# Illuminating Controls on Solute and Water Transport in the Critical Zone

Jesse Benjamin Radolinski

Dissertation submitted to the faculty of the Virginia Polytechnic Institute and State University in partial fulfillment of the requirements for the degree of

**Doctor of Philosophy**

In

School of Plant and Environmental Sciences

**Committee**:

Ryan. D. Stewart

Kang Xia

W. Cully Hession

W. Lee Daniels

September 26, 2019

Blacksburg, Virginia

Keywords: preferential flow, neonicotinoids, veterinary antibiotics, evapotranspiration, evapo-concentration, soil structure, stable isotopes, deuterium

Illuminating Controls on Solute and Water Transport in the Critical Zone

Jesse Benjamin Radolinski

ACADEMIC ABSTRACT

Earth's near-surface environment sustains nearly all terrestrial life, yet this critical zone is threatened by the environmental migration of new and potentially harmful compounds produced to support a growing human population. Traditional transport equations often fail to capture the environmental behavior of these emerging contaminants due to issues such as flow heterogeneity. Thus, there is a need to better evaluate controls on pollutant partitioning in Earth's critical zone. Our first study investigated the transport and distribution of the neonicotinoid insecticide thiamethoxam (TMX) by growing TMX-coated corn seeds in coarse vs fine-textured soil columns maintained with versus without growing corn plants. Fine-textured soil transported TMX at concentrations that were two orders of magnitude higher than coarse-textured soil, due to preferential flow in the fine-textured soil columns and higher evapotranspiration (ET) concentrating more TMX in the coarse-textured soil. Living plants increased the concentration of TMX at depth, indicating that growing plants may drive preferential transport of neonicotinoids. For the second study we planted TMX-coated corn seeds and maintained field plots with and without viable crops ($n$ = 3 plots per treatment), measuring TMX concentrations in three hydrological compartments (surface runoff, shallow lateral flow, and deep drainage) and soil. TMX was transported in the highest concentrations via surface runoff, while also showing continual migration within the subsurface throughout the growing season. Plants facilitated downward migration of TMX in soil yet restricted losses in drainage. For our final study, we used a simple isotope mixing method to evaluate how preferential flow alters the influence of compound chemical properties on solute transport. We applied deuterium-labeled rainfall to plots containing manure spiked with eight veterinary antibiotics with a range of mobility, and quantified transport to suction lysimeters (30 and 90 cm). We showed that low preferential flow (<20%) eliminates the influence of compound chemical properties and, contrary to conventional understanding, more preferential flow (~ >20%) amplifies these chemical controls, with more mobile compounds appearing in significantly higher concentrations than less mobiles ones. Altogether, we provide a refined understanding of solute partitioning in the critical zone necessary to improve process-based transport modeling.

Illuminating Controls on Solute and Water Transport in the Critical Zone

Jesse Benjamin Radolinski

## GENERAL AUDIENCE ABSTRACT

Earth's near-surface environment sustains nearly all terrestrial life, yet this critical zone is threatened by the environmental migration of new and potentially harmful pollutants produced to support a growing human population. Additionally, traditional mathematical methods fail to accurately describe the behavior of these emerging pollutants in soils due to complex flow patterns. Thus, scientists need to better understand how these pollutants contaminate water bodies in the critical zone. We first conducted a greenhouse experiment to understand and measure the amount of the neonicotinoid insecticide thiamethoxam (TMX) that could move from coated corn seeds through the soil environment. Water draining from fine-textured soil had >100 times more TMX than water draining from course-textured soil, due to commonly occurring fractures/cracks in the finer-particle soil and more evaporation from soil and plant leaves sequestering TMX in the sandy soil. Growing plants amplified TMX movement through soil voids to lower depths. We then conducted a field study to determine how much TMX could move to the surrounding environment throughout the corn growing season. We found that plants aided in downward movement of TMX yet restricted total losses from the plot overall by removing soil water. Our third study investigated the degree to which chemical pollutant properties control movement of solutes when water flows preferentially through soil void space. Common dairy manure was spiked with eight pollutants ranging in chemical attraction to soil and was added to an agricultural field. After irrigation, we found that when total drainage water was less than 20% derived from preferential flow, chemical properties had a negligible effect on the amount of pollutant in draining soil water. Contrary to conventional understanding, when draining water contained more than 20% preferential flow, chemical properties had a strong influence on the amount of pollutant detected. Altogether, we provide new understanding of how solutes move though the critical zone. These findings are necessary to create mathematical tools that more accurately depict pollutant behavior below-ground.

## Acknowledgements

First, thanks to all of my committee members for their guidance and patience throughout my time at Virginia Tech. Learning from their diverse expertise helped me grow as a scientist. Thanks to my advisor, Dr. Ryan Stewart, for being the man and always being available at the most critical times. Thank you Dr. Xia for your constant encouragement, enthusiasm, and analytical insight. Thanks to all my lab mates, especially Ayush Joshi Gyawali and Jingjing Chen, for their support and just generally making every experience more enjoyable. Thanks to Junxue Wu and Hanh Le for their invaluable help with analytical analyses in the Xia Lab. Thanks to Sheldon Hillaire for collaboration in the field—rain or shine. Thanks to the following undergraduates for quality help in the field and lab: Kait Palys, Mayanni McCourty, Ben Spencer, Alexis Gillmore, Victoria Schluszas and Aaron Cleveland. I would like to thank Aaron Cleveland and Alexis Gillmore, specifically, for being a tremendous help during the wildest days of the antibiotic field experiment. Thanks to Brandon Lester for going full MacGyver when necessary. Thanks to Mike Brosius for his expertise and assistance with rainfall simulations. Thanks to Kelly Peeler for help with isotope analyses. Thanks to family and friends for support. Most importantly, thank you to Taqueria el Paso in Christiansburg for the best tacos that man can produce. There are few things on this rock better than good, authentic tacos. Tacos provided bliss in a background of adversity and were thus critical to the completion of this degree. No, I am not being to paid write this love letter.

**Table of Contents**

# Chapter 1. Introduction

The thin section of the Earth's subsurface that extends from the bottom of the local water table to the top of vegetation, known as the critical zone, supports nearly all terrestrial life. A growing human population has exposed new and potentially harmful compounds to the critical zone in ever increasing loads, often at the expense of water quality. Additionally, the environmental behavior of these emerging contaminants is not well captured by traditional transport models due to heterogeneous flow conditions (e.g., preferential flow through soil macropores) [*Beven and Germann*, 2013; *Hassanpour et al.*, 2019; *Richard and Steenhuis*, 1988], thus there is a need to re-evaluate controls on subsurface partitioning of these pollutants.

One class of emerging contaminants includes the neonicotinoid insecticides that coat the seeds of 140+ crops worldwide [*Elbert et al.*, 2008; *Main et al.*, 2015]. These chemicals are water soluble and highly toxic to non-target invertebrates (e.g., honeybees), thus eliciting concern of environmental transport. Marketed as a more environmentally-friendly alternative to spray application, seed dressings now account for > 60% of all global neonicotinoid application [*Jeschke et al.*, 2011]. However, ~2-20% of the compounds are translocated into plant tissue and the remainder is introduced directly to the soil environment [*Sanchez-Bayo*, 2014a]. Neonicotinoids are detected in surface water bodies [*Main et al.*, 2016; *Starner and Goh*, 2012a; *Stone et al.*, 2014], groundwater [*Lamers et al.*, 2011], and drinking-water [*Klarich et al.*, 2017], yet a definitive link to seed applications has yet to be identified.

Similarly, veterinary antibiotics (VAs) are a group of emerging contaminants that are chemically diverse and environmentally ubiquitous. The U.S. purchases nearly 66 million kg of VAs annually to support the animal production industry; many of which are labeled as critically

important to the World Health Organization's strategy for controlling global antibiotic resistance [*Chen et al.*, 2018; *Collignon et al.*, 2016]. As much as 80% of initial antibiotic doses to livestock can be still be found in animal waste [*Chen et al.*, 2018; *Montforts et al.*, 1999]. This waste is often applied as cheap fertilizer in agricultural systems [*Heuer et al.*, 2011], furthering the potential transport of VAs [*Le et al.*, 2018] and establishment of antibiotic resistant organisms [*D'Costa et al.*, 2011; *Wind et al.*, 2018]. Once VAs are exposed to the soil environment, a variety of reactive chemical structures translate to complex solute distributions below-ground. These compounds can largely partition into soil organic matter [*Wegst-Uhrich et al.*, 2014], sorb strongly to soil mineral surfaces [*Chee-Sanford et al.*, 2009], or exist primarily in the aqueous phase [*Boxall et al.*, 2002], with high susceptibility to macropore flow [*Kay et al.*, 2004; *Kay et al.*, 2005a; b]. VAs can thus be transported through a given soil at velocities similar to or several orders of magnitude slower than water [*Boy-Roura et al.*, 2018]. As a result, VAs stand as potentially ideal compounds to study how preferential flow alters chemical retention within soils.

Preferential (i.e., non-equilibrium) flow occurs when infiltrating water moves through fractures or voids in porous media, bypassing the soil matrix and causing steep increases in flow rates without analogous or uniform increases in water pressure [*Beven and Germann*, 2013; *Flühler et al.*, 1996; *Jarvis*, 2007b]. Preferential flow is ubiquitous in natural soils [*Flury et al.*, 1994; *Graham and Lin*, 2011; *Hardie et al.*, 2011; *Nimmo*, 2012], often resulting in orders of magnitude higher contaminant leaching than estimated assuming a homogenous soil matrix [*Allaire et al.*, 2009; *Radolinski et al.*, 2018b]. A contaminant's chemical affinity for the soil matrix is generally thought to dictate the total amount of solute transported to a given outlet (i.e., stream, aquifer, tile drain etc.) per unit time. However, these chemical controls may be altered as

drainage water preferentially bypasses the soil matrix [*Barbash and Resek*, 1996; *Klein*, 1994]. Some numerical simulations have suggested that immobile compounds (i.e. with high $K_d$, high $K_{oc}$) can be more sensitive to non-equilibrium flow [*Larsson and Jarvis*, 2000]. Others studies report that the total mass transport of more mobile compounds may be reduced by up to 50% with preferential flow when compared to modeled flow through a homogenous medium [*Larsson and Jarvis*, 1999]. Preferential flow is thought to weaken these chemical controls on contaminant mobility [*Larsson and Jarvis*, 2000] or eliminate them altogether [*Ghodrati and Jury*, 1992], yet no study to date has defined the degree of preferential flow required to dampen this chemical influence.

Stable isotopes of water (e.g., $^{2}H$ and $^{18}O$) are naturally abundant in Earth's hydrological cycle as components of water itself, making them ideal for identifying hydrological flow paths [*Gazis and Feng*, 2004] and determining water residence time [*Hrachowitz et al.*, 2013; *McGuire and McDonnell*, 2006]. These tracers are used traditionally to detect preferential flow by tracking water transit through hydrological systems [*White et al.*, 1984]; however, they are particularly useful for identifying water sources [*Good et al.*, 2015]. For this reason, stable isotopes can be used to fingerprint water slowly flowing through the soil matrix versus more rapid bypass flow [*Stumpp and Maloszewski*, 2010; *Stumpp et al.*, 2007; *Vogel et al.*, 2010]. Thus, these tracers can be an effective tool for isolating and quantifying preferential flow.

In this dissertation, we aimed to: 1) quantify the environmental transport of two emerging contaminant classes (neonicotinoids + VAs), and 2) use these solutes to evaluate fundamental controls on contaminant mobility in the critical zone. These two objectives were met with three studies, each presented as a chapter. The first study sought to quantify the physical transport of the common neonicotinoid thiamethoxam (TMX) from corn seed coatings under environmentally

relevant conditions. We performed a greenhouse study to understand the role of plant growth on neonicotinoid transport, using columns with two soil textures (fine vs coarse textured), two lengths (20 and 60 cm), and comparing the presence versus absence of viable corn plants. Using insight from this greenhouse study, we further addressed the role of plant growth on neonicotinoid transport by quantifying the movement of TMX through runoff, shallow later (<72 cm), and deep (110 cm) drainage with and without viable corn plant growth throughout the growing season. For our final study, we used a simple isotope mixing method to evaluate how and the degree to which preferential flow alters chemical controls on solute transport. We conducted deuterium-labeled rainfall simulations on a field containing VA-spiked dairy manure, and collected subsurface water samples using suction lysimeters. Together, this approach allowed us to quantify the amount of preferential flow and VA concentrations represented in each sample.

# Chapter 2. Transport of a neonicotinoid pesticide, thiamethoxam, from artificial seed coatings

Jesse Radolinski, Junxue Wu, Kang Xia, and Ryan D. Stewart

Published in *Science of the Total Environment*:

Radolinski, J., J. Wu, K. Xia, and R. Stewart (2018), Transport of a neonicotinoid pesticide, thiamethoxam, from artificial seed coatings, *Science of the Total Environment*, *618*, 561-568. https://doi.org/10.1016/j.scitotenv.2017.11.031

## 2.1 Abstract

Neonicotinoid insecticides coat the seeds of major crops worldwide; however, the high solubility of these compounds, combined with their toxicity to non-target organisms, makes it critical to decipher the processes by which they are transported through soils and into aquatic environments. Transport and distribution of a neonicotinoid (thiamethoxam, TMX) were investigated by growing TMX-coated corn seeds in coarse-textured and fine-textured soil columns (20 and 60 cm lengths). To understand the influence of living plants, corn plants were terminated in half of the columns (no plant treatment) and allowed to grow to the V5 growth stage (33 days of growth) in the other half (with plant treatment). TMX was analyzed in leachate 12 times over 33 days and in bulk soil after 8, 19, and 33 days of corn growth. All 20 cm columns leached TMX at levels exceeding the United States Environmental Protection Agency benchmark for aquatic invertebrates (17.5 µg $L^{-1}$). TMX migrated from seeds to adjacent bulk soil by the eighth day and reached deeper soil sections in later growth stages (e.g., 30-45 cm depth by Day 33). Fine-particle soils transported over two orders of magnitude more TMX than coarse-textured soils (e.g., 29.9 µg vs 0.17 µg, respectively), which was attributed to elevated evapotranspiration (ET) rates in the sandy soil driving a higher net retention of the pesticide and to structural flow occurring in the fine-textured soil. Living plants increased TMX concentrations

at depth (i.e., 30-60 cm) compared to the no plant treatment, suggesting that corn growth may drive preferential transport of TMX from coated seeds. Altogether, this study showed that neonicotinoid seed coatings can be mobilized through soil leachate in concentrations considered acutely toxic to aquatic life.

## 2.2 Graphical Abstract

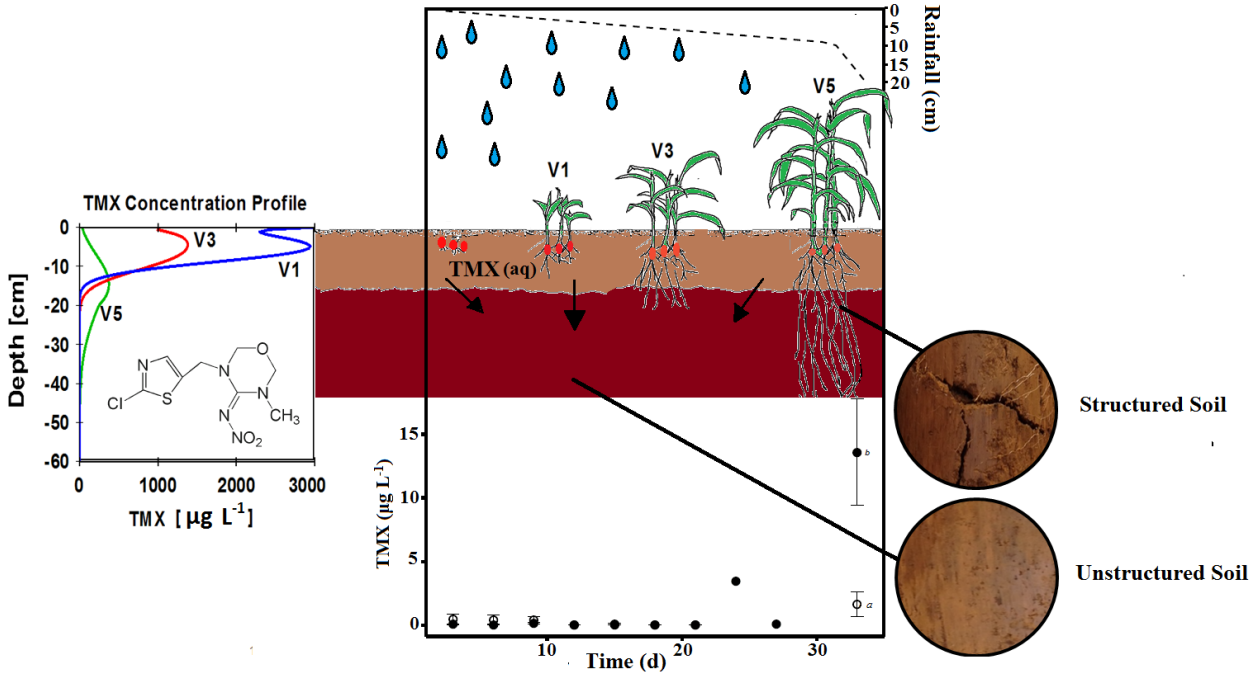


## Keywords

Soil Structural Features, Evapo-concentration, Evapotranspiration, Corn Stage, Insecticide

## 2.3 Introduction

Each year more than 20,000 tonnes of neonicotinoids are produced [*Codling et al.,* 2016] and applied to 140 + crops worldwide [*Elbert et al.,* 2008; *Main et al.,* 2015], with an estimated global market value of ~$2.6 billion [*Goulson and Kleijn*, 2013; *Jeschke et al.,* 2011]. Imidicloprid (IMD), thiamethoxam (TMX), and clothianidin (CLO) are the most common neonicotinoids, and are used extensively as seed coated insecticides. These three compounds have high selectivity for the insect nicotinic acetylcholine receptor, which makes them an effective pesticide against a broad spectrum of invertebrate pests while remaining relatively non-toxic to mammals [*Jeschke and Nauen*, 2007; *Jeschke et al.,* 2011; *Zalom et al.,* 2005]. Despite their effectiveness as insecticides, neonicotinoids have been scrutinized for high toxicity to non-target invertebrate organisms and insectivorous birds [*Douglas et al.,* 2015; *Hallmann et al.,* 2014], including an association with significant declines in bee populations [*Alix et al.,* 2009; *Sanchez-Bayo and Goka*, 2014; *Sandrock et al.*, 2014; *Whitehorn et al.*, 2012].

Globally, more than 60% of all neonicotinoids are applied via seed dressings [*Goulson and Kleijn*, 2013]. Neonicotinoid seed coatings are advertised to provide continued protection from insect herbivory throughout the growing season, as the highly soluble compounds move into the root zone, enter the plant, and arm its aboveground tissue [*Jeschke et al.,* 2011; *Jones et al.,* 2014; *Zalom et al.,* 2005]. Because they are applied directly to the plant roots, seed coatings typically have lower amounts of active pesticides compared to spray applications (in terms of g $ha^{-1}$) and are therefore often considered to be more environmental friendly [*Jeschke et al.,* 2011]. However, only 2-20% of the pesticide is taken up by the target crop, with the remainder left in the soil environment where it may become transported into ground water and eventually incorporated into surface water systems [*Sanchez-Bayo,* 2014b]. Neonicotinoids can be applied

as corn coatings at amounts up to 1.25 mg per seed. Using corn production (typical planting rate: 74,000 seeds $ha^{-1}$) as an example, an estimated 3,300 tonnes of neonicotinoids can be applied each year to the 36 million hectares of maize in the United States [*USDA*, 2017]. If only 20% of the neonicotinoids are taken up by the corn plants, then up to 2,700 tonnes of neonicotinoids may be mobilized in the surrounding environment. As a possible consequence, neonicotinoids are now detected in surface waters across North America [*Hladik et al.*, 2014b; *Main et al.*, 2015; *Schaafsma et al.*, 2015]. In regions with intensive soybean and maize production, neonicotinoids have been detected in nearly all surface water bodies [*Hladik et al.*, 2014b; *Schaafsma et al.*, 2015], with seed coatings identified as the most likely source. However, the linkage between seed coatings and the aquatic environment as not been directly assessed, and no work to date has identified or quantified the underlying mechanisms by which neonicotinoids are transported from agricultural fields.

Neonicotinoids have moderate to high leaching potential, with leaching patterns largely explained by the aqueous solubility of the compounds.[*Banerjee et al.*, 2008; *Cox et al.*, 1997; *Cox et al.*, 2001; *Gupta et al.*, 2008; *Katagi*, 2013; *Kurwadkar et al.*, 2014a; *Leiva et al.*, 2015; *Oi*, 1999]. Leaching typically increases with soil water content; for example, the half-life of thiamethoxam (TMX) in soil columns decreased from 301 days to 46 days as soil water content increased from dry to near-saturated conditions, with degradation rates increasing with TMX concentration [*Gupta et al.*, 2008]. Because neonicotinoids are polar, highly soluble, and exhibit low affinity for soil mineral matrix, the partial equilibrium conditions provided by a rain storm may promote leaching via bulk flow or advection [*Hu and Brusseau*, 1996; *Katagi*, 2013; *Kurwadkar et al.*, 2014a; *Oi*, 1999].

Soil structural features, which arise as unconsolidated soil material arranges into a more stable hierarchy of aggregates, often form secondary pore networks that may affect solute transport. As soil water pressure increases during a rain event, flow can preferentially follow these structural pathways and bypass the soil matrix, where water is tightly held at more negative potentials [*Jarvis*, 2007b]. This non-equilibrium flow can result in pesticides being rapidly mobilized through the soil profile [*FOCUS*, 2001; *Jarvis*, 2007b; *Molz*, 2015]. For example, mass balances performed on the herbicide bentazone have showed that up to 8% of the applied dose can be lost through soil structural pathways, resulting in concentrations as high as 200 μg $L^{-1}$ in tile drainage [*FOCUS*, 2001]. Thus, it is important to understand if neonicotinoids can also be mobilized via flow through soil structural pathways.

The transport and distribution of pesticides in soil is also further complicated by the presence of plants. For instance, maize can apply suction forces well above 9.5 bars [*Ionescu*, 1969]. For highly soluble compounds such as neonicotinoids, this plant-induced suction could translate to a vertical stratification in the soil profile, in which neonicotinoids can remain close to the soil surface under stable unsaturated conditions. On the other hand, roots may increase the size of soil structural pathways, which can cause increased preferential leaching [*Bundt et al.*, 2000; *Jørgensen et al.*, 2002]. Such plant-related processes have not yet been well-studied in the context of pesticide transport.

The primary aim of this study was to quantify the transport of thiamethoxam (TMX) from coated corn seeds in fine-textured and coarse-textured soils, while also accounting for the roles of soil structure and viable plants. We hypothesize that: i) coarse-textured soil will transport more TMX than fine-textured soil with intact structural features, ii) structured soil will transport more than unstructured soil of the same texture, and iii) the presence of viable plants will result

in less leaching of the pesticide from soil columns. Since seed coatings are the dominant form of neonicotinoid application for many crops, direct measurements of their movement from the seeds is an imperative step in assessing the overall environmental impact of this practice.

## 2.4 Materials and methods

### 2.4.1 Soil characterization

Soils were taken from pastures in New Kent County and Whitehorne (Montgomery Co.), VA. The New Kent soil was a Bojac series (Typic Hapludult) and coarse-textured (hereafter referred to as a "sand"). The Whitehorne soil was a Shottower series (Typic Paleudults) and a fine-textured, moderately structured soil (hereafter referred to as a "loam").

Intact soil cores (stainless steel, 2.5 cm x 5 cm) taken from the two sites were analyzed for bulk density [M $L^{-3}$] and saturated hydraulic conductivity ($K_s$) [L $T^{-1}$]. Samples were collected every 5 cm depth from the surface to 30 cm depth ($n$ = 6 cores per depth increment). The 0-20 cm cores were considered to represent the Ap horizon and the 20-30 cm cores were considered to represent the upper Bt horizon. $K_s$ was determined using the falling head method with a UMS KSAT Benchtop Saturated Hydraulic Conductivity Instrument (UMS Inc.; Munich, Germany). $K_s$ was determined per the manufacturer's recommendation as:

$$K_s = bL\left(\frac{A_{burette}}{A_{sample}}\right) \quad (1)$$

where $A_{burette}$ [$L^2$] is the cross-sectional area of the water column, $A_{sample}$ [$L^2$] is the cross-sectional area of the sample, L is the length of the sample, and b is an exponent determined via curve-fitting between measured pressure head ($h$, starting at some initial pressure head $h_0$) and time:

$$h(t) = h_0 e^{-bt} \quad (2).$$

Loose soil samples from the Ap (0-20 cm) and Bt (20-60 cm) horizons were air dried, sieved to 2 mm, and analyzed for pH, cation exchange capacity (CEC) [Mol $M^{-1}$], total organic carbon (TOC) [M $M^{-1}$], and texture. Five replicates ($n$ = 5) samples were used per test; additional details regarding the soil CEC, pH, TOC, and texture measurements are found in Appendix A. TMX sorption coefficient ($K_d$) [$L^3$ $M^{-1}$] and sorption coefficient normalized to soil organic carbon content ($K_{OC}$) [$L^3$ $M^{-1}$] were determined via EPA method 835.1230 [*USEPA*, 2008] using composite soil samples collected from the two field locations**.** Soil physiochemical and hydraulic properties are shown in **Table 2.1**.

2.4.2 Columns design and preparations

At each soil collection site, 12 m long by 0.3 m wide areas were excavated to a depth of 20 cm, exposing the subsurface Bt horizons. At the New Kent site, seventeen long (60 cm) and eight short (20 cm) columns were hand-packed using soil from the trench. All columns were made using 20 cm (inner diameter) Schedule 40 PVC Pipe. The 20 cm columns were packed with the Ap soil. For the 60 cm columns, the upper 20 cm and lower 40 cm were packed with the Ap and Bt soils, respectively. All fill soil was homogenized by hand and plant material and roots were removed. Soil layers were packed with a wooden piston (10 cm diameter) to match the measured *in situ* dry bulk density. The two column lengths were chosen to isolate the effects of the Ap and Bt layers. At the Whitethorne site, a Giddings Rig was used to collect sixteen semi-intact cores (with 20 cm inner diameter PVC pipe) that were 60 cm in length, of which the lower 40 cm came from the extracted soil (moderate, fine, subangular, blocky structure). These columns therefore included soil structure within the Bt horizon, and are referred to as the "structured loam" treatment. In addition, an "unstructured" loam treatment was created using

five 60 cm tall columns that were filled with sieved (< 2 mm) and repacked Bt (20-60 cm) and Ap soil (0-20 cm) from the Whitethorne site. The upper 20 cm of all other loam columns, as well as ten additional 20 cm ("short") columns, were packed using the local Ap soil as described above. Column packing resembled *in situ* bulk densities, though some minor adjustments were made after packing, as detailed in the Appendix A.

All columns were saturated with a 0.005 M $CaCl_2$ artificial rain solution for 48 hours and left to drain completely for another 48 hours prior to planting corn seeds [*Kurwadkar et al.*, 2014a; *USEPA.*, 2008]. This step was included to purge air-filled pores, force out large soil macrofauna, and remove background TMX (for more information on background TMX, see Appendix A). After the columns stopped draining, three Cruiser Extreme® 1250 corn seeds (Syngenta; Greensboro, NC) were planted in each column to a depth of 4 cm [*Roger et al.*, 2013]; this amount corresponded to the recommended maximum yield planting density of 95,000 plants $ha^{-1}$ [*Lauer*, 2009]. Preliminary analysis revealed that each seed carried 0.6 mg of TMX.

2.4.3 TMX transport/leaching study

Forty columns ($n$ = 17 for sand and $n$ = 23 for loam) were chosen for the leaching study (**Figure A1**). Within each soil texture class, columns were separated into a "with plant" treatment, where corn plants were allowed to grow, and a "no plant" treatment where seedlings were severed upon emergence to control for corn growth. This design was to understand the influence of the plant on the transport process. Each treatment was replicated 4-5 times by column lengths (20 cm and 60 cm) ($n$ = 4-5). The five "unstructured" 60 cm loam columns were assigned the "with plant" treatment, for direct comparison to structured loam columns with viable corn. Soil columns were housed in a greenhouse at 24 °C, and exposed to 400-watt growth lights for 14 hours and 10 minutes, daily. The hours of daylight were consistent with that of May

15th, 2015 in Blacksburg, VA, which was chosen to represent the median day length for the first month of the corn growing season [*Brann et al.*, 2009; *Straw*, 2009].

The columns were watered every 3 days for a 30 day growing period with 300 mL (0.9 cm) of 0.005 M $CaCl_2$ solution each time. Volume and frequency of watering were chosen to reflect mean precipitation and return periods, based on Virginia precipitation data from 1952-2012 [*UVA*, 2015]. The watering solution was applied at a rate of 70 mm $hr^{-1}$ using a calibrated polyethylene cylinder [*SERA-17*, 2008]. On Day 31, a large rainstorm event of 9 cm (3 L) was simulated, representing the mean daily maximum rainfall for March-April at the sites [*UVA*, 2015]. Leachate was continuously collected from the bottom of each column. Samples were taken for analysis of TMX concentration and the collection containers were then emptied prior to each watering event (12 events total over 33 days). A simplified mass balance was then used to estimate cumulative evapotranspiration [L] by subtracting the amount of cumulative leachate from the cumulative simulated rainfall (as discussed in more detail in the Appendix A). The daily evapotranspiration rate [$L\ T^{-1}$] was calculated by dividing the cumulative amount by the number of elapsed days (i.e., 33 days). This approach assumed that evapotranspiration was constant throughout the experiment, which was likely reasonable given the near constant temperature and humidity conditions in the greenhouse, particularly for the "no plant" columns.

**Table 2.1: Soil physiochemical properties.**

| Soil | Depth (cm) | Texture | Sand (%) | Silt (%) | Clay (%) | Bulk Density (g $cm^{-3}$) | Porosity (%) | TOC (%) | pH | CEC (cmol $kg^{-1}$) |
|---|---|---|---|---|---|---|---|---|---|---|
| **Loam Ap** | 0-20 | loam | 38.7 | 43.6 | 17.7 | 1.37 ± 0.093 | 49 | 1.12 ***a*** | 5.8 | 4.7 ± 0.15 ***a*** |
| **Loam Bt** | 20-60 | loam | 33.4 | 40.1 | 26.4 | 1.64 ± 0.130 | 39 | 0.3 ***c*** | 5.9 | 4.5 ± 0.75 ***a*** |
| **Sand Ap** | 0-20 | loamy sand | 85.9 | 7.69 | 6.41 | 1.52 ± 0.108 | 44 | 1.46 ***b*** | 4.8 | 3.5 ± 0.50 ***b*** |
| **Sand Bt** | 20-60 | fine sand | 87.4 | 9.91 | 2.71 | 1.67 ± 0.070 | 38 | 0.49 ***c*** | 4.1 | 1.8 ± 0.33 ***c*** |

*Different letters* denote significant differences ($p \leq 0.05$). Bulk Density and Cation Exchange Capacity (CEC) are expressed as mean ± standard deviation.

2.4.4 TMX distribution and movement in soil

The remaining 33 columns were used to measure TMX uptake into corn plants and movement into surrounding soil. These columns were destructively sampled at corn stages V1 (8 columns; $n$ = 4/soil texture), V3 (8 columns; $n$ = 4/soil texture), and V5 (17 columns that were also used in the Leaching Study, as detailed in **Figure A1**), which respectively corresponded to 8 19, and 33 days after planting. Corn growth stages were determined by counting corn "collars", e.g. stage V1 corresponds to one corn collar following the development of the first leaf [*McWilliams et al.*, 2010]. At growth stages V1 and V3, the sampled columns ($n$ = 4/soil texture/growth stage) were cut longitudinally with a jig saw, destructively sampled, and measured for TMX concentrations. At growth stage V5, eight of the 60 cm "with plant" leaching columns, along with another nine "no plant" leaching columns ($n$ = 4 for sand and 5 for loam), from the Leaching Study ($n$ = 4/soil texture), were destructively sampled. Because TMX in plant tissue represented a minor contribution to the initial input from seed coatings (< 0.5 %), the current study reports TMX movement and distribution in soil. TMX was analyzed in rhizosphere, root soil, and in bulk soil (0-30 cm, 30-45 cm, and 45-60 cm depth intervals) (as discussed in the Appendix A). Methods for collection of root soil and rhizosphere soil are described by *Cushman* [2017].

To focus on providing definitive evidence of any mobilization of TMX in the soil profile, TMX distribution in bulk soil was reported. The TMX measured in root soil and rhizosphere soil were grouped together as a lumped average deemed the "plant-associated" TMX. This grouping allowed for contrast between soil that is associated with plant tissues versus that which is in the bulk soil, and thus assumed to be environmentally available. In the case of

the “no plant” treatments, the “plant-associated” TMX consisted only of soil associated with seed and decayed root tissue.

### 2.4.5 Statistical analysis

TMX concentrations and mass recovered in the soil profile were analyzed using two-way ANOVA. These tests were conducted on log transformed data by bulk soil depths of 0-30 cm and 30-45 cm, and rank transformed data for the 45-60 cm section. Rank transformation was used as a way to transform data to normality and provided an avenue for parametric factorial comparisons (e.g. two-way ANOVA), which is the functionally equivalent to traditional non-parametric tests [*Conover*, 2012; *Conover and Iman*, 1981]. For soil analysis, texture (sand and loam) and corn stage (V1, V3, V5, and a combined V5-no plant) were treated as factors. The V5-no plant combination was created to identify the corn plant’s influence on TMX distribution. Two-way ANOVAs were tested on TMX concentration in final leachate, TMX mass transport data, and total leachate volume, where texture and plant influence (plant and no plant) were treated as factors. TMX transport data were rank transformed to normality for 60 cm columns and log transformed for 20 cm columns. A one way Kruskal Wallis test was also conducted to compare TMX transported in structured versus unstructured loam treatments. Normality was determined via visual inspection of histogram and normal quantile plot results. Homogeneity of variances was confirmed via Fligner’s test. Tukey’s multiple comparisons test was run on all resulting ANOVA results. All statistical tests were conducted in R version 3.2.2 with $\alpha = 0.05$.

## 2.5 Results and Discussion

The saturated hydraulic conductivity ($K_s$) measurements from the soil cores showed that the loam soil had much higher variability, both between the Ap and Bt horizons and between samples within each horizon (**Figure 2.1**). The median $K_s$ value for the loam Ap horizon was 860 cm $d^{-1}$,

which was approximately two times greater than the median $K_s$ value for the sand Ap (410 cm $d^{-1}$). The median $K_s$ values for the loam Bt horizon, on the other hand, was 36 cm $d^{-1}$, which was nearly a factor of 10 less than the $K_s$ value for the sand Bt horizon (300 cm $d^{-1}$). However, individual cores within the loam Bt horizon showed $K_s$ values as high as 1100 cm $d^{-1}$, which exceeded all values measured for the sand Bt horizon. Taken together, these $K_s$ estimates show that the loam soil has greater variability in its hydraulic conductivity, which we hypothesize to be an indication of preferential flowpaths, for example due to soil structure or connected biopores. We also hypothesize that the unstructured loam columns would have lacked these preferential pathways due to the repacking process, and that the hydraulic conductivity of those columns would be better represented by the lowest, rather than the highest, $K_s$ readings.

TMX leaching was minimal in all treatments for the first 30 days of the experiment; however, TMX was detected in leachate for all columns following the final (9 cm) precipitation event on day 31 (**Figure 2.2**). Texture played a significant role in TMX transport through the 20 cm columns (two-way factorial ANOVA, $p = 0.008$), as sand columns transported higher concentrations of TMX during the final leaching event compared to the loam columns (sand, with plant vs loam, with plant; Tukey, $p = 0.03$; **Figure 2.2a**). No significant differences were found between treatments for total drainage and total TMX mass transported, and plants showed no significant effect on TMX leaching in terms of mass transport, final leachate concentration, and drainage in 20 cm columns (two-way factorial ANOVA, Tukey, $p > 0.05$; **Figure 2.2a and b**). All 20 cm columns leached TMX at concentrations above the United States Environmental Protection Agency (EPA) benchmark for acute toxicity to aquatic invertebrates [*Anderson et al.*, 2013] (**Figure 2.2a**). This finding suggests that surface soil horizons in agricultural systems may

be capable of transporting harmful concentrations of TMX, particularly during more intense/longer duration rainfall events.

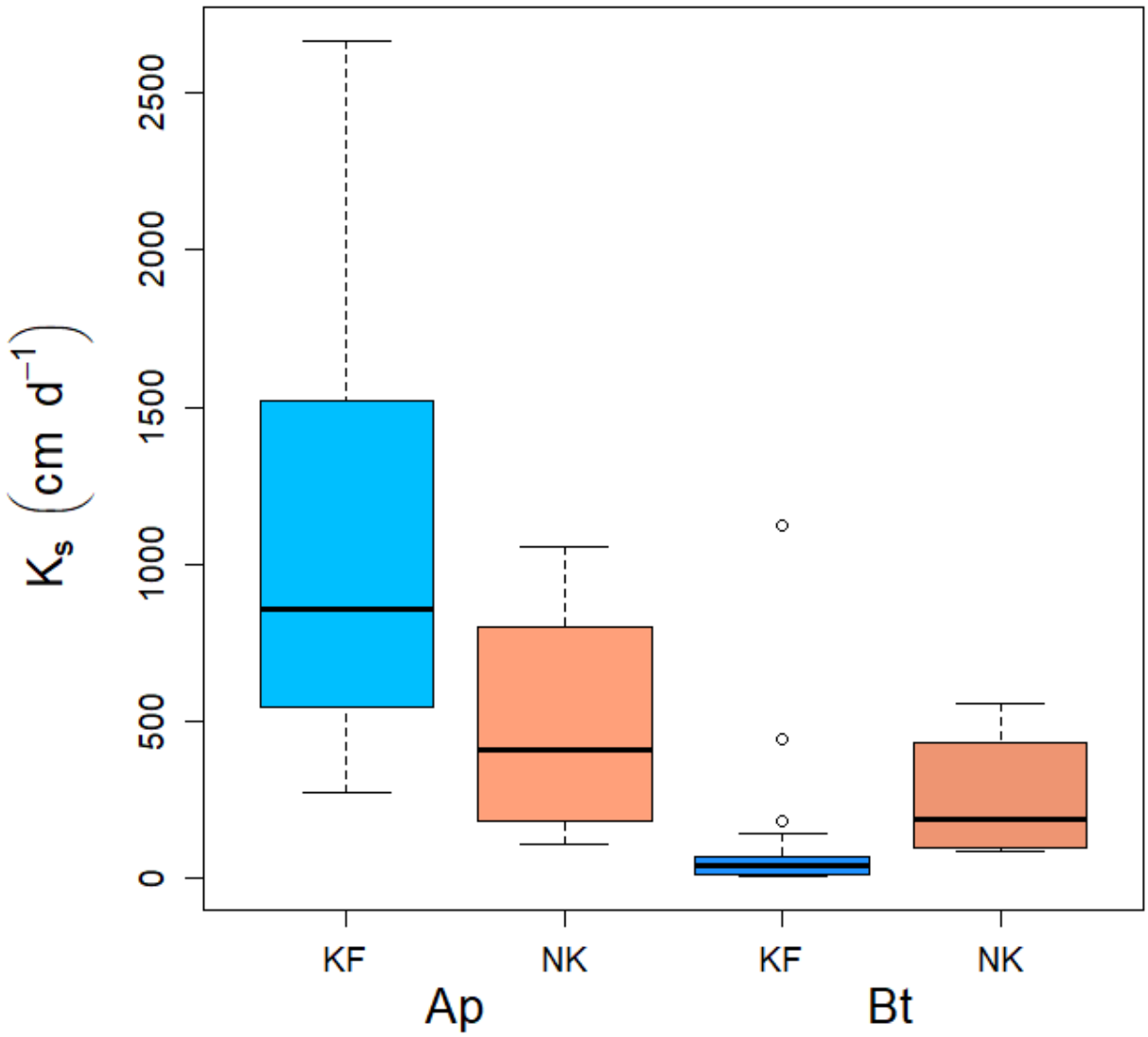


**Figure 3.1**: Saturated hydraulic conductivity ($K_s$) values (cm $d^{-1}$) measured for the upper Ap and lower Bt horizons from the two studied soils (KF = Kentland Farm "loam" soil; NK = New Kent "sand" soil). $n$ = 17 for KF/$A_p$; $n$ = 12 for NK/$A_p$; $n$ = 21 for KF/$B_t$; $n$ = 8 for NK/$B_t$.

Contrary to the 20 cm columns, in the 60 cm columns the structured loam column soil facilitated greater TMX transport than the sand, with greater cumulative mass leaching over the course of the experiment (**Figure 2.2f**), and higher TMX concentrations during the final 3 L

irrigation event (two-way factorial ANOVA, $p < 0.001$; **Figure 2.2e**). Viable corn plants had no effect on TMX transport in terms of mass or concentration (two-way factorial ANOVA, $p > 0.05$). Soil texture affected the total leachate volume; however, the difference was attributed to a higher volume of leachate in loam columns without viable plants compared to sand columns with plants (Two-Way factorial ANOVA, $p = 0.006$; Tukey, $p = 0.007$; **Figure 2.2f**). Soil structure also had a significant effect, as the structured loam columns transported more TMX mass, contained a higher concentration in final leachate, and yielded a higher drainage volume than the unstructured loam columns (Kruskal-Wallis, $p = 0.03$, $p = 0.007$, $p = 0.03$, respectively; **Figures 2c and d**). It should also be noted that even unstructured loam transported TMX at higher concentrations in the final leachate than the sand columns (unstructured loam, $1.65 \pm 1.96$ μg $L^{-1}$; sand, $0.18 \pm 0.10$ μg $L^{-1}$; both containing viable plants), possibly due to the sand having high near-surface evapotranspiration over the course of the experiment (see ET discussion below).

In the soil distribution study, TMX was detected in the 0-30 cm bulk soil (outside of rhizosphere and root soil) as early as 8 days after planting (i.e., the V1 growth stage), with average concentrations as high as 75 μg $kg^{-1}$ (sand columns at V1 corn stage; **Figure 2.3a**). The appearance of TMX in bulk soil was complemented by migration of the pesticide from plant-associated soil (plant-associated soil: **Figure 2.4;** bulk soil: **Figure 2.3**). By the V5 corn stage (33 days after planting), TMX had moved into the 30-45 cm and 45-60 cm soil sections in significant concentrations (Tukey, $p < 0.001$), though the majority of TMX still remained in the 0-30 cm bulk soil.

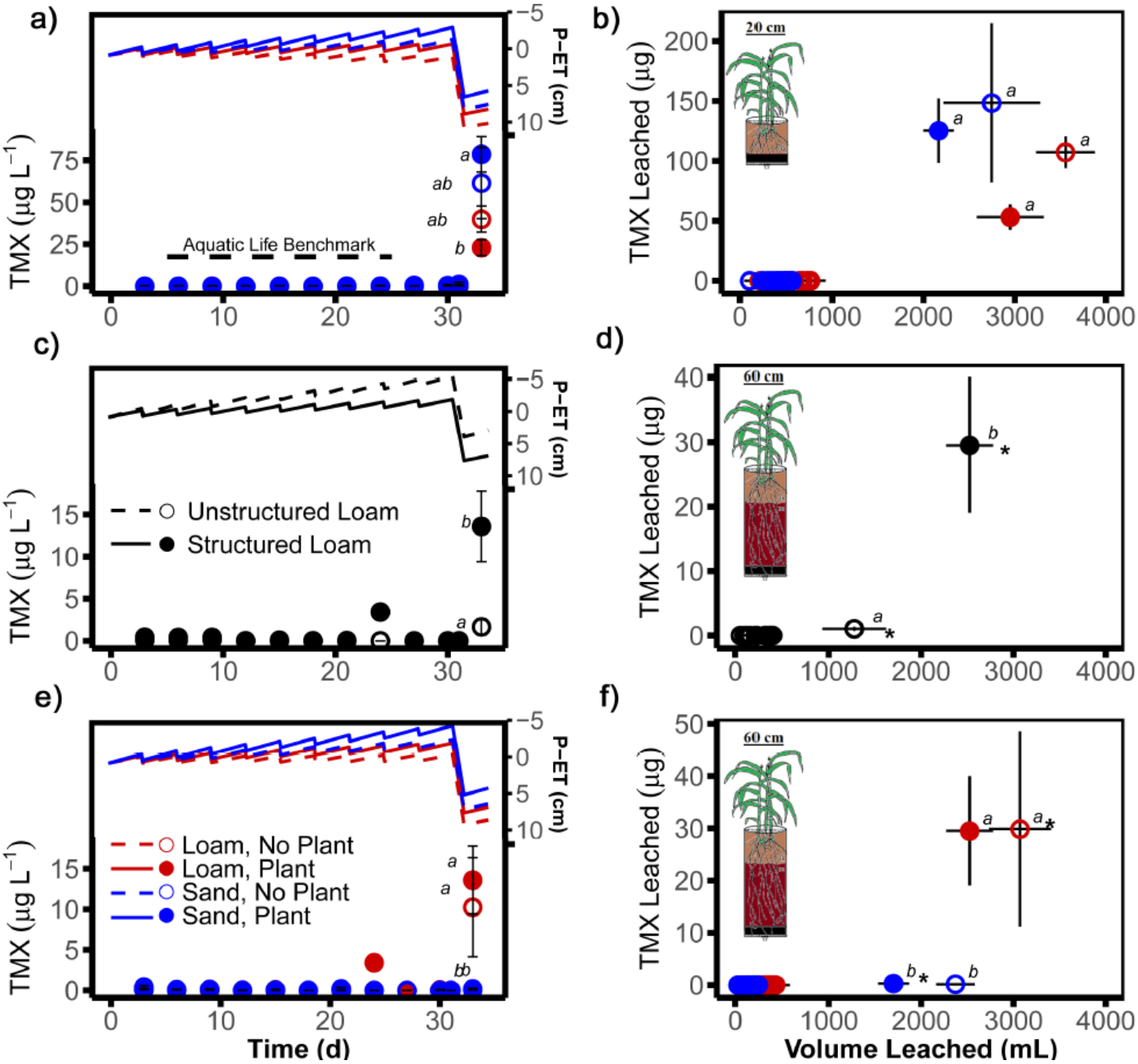


**Figure 2.2**: TMX concentration in leachate vs time with Cumulative Rainfall/Cumulative Evapotranspiration Deficit (P – ET) **(left),** and mass of TMX transported vs cumulative drainage (**right**). Column-plant graphics specify the column size for that row of panels (e.g. first row depicts 60 cm column results). *Different letters* denote significant differences for Y variable, while (∗) designates differences along the x axis ($p \leq 0.05$). Error bars represent standard error. Missing SEs indicate $n = 1$ column at time of measurement. The dashed black line in **a)** represents the Environmental Protection Agency benchmark for acute toxicity to aquatic invertebrates (17.5 µg L$^{-1}$) [*Anderson et al.*, 2013].

Corn stage showed a significant effect on TMX concentration and recovered mass for all depth intervals (two-way factorial ANOVA, $p < 0.001$). TMX concentrations in bulk soil were generally higher in the sand compared to the loam soil; however, texture only significantly affected TMX distribution in the 0-30 cm section at the V5 corn stage (two-way factorial ANOVA, $p < 0.001$; Tukey, $p < 0.001$; **Figure 2.3a**). Further, using the experimentally determined sorption coefficient from sand columns ($K_d$ = 0.5 L kg$^{-1}$), the liquid phase concentration could be as high 150 μg L$^{-1}$, which exceeds the EPA's aquatic life benchmark of 17.5 μg L$^{-1}$ by nearly an order of magnitude [*Anderson et al.*, 2013]. This predicted liquid phase concentration was within a factor of two of the concentration measured in the leachate from 20 cm tall sand columns (e.g. 75 μg L$^{-1}$), showing that the $K_d$ value determined in the laboratory from small-scale samples was applicable to the larger-scale columns.

Because sandy soils typically have larger, less reactive particles and higher hydraulic conductivity than finer-textured soils, it is often assumed that coarse-textured soils will transport more solutes (e.g. pesticides) than finer-textured particle soils [*Katagi*, 2013; *Mallants et al.*, 2011]. This assumption is supported by the measured soil physiochemical (compared with loam, sand had lower measured $K_d$ of 0.5 L kg$^{-1}$ and $K_{oc}$ of 57.9 L kg$^{-1}$; also lower measured CEC value of 1.8-3.5 cmol kg$^{-1}$) and hydraulic (e.g., the sand produced higher median $K_s$ values than the loam in the $B_t$ horizons; **Figure 2.2.1**) properties, as well as by the TMX mobilization observed in the 20 cm sand columns (**Figure 2.2a** and **Figure 2.2b)**. However, in the 60 cm columns the loam soil was associated with greater TMX transport (**Figure 2.2e** and **Figure 2.2f**) and less retention than the sand (**Figure 2.3**) despite its physiochemical properties appearing to favor more pesticide retention relative to the sand (compared with sand, higher measured $K_d$ of 0.8 L kg$^{-1}$ and $K_{oc}$ of 127 L kg$^{-1}$; also larger measured CEC value of 4.5-4.7 meg 100g$^{-1}$**)**. Higher levels

of the pesticide leaching from structured loam columns (compared to unstructured loam; **Figure 2.2c** and **Figure 2.2d**) and greater variation in measured $K_s$ in structured loam columns (**Figure 2.2.1**) suggest that pore heterogeneity and preferential flow [*Øygarden et al.*, 1997] may have driven TMX transport. For example, the cumulative mass of leached TMX was more than two orders of magnitude higher in the structured loam soils than the sand (e.g., 29.9 µg vs 0.17 µg for the no plant treatments; **Figure 2.2f**). This trend was apparent with and without the presence of viable plants, and suggests that structural flow pathways located in the intact loam $B_t$ horizon may have become activated during rain events. This process likely then, allowed for downward advection of TMX through the profile. In this experiment soil structure was thus seen to be a more important control on TMX transport than soil texture, which has several implications. For one, using repacked columns for transport studies may prove inadequate for representing well-structured soils, and such experimental setups may under-predict neonicotinoid movement. Also, the adoption of "soil health" building agricultural practices such as no tillage and cover crops, which provide greater soil macroporosity and preferential flow, may be unexpectedly increasing the likelihood of pesticide transport [*Alletto et al.*, 2010].

Further, the significantly higher evapotranspiration estimates shown in 60 cm sand columns (loam, with plant vs sand, with plant; **Table 2.2**), coupled with higher observed concentrations of TMX in the soil profile (sand vs loam; **Figure 2.3**), suggest that evapotranspiration may have concentrated much of the TMX at or near the soil surface, in a process referred to here as "evapo-concentration." The loam soils also likely experienced some evapo-concentration, though the effect was more muted in the structured loam columns (i.e., more total TMX leached by the end of the experiment even though total leachate amount only differed statistically between the structured loam with no plants and sand with plants; **Table 2.2**)

and was more pronounced in the unstructured 60 cm loam columns, which showed the greatest amount of evaporation (**Table 2.2**). By comparison these results suggest that macropore networks within structured soils may reduce evaporation of water and evapo-concentration of soluble pesticides like TMX. These reductions may result from a combination of two processes: 1) leaching via preferential flow can remove water and soluble compounds from the system altogether, and 2) macropores can limit the ability of water to move back up towards the drying front via capillary rise, due to the relatively low tensions of water held in those pores. Also, in nearly all cases the columns with viable plants yielded less drainage water (thus displaying higher estimated ET; **Figure 2.2** and **Table 2.2**) and transported less TMX mass (excluding 60 cm sand columns) than the equivalent "no plant" columns (**Figure 2.2**), though the differences were not significant. Still, these observations indicate that evapo-concentration (aided by viable plants) likely retarded any noticeable downward migration of TMX so long as cumulative ET exceeded cumulative precipitation, P (i.e., $P - ET < 0$).

Corn plants influenced the distribution of TMX in the 30-45 cm bulk soil section (two-way factorial ANOVA, $p < 0.05$; **Figure 2.3b**), which can be seen as higher concentrations detected in columns containing viable plants compared to those controlled for plant growth in the V5 corn stage (i.e., after 33 days of growth). Corn plants appear to have amplified the downward mobilization of TMX (**Figure 2.3**), which may be linked to a more massive and extensive root network (**Figure 2.5**) present in the V5 corn stage. Higher concentrations of TMX were detected in plant-associated soil for columns without viable corn plants at V5 (sand; Tukey, $p < 0.01$; **Figure 2.4**), which further illustrates the plant-assisted movement of this compound; however, this observation may be partially attributed to accelerated decomposition of TMX in the presence

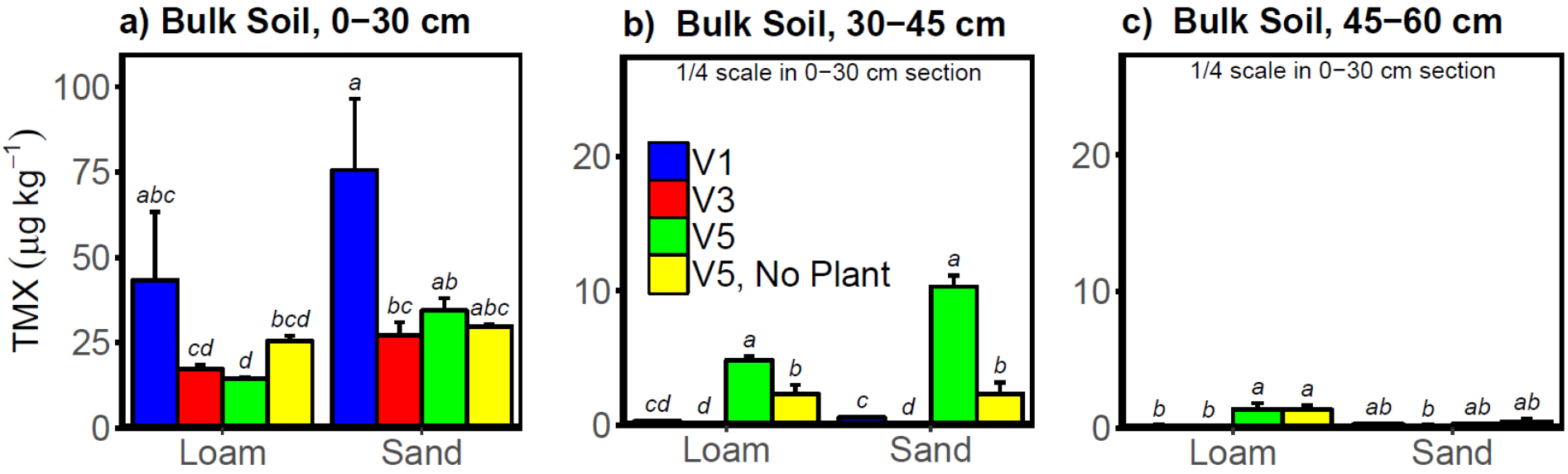


**Figure 2.3**: TMX concentration detected in bulk soil fractions 0-30 cm **a)**, 30-45 cm **b)**, and 45-60 cm **c)** over three corn stages (V1, V3, and V5). Error bars represent SE and *different letters* represent significant differences ($p \leq 0.05$). Y axes in 30-45 cm and 45-60 cm fractions are 25% that of the 0-30 cm section.

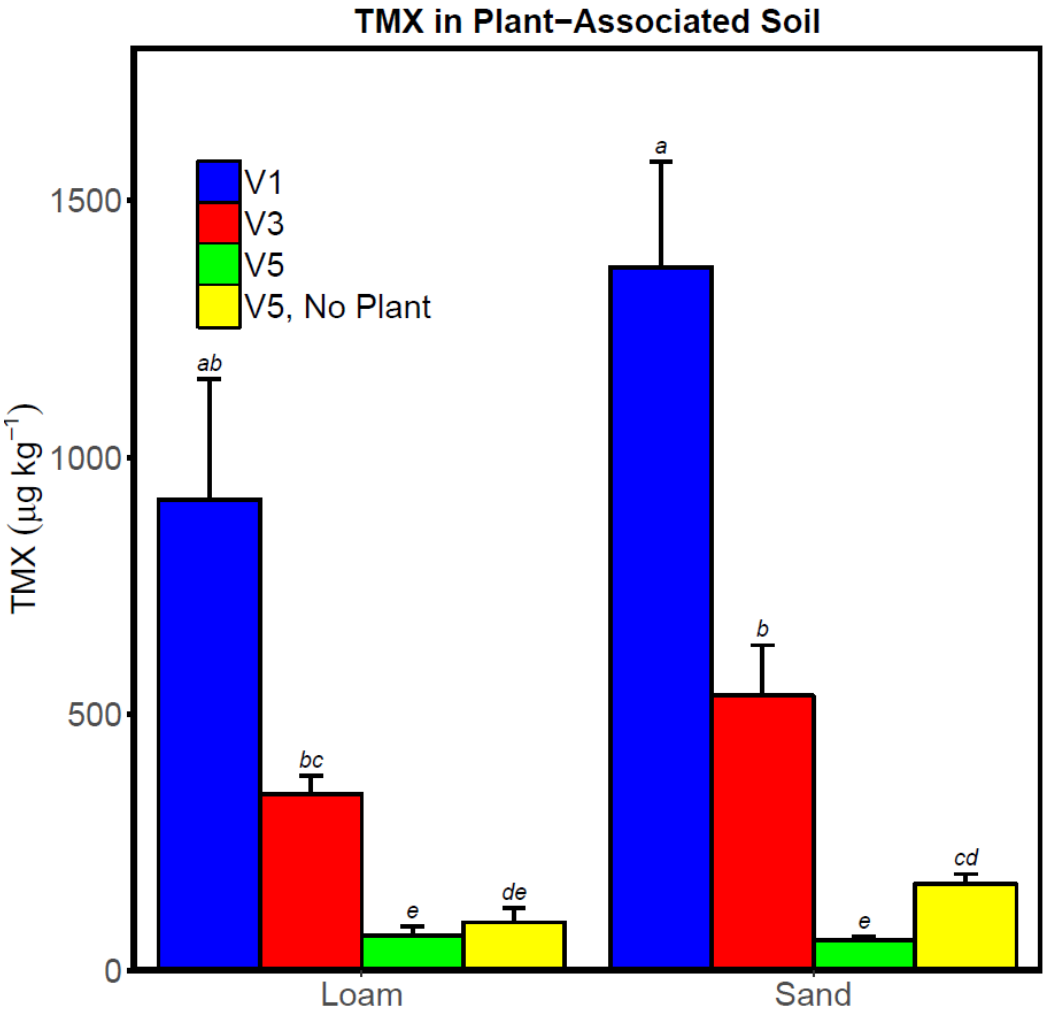


**Figure 2.4**: TMX concentration detected in plant-associated soil (lumped average between root and rhizosphere soil). V5 No Plant treatment represents seed soil (see description in Methods section). Error bars represent SE and *different letters* represent significant differences ($p \leq 0.05$)

of root exudates [*Akbar and Sultan*, 2016]. Altogether, root-facilitated preferential transport of TMX exceeded preferential retention of TMX via root water uptake or localized evapo-concentration. As such, living plant roots may provide a previously unrecognized conduit for pesticide leaching, though it is not yet known if this process is relevant in field settings.

**Table 2.2: Estimated Cumulative Evapotranspiration (ET) and Average Daily ET Rate in: a) Small (20 cm) Columns; b) Tall (60 cm) Columns from Soil Structure Study; and c) Tall (60 cm) Columns Without an Unstructured Loam Treatment**

| | Texture | Column Size (cm) | Plant Influence | Structure | Cumulative ET (cm) | ET Rate (cm $d^{-1}$) |
|---|---|---|---|---|---|---|
| **a)** | Loam | 20 | Plant | *NA* | 11 ± 2.3 ***a*** | 0.32 ± 0.035 |
| | Loam | 20 | No Plant | *NA* | 8.7 ± 2.6 ***a*** | 0.26 ± 0.069 |
| | Sand | 20 | Plant | *NA* | 13 ± 0.92 ***a*** | 0.40 ± 0.028 |
| | Sand | 20 | No Plant | *NA* | 11.3 ± 3.4 ***a*** | 0.34 ± 0.10 |
| **b)** | Loam | 60 | Plant | Structured | 12 ± 2.1 ***b*** | 0.36 ± 0.024 |
| | Loam | 60 | Plant | Unstructured | 16 ± 1.4 ***a*** | 0.48 ± 0.067 |
| **c)** | Loam | 60 | Plant | *NA* | 12 ± 2.1 ***b*** | 0.36 ± 0.024 |
| | Loam | 60 | No Plant | *NA* | 10 ± 2.1 ***ab*** | 0.31 ± 0.064 |
| | Sand | 60 | Plant | *NA* | 14.6 ± 1.07 ***a*** | 0.44 ± 0.032 |
| | Sand | 60 | No Plant | *NA* | 12 ± 1.3 ***ab*** | 0.37 ± 0.040 |

Values are expressed as mean ± standard deviation and *different letters* denote significant differences ($p \leq 0.05$). *NA* is used to distinguish the Soil Structure Study from other soil columns. Section **a),** row 1 and **b),** row 1 are equivalent, as they depict the same soil column

TMX concentrations found in the near-surface bulk soil were sufficiently high to pose environmental threats. For example, given the 75 μg $kg^{-1}$ concentration measured in the sand columns at the V1 growth stage, only 0.5 g of that soil would contain enough pesticide to kill 50% of any given honeybee population [*Anderson et al.*, 2013; *Sanchez-Bayo and Goka*, 2014]. Likewise, the leachate from the 20 cm tall columns (which represents the mobile compounds in the near-surface soil) had measured concentrations as high 75 μg $L^{-1}$, which exceeds the EPA's aquatic life benchmark of 17.5 μg $L^{-1}$ by nearly a factor of five [*Anderson et al.*, 2013]. TMX concentrations at depths below 30 cm may also be of concern. For instance, the 30-45 cm bulk soil in the sand columns with viable plants showed TMX concentrations as high as 10 μg $kg^{-1}$ TMX at corn stage V5, which translates to 20 μg $L^{-1}$ (using the experimentally-determined sorption coefficient of $K_d$ = 0.5 L $kg^{-1}$). This value again exceeds the EPA benchmark and is sufficiently elevated to induce tissue necrosis to some aquatic invertebrates [*Uğurlu et al.*, 2015]. The maximum concentration in the 30-45 cm bulk soil occurred nearly 20 days after the maximum concentration was detected in the 0-30 cm section, indicating that TMX mass was migrating downward in response to percolating water. Thus, while the leachate from the 60 cm sand columns had only trace amounts of TMX by the end of the experiment (**Figure 2.1e and f**), continued rainfall (or lower ET) would have likely led to deeper migration and eventual leaching of the pesticide.

This experiment provided a conservative simulation of TMX mobilization in soils (e.g. low rainfall, repacked Ap and some Bt horizons), whereas field conditions could potentially favor even greater mobilization and transport of this compound.

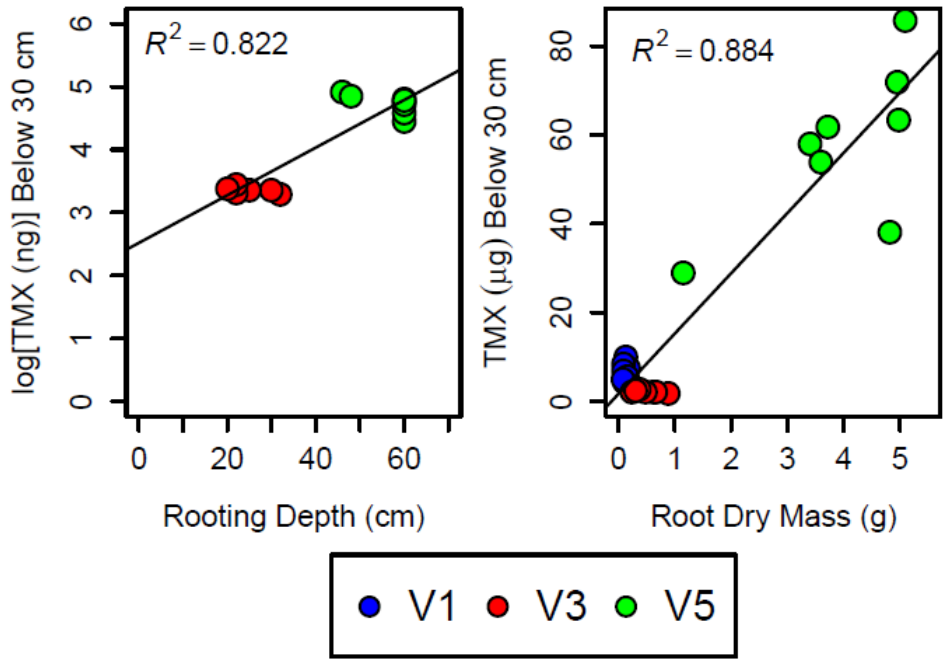


**Figure 2.5**: Linear relationship between: the mass recovered below the 0-30 cm bulk soil section, rooting depth (**left;** log transformed), and root dry mass (**right**). Root length was not recorded for V1 columns.

For example, greenhouse conditions (e.g., constant air circulation and the use of growth lights) likely enhanced evapotranspiration rates compared to field settings, resulting in greater evapo-concentration (as seen in **Table 2.2** and in the P – ET estimates shown in **Figure 2.2**). In addition, agricultural systems often are subjected to one or more large-scale rainfall events throughout the growing season, [*Kunkel et al.*, 2013] rather than a consistent regiment of small-scale events (e.g., the 0.9 cm of rainfall applied every three days) that was applied in this study.

## 2.6 Implications and Conclusions

Seed coatings account for ~60% of the global product use [*Goulson and Kleijn*, 2013]. However, no previous study has definitively proven that neonicotinoids, once planted, can become transported from crop seed coatings. This study establishes that neonicotinoid can be

transported in concentrations considered acutely toxic to aquatic life. If similar conditions exist in field soils that have well-connected macropore (e.g. the structured loam in this study) and/or tile-drain networks, then TMX could reach ground water and surface water systems at potentially harmful concentrations. These results also imply that plant growth and development may enhance neonicotinoid leaching, as the preferential transport along roots and root channels appear to have exceeded the ability of the plants to systematically uptake and retain TMX. This effect may become even more pronounced during short, high-intensity rainfall events, during which time neonicotinoid compounds can become mobilized via rapid preferential flow.

Even in the absence of preferential flow, TMX may become leached from soils over time. Given that the half-life of TMX can exceed 350 days, [*Goulson and Kleijn*, 2013], the compound could persist in fields during the growing season (i.e., when evapo-concentration would be greatest) and then become leached during the non-growing season (i.e., when evapo-concentration conditions would diminish). Future neonicotinoid application rates may also increase in response to greater pest pressures (for example driven by changes in climate conditions and weather variability; *Koleva and Schneider* [2010]), which could further increase concentrations and mobility of these compounds in the environment. Based on these findings, we expect that this study will serve as a reference for environmental risk assessment of neonicotinoids and a serve as material for pesticide transport modeling.

# Chapter 3. Plants mediate precipitation-driven transport of a neonicotinoid pesticide

Jesse Radolinski, Junxue Wu, Kang Xia, W. Cully Hession, and Ryan D. Stewart

Published in *Chemosphere:*

Radolinski, J., J. Wu, K. Xia, W. C. Hession, and R. D. Stewart (2019), Plants mediate precipitation-driven transport of a neonicotinoid pesticide, *Chemosphere*, *222*, 445-45. https://doi.org/10.1016/j.chemosphere.2019.01.150

## 3.1 Abstract

Neonicotinoid insecticides provide crop protection via water solubility and systemicity, yet these chemical characteristics, combined with high toxicity to non-target invertebrates (e.g., honeybees), elicit concern of environmental transport. Neonicotinoids have been detected in soil and surface water throughout North America; however, no investigation has defined a direct connection to planted seed dressings. We quantified the physical transport of thiamethoxam (TMX), a neonicotinoid, under field conditions. We planted TMX-coated corn seeds and maintained plots with and without viable crops ($n$ = 3 plots per treatment) to determine plant influence on pesticide transport. TMX concentrations were measured in soil and drainage throughout the growing season. Storm-generated runoff was the dominant transport mechanism (maximum TMX concentration 1.72 ± 0.605 μg $L^{-1}$; no viable plants), followed by shallow (<72 cm) lateral drainage (0.570 ± 0.170 μg $L^{-1}$; no viable plants), and deep (110 cm) drainage (0.170 ± 0.265 μg $L^{-1}$; viable plants). Soil samples confirmed vertical and lateral movement within 23 and 36 days of planting, respectively. Plants facilitated downward migration of TMX in soil but restricted TMX drainage. Altogether, these study results revealed that neonicotinoids can be transported from seed coatings both above and through the soil profile, which may enable migration into surrounding ecosystems. [*Radolinski et al.*, 2019]

## 3.2 Graphical Abstract

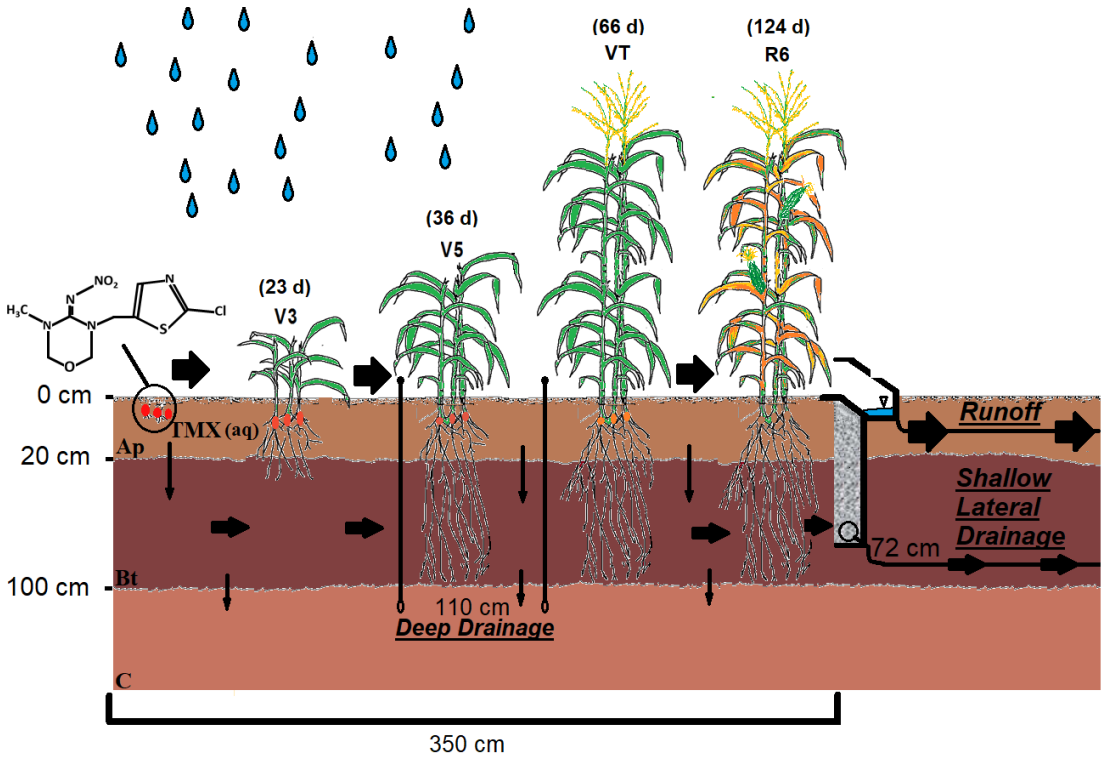


**Note:** The sizes of flux arrows reflect relative differences in drainage losses of TMX as detailed in the manuscript.

## 3.3 Introduction

Neonicotinoids have become the most extensively used class of insecticide worldwide as a result of a few novel chemical characteristics. These compounds exhibit low toxicity to mammals[*Miranda et al.*, 2011], have a high selectivity for the invertebrate nicotinic acetylcholine receptor (*n*AChR)[*Jeschke et al.*, 2011], and are water soluble (0.19-840 g $L^{-1}$)[*Jeschke et al.*, 2011; *Kurwadkar et al.*, 2014b], making them a top choice for systemic crop protection. Seed companies have resorted to coating the seeds of 140+ crops worldwide under the assumption that these compounds will be mostly taken up into the plant tissue and arm the crop throughout the growing season [*Anderson et al.*, 2015], as opposed to conventional broadcast or foliar applications that present a higher risk of direct environmental exposure

[*Limay-Rios et al.*, 2016]. Nevertheless, high *n*AChR selectivity makes neonicotinoids lethal in sub-ppm levels to non-target organisms such as honeybees[*Sanchez-Bayo and Goka*, 2014; *Tosi et al.*, 2017; *Whitehorn et al.*, 2012] and aquatic invertebrates[*Anderson et al.*, 2013]. Neonicotinoids have also been linked to increased mortality of insectivorous birds [*Hallmann et al.*, 2014]. Additionally, their water solubility and low affinity for the soil matrix [*Kurwadkar et al.*, 2014b; *Zhang et al.*, 2018a] elicit concern of transport to aquatic environments. Seed coatings now account for more than 60% of global neonicotinoid application[*Goulson and Kleijn*, 2013]; however, research has shown that a maximum of 20% of the applied dose is recovered in plant tissue[*Sanchez-Bayo*, 2014a] with the remainder left in the soil environment.

Previous laboratory and greenhouse studies have suggested that plant growth and development may influence neonicotinoid mobility in the soil. For example, as soil water content decreases during the growing season, corn (*Zea mays* L.) can apply suction forces of over 9.5 bars[*Ionescu*, 1969], which may limit solute mobilization. Thus, plant-mediated evapotranspiration may retard downward migration of neonicotinoids, resulting in more evapo-concentration of the compounds near the root zone [*Radolinski et al.*, 2018a]. Researchers have also noted that neonicotinoids and other highly soluble pesticides develop a stronger affinity for the soil matrix with time, such that the sorption coefficient $K_d$ increases. This process may reflect rate-limited migration into more protected sorption sites such as intra-aggregate micropores, thereby limiting transport and increasing retention time [*Katagi*, 2013; *Larsson and Jarvis*, 1999; *O'Dell et al.*, 1992; *Oi*, 1999]. Still, non-equilibrium flow conditions resulting from high rainfall events may also drive downward advection or bulk flow of neonicotinoids and other solutes through newly formed root channels [*Bundt et al.*, 2000; *Radolinski et al.*, 2018a].

As a possible result of these advective pathways, the three most abundant neonicotinoids, imidicloprid (IMD), thiamethoxam (TMX), and clothianidin (CLO), are now detected in soil,[*Jones et al.*, 2014] surface water bodies [*Main et al.*, 2016; *Starner and Goh*, 2012a; *Stone et al.*, 2014], groundwater [*Lamers et al.*, 2011], and drinking water[*Klarich et al.*, 2017]. *Starner and Goh* [2012b] detected IMD in 67 of 75 (89%) surface water samples collected in southern California, 14 of which exceeded the US Environmental Protection Agency's (EPA) chronic invertebrate aquatic life benchmark of 1.05 μg $L^{-1}$. Other studies in Ontario, Canada [*Schaafsma et al.*, 2015] and Iowa, USA [*Hladik et al.*, 2014b], detected neonicotinoid contamination in 100% of surface water bodies, likely related to the soybean and corn production of those regions. Both analyses showed that spring snowmelt [*Schaafsma et al.*, 2015] and large rainfall events [*Hladik et al.*, 2014b] early in the growing season increased pesticide concentration in surface waters, with neonicotinoid-treated seeds identified as the most likely source. Neonicotinoid transport has been proven via dust drift associated with seed coatings and planting equipment[*Girolami et al.*, 2013; *Greatti et al.*, 2006; *Tapparo et al.*, 2012], although this contamination was exclusive to the time of planting [*Nuyttens et al.*, 2013] and did not account for the majority of pesticide introduced into soil with planted seeds.

Laboratory and greenhouse studies have identified subsurface leaching as a potential mechanism for neonicotinoid movement from seed coatings. For instance, a recent laboratory experiment concluded that 24 h of inundation may drive up to 95% of seed-applied neonicotinoid mass into solution [*Smalling et al.*, 2018], while a different greenhouse study determined that seed-coated neonicotinoids could mobilize in soil under environmentally relevant conditions [*Radolinski et al.*, 2018a]. Still, transport in the field remains less certain. Three recently published field-scale experiments examined neonicotinoid transport from seed coats [*de Perre et*

*al.*, 2015; *Hartz et al.*, 2017; *Wettstein et al.*, 2016] yet those studies did not quantify pesticide concentrations relative to background residues in soil, thus failing to isolate any direct effects from seed coatings. The studies also lacked sufficient hydrological data to identify and model soil and environmental controls on neonicotinoid transport. Thus, there exists a critical need to identify the mechanisms by which seed-coating pesticides mobilize through agricultural fields.

The purpose of this study was to quantify the transport of the common neonicotinoid thiamethoxam from commercially available TMX-coated corn seeds in a field setting and to identify the influence of viable plants throughout the growing season. We hypothesized that: i) TMX would become transported via multiple pathways, including surface runoff, shallow lateral drainage, and leaching below the corn root zone; ii) vertical and lateral transport of TMX would be detected in soil; and iii) higher concentrations of TMX would be detected in deep drainage for plots containing viable plants (compared to plots controlled for plant growth) due to preferential, vertical transport along newly formed root channels. By assessing neonicotinoid transport from planted seed coatings in the field, this study aims to provide the first direct connection between this widespread pesticide application method and potential environmental contamination.

## 3.4 Materials and Methods

### 3.4.1 Site Description and Soil Characterization

The field experiment was conducted at the Virginia Tech Urban Horticulture Center in Montgomery County, Virginia, on a 5% southeast facing slope. The soil was a Groseclose loam series (*Typic Hapludult*). The site had been in pasture for 10 years prior to the experiment, so the ground was tilled to a depth of 30 cm in spring and summer of 2015. The soil contained no background TMX, as determined using an LC-MS/MS analyzer (additional details on TMX analysis in soil, plant and water samples are presented in the Appendix B).

Intact cores (5 x 5 cm) were taken from three depths representing distinct soil horizons: Ap (0-5 cm), Bt (25-30 cm), and C (105-110 cm). Cores were used to determine soil bulk density [$M\ L^{-3}$], porosity [$L^3\ L^{-3}$], saturated hydraulic conductivity ($K_s$) [$L\ T^{-1}$], and water retention ($n$ = 6 cores per horizon). $K_s$ was measured using the falling head method with a UMS KSAT Benchtop Saturated Hydraulic Conductivity Instrument (UMS Inc., Munich, Germany). Unconsolidated soil samples were collected ($n$ = 6 per horizon), air dried, sieved to 2 mm, and analyzed for cation exchange capacity (CEC), pH, total organic carbon (TOC), and texture. CEC was measured colorimetrically via ammonium acetate at pH 7 using a Lachat Quickchem 8500 autoanalyzer (Lachat, Loveland, USA), soil pH was measured in a 1:1 slurry (soil: $CaCl_2$), TOC was quantified by dry combustion using a Vario MAX CNS macro elemental analyzer (Elementar, Hanau, Germany), and textural analysis was conducted via the pipet method.[*Day*, 1965] Soil physiochemical and hydraulic properties are shown in **Table 3.1**.

### 3.4.2 Field Plot preparation and experimental design

Six runoff plots (300 cm x 350 cm) were constructed using sheet metal (30 cm tall, installed to approximately 15 cm depth) as borders to contain overland flow (see **Figure B1**). On the downslope side of each plot, a trench was excavated (10 cm wide x 300 cm long x 72 cm deep), lined with 10 cm ID perforated PVC pipe, and filled with coarse gravel to collect shallow lateral flow. A second PVC trough (13 cm wide x 300 cm long x 10 cm deep) was installed on the surface to collect surface runoff. Runoff and shallow lateral flow drainage were piped to separate, unlined 200 L steel barrels that were fitted with pressure transducers (HOBO U-20 L level logger; Onset, Bourne, USA) to determine drainage volume. Two suction lysimeters (1 bar, ceramic cups) were installed at random locations within each plot to a depth of 110 cm to collect TMX in gravity-driven deep drainage below the root zone. Tensiometers (Spectrum

Technologies, Aurora, USA) and soil water content probes (Decagon Devices 5TM, Pullman, WA) were installed at random locations within each plot (30 cm and 110 cm depths; 1 of each probe per depth per plot) to measure soil matric potential [$M\ L^{-1}\ T^{-2}$] and soil water content [$L^3\ L^{-3}$]. A flow-through rain gauge (Spectrum Technologies, Aurora, USA) was used to record rainfall [L]. All loggers recorded at 15 min intervals. Daily potential evapotranspiration ($ET_o$; [L]) was determined using the FAO $ET_o$ calculator.[*Raes and Munoz*, 2009]

Prior to planting, agronomic rates of lime and fertilizer were applied. Cruiser Extreme® 1250 corn seeds (Syngenta; Greensboro, USA) were sowed to a depth of 4 cm within each plot as six 50 cm wide rows at a spacing of 33 cm, approximating a planting rate of 59,000 plants $ha^{-1}$, as recommended for the state of Virginia [*Brann et al.*, 2009; *DCR*, 2015]. Though 80 cm row spacing is sometimes recommended for increased corn yield, the 50 cm width chosen in this study has been shown to reduce yield by as little as 3% [*Brann*, 1998], while better accommodating our 300 x 350 cm plots. Each seed carried 1.21 ± 0.04 mg of TMX in its seed coating (from $n = 4$ tested seeds) based on LC-MS/MS analysis. To understand the role of viable plants on the transport process, half of the plots were controlled for growth by snipping the plant upon emergence ("no viable plant" treatment; $n = 3$), while the remaining plots sustained viable corn plants ("viable plant" treatment; $n = 3$) throughout the 124-day growing season (June 6$^{th}$ – October 4$^{th}$, 2016). The experiment followed a complete randomized design with one factor (plant presence) and two treatment levels (viable and no viable plants), whereby treatments were assigned randomly to each of the 6 plots.

**Table 3.1.**

Soil physiochemical properties. CEC = Cation Exchange Capacity; $\rho_b$ = Bulk Density; $K_s$ = Saturated Hydraulic Conductivity; TOC = Total Organic Carbon.

| Horizon | Depth (cm) | Texture | Sand (%) | Silt (%) | Clay (%) | CEC (cmol $kg^{-1}$) | Porosity (%) | $\rho_b$ (g $cm^{-3}$) | $K_s$ (cm $d^{-1}$) | pH (-) | TOC (%) |
|---|---|---|---|---|---|---|---|---|---|---|---|
| **Ap** | 0-20 | silt loam | 24.0 | 62 | 13.9 | 8.5 ± 0.9 | 58 ± 0.03 | 1.26 ±0.09 | 4460 ± 1670 | 5.7 ± 0.3 | 2.00 ± 0.45 |
| **Bt** | 20-100 | silty clay loam | 14.7 | 46.4 | 38.9 | 8.4 ± 2.6 | 53 ± 0.04 | 1.49 ±0.12 | 50.4 ± 99.3 | 4.4 ± 0.2 | 0.25 ± 0.06 |
| **C** | 100+ | clay | 4.1 | 20.9 | 75.0 | 12 ± 2.7 | 60 ± 0.03 | 1.34 ±0.05 | 81.2 ± 81.4 | 6.4 ± 0.1 | 0.40 ± 0.03 |

CEC, porosity, bulk density, $K_s$, pH and TOC are expressed as mean ± standard deviation.

3.4.3. Water Sampling

Drainage water samples from the three measured hydrologic compartments (runoff, shallow lateral flow, and deep drainage) were collected following nine rain events throughout the growing season (see **Table B1**). Runoff and shallow lateral drainage samples were retrieved from storage barrels and deep drainage was extracted from lysimeters by applying 60 kPa of suction for 10 minutes. It should be noted that the final rainfall event produced drainage volumes that exceeded the capacity of our storage barrels (>117 L); therefore, the final drainage volumes were estimated as the steady state water level at the time of sampling. Following retrieval from the field, all drainage samples were analyzed for TMX using method described in Appendix B with limit of quantitation (*LOQ*), limit of detection (*LOD*), and recoveries of 0.01 µg $kg^{-1}$, 0.005 µg $kg^{-1}$, and 104.2 ± 5.3%, respectively. Additionally, as a simple means of representing the effect of viable plants on TMX transport via drainage, we calculated a simple response ratio ($R_r$) as:

$$R_r = \frac{[TMX_{plant}]}{[TMX_{no\ plant}]} \quad (1)$$

where $TMX_{plant}$ and $TMX_{no\ plant}$ represent concentrations of TMX in shallow lateral drainage for plots containing viable and no viable plants, respectively. We present these data as the natural logarithm of $R_r$ ($\ln R_r$) such that more negative values of $\ln R_r$ correspond to more plant restriction of TMX transport.

3.4.4. Soil and Plant Sampling

TMX distribution in soil was measured at four corn growth stages (V3, V5, VT, and R6, corresponding to 23, 36, 66, and 124 days, respectively). Soil sampling periods were

chosen to assess subsurface mobility of TMX during early (V3), middle (V5), and peak (VT) vegetative growth stages and one final point for physiological maturity (i.e., R6, which represents the end of the corn growing season) [*McWilliams et al.*, 2010]. At each of these four times, replicated 2 cm diameter by 5 cm tall soil samples were collected from the Ap (0-5 cm) and Bt (25-30 cm) horizons, with samples collected within the corn seed planting row (± 2 cm from row center) and in between corn rows (25 cm from planting rows; see **Figure B2** for a spatial description of soil sampling). Three samples were composited together into 1 sample per location (in-row versus between row) within each plot, which was then analyzed for TMX using the method described in Appendix B with *LOQ, LOD,* and recoveries of 0.01 µg $kg^{-1}$, 0.005 µg $kg^{-1}$, and 98.6 ± 13.3%, respectively.

3.4.5. Statistical Analysis

One-way ANOVAs were used to compare per-event TMX concentrations [M $L^{-3}$] and final cumulative TMX mass [M], and drainage volumes [$L^3$] between "with viable plants" vs "no viable plants" treatments for each hydrologic compartment (surface runoff, , shallow lateral drainage ≤ 72 cm, deep drainage at 110 cm). For soil concentrations [M $M^{-1}$], data were subjected to two-way ANOVAs per combination of location (next to plant vs between rows) and horizon ($A_{p,}$, 0-5 cm vs $B_t$, 25-30 cm) using plant influence and corn stage (V3, V5, VT and R6) as factors. All data were rank transformed and analyzed for normality and homogeneity of variances using Fligner's test. Factorial ANOVA results were subjected to multiple comparisons via Tukey HSD. R version 3.2.2 was used to conduct all statistical analyses with $\alpha = 0.05$.

## 3.5 Results and Discussion

Because our previous greenhouse investigations [*Cushman*, 2017; *Radolinski et al.*, 2018a] and the current study have shown that TMX uptake into corn plants represented a minor fraction of

the applied seed dose (< 0.1%), the distribution of TMX in the drainage and soil is the focus of the current report. Thiamethoxam was detected in all three drainage compartments (surface runoff, shallow lateral drainage ≤ 72 cm, and deep drainage at 110 cm) as early as 10 days after planting and throughout the corn growing season (**Figure 3.1**). Though concentrations of TMX detected in drainage generally reflected each compartment's proximity to the seed source (runoff > shallow lateral drainage > deep drainage; **Figure 3.2**), TMX was transported in similar concentrations via shallow lateral drainage (no viable plants, 0.020 ± 0.0264 μg $L^{-1}$; **Figure 3.1b**) and deep drainage (no viable plants, 0.022 ± 0.017 μg $L^{-1}$; **Figure 3.1c**) following the first rain event. The total percent of seed-coated TMX quantified in drainage for viable plants (0.27 ± 0.02 %; **Table B1**) are comparable to estimates of total neonicotinoid losses to tile drains in sugar beet fields (same order of magnitude as IMD) [*Wettstein et al.*, 2016]. TMX concentrations in surface runoff and shallow lateral drainage from viable plant plots reached seasonal peaks by the V5 corn stage (~4 weeks), whereas plots with no viable plants showed more delayed and higher peak concentrations. Plants also affected late-summer concentrations in deep drainage, when TMX was only detected in the no-viable plant plots.

The cumulative mass transported via runoff and shallow lateral flow generally increased in response to storm-generated drainage (**Figure 3.2**), though drainage losses were more reduced following peak concentrations and less apparent for plots containing viable plants. Altogether, early detection of TMX in runoff, shallow lateral drainage, and analogous vertical migration to a depth of 110 cm indicate that the compound has a high potential for advective transport. Further, TMX detection through 113 days of plant growth suggest that transport is possible throughout the growing season, even as the mass of TMX available for transport decreases.

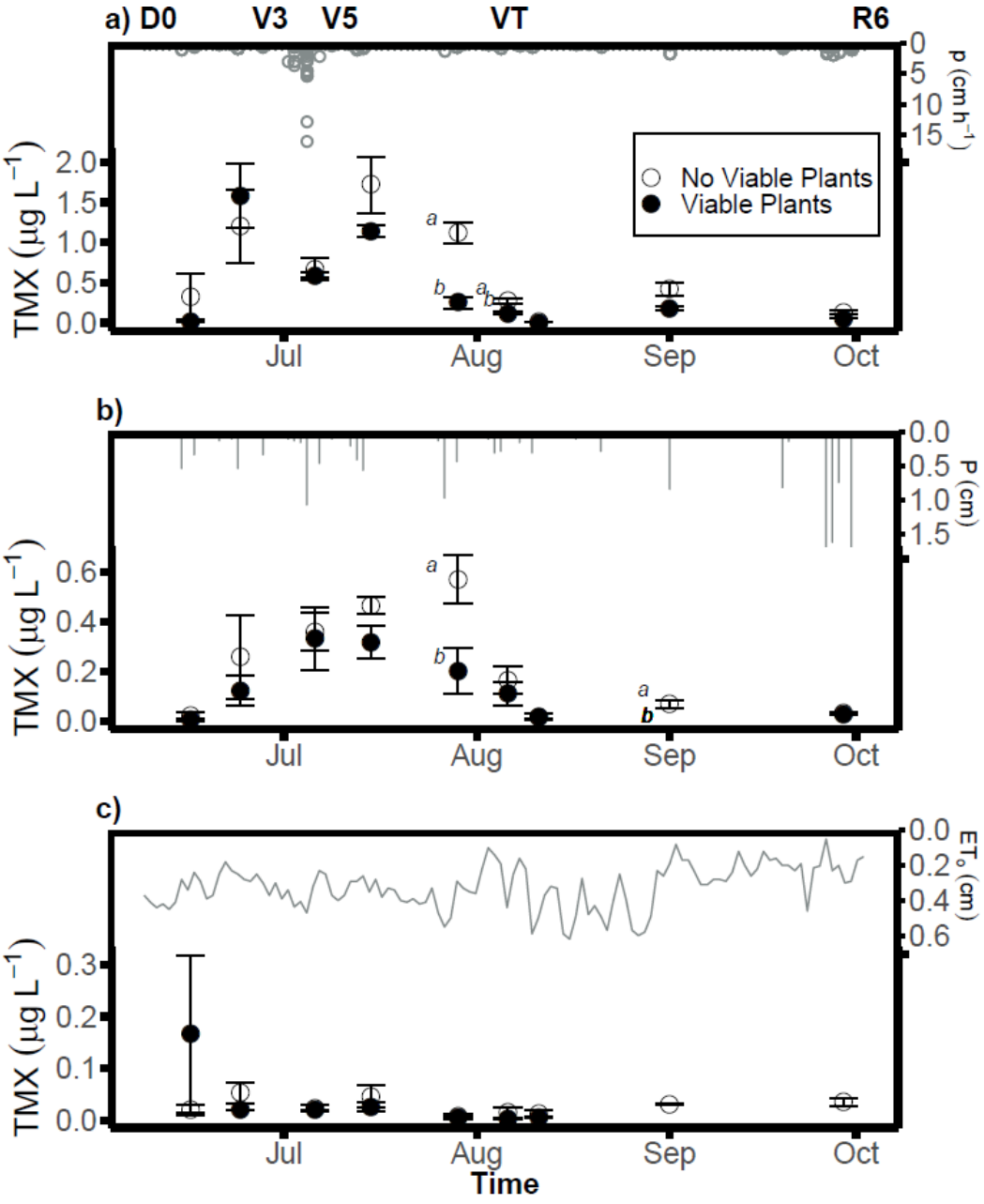


**Figure 3.1.** TMX concentrations detected throughout the 2016 corn growing season in **a)** surface runoff, **b**) shallow lateral drainage at 72 cm in the $B_t$ horizon, and **c)** deep drainage collected via suction lysimeters at 110 cm in C horizon. The rainfall intensity (p), rainfall accumulation (P) and daily potential evapotranspiration ($ET_o$) are plotted in the top panel of **a)**, **b)**, and **c)**, respectively. Time of planting (D0) and corn growth stages (V3, V5, VT, and R6) are shown above **a)** as a reference for time of soil sampling. Error bars represent standard error (SE; $n = 3$). *Different letters* denote significant differences between plant and no viable plants treatments at each sampling event ($p \leq 0.05$). The "**b**" for the 9/01/16 event in panel **b)** denotes differences in concentration between detectable (no viable plant) and non-detectable (viable plant) samples. Viable plant plots yielded no water for lysimeter sampling for the final 2 rain events in **c)**.

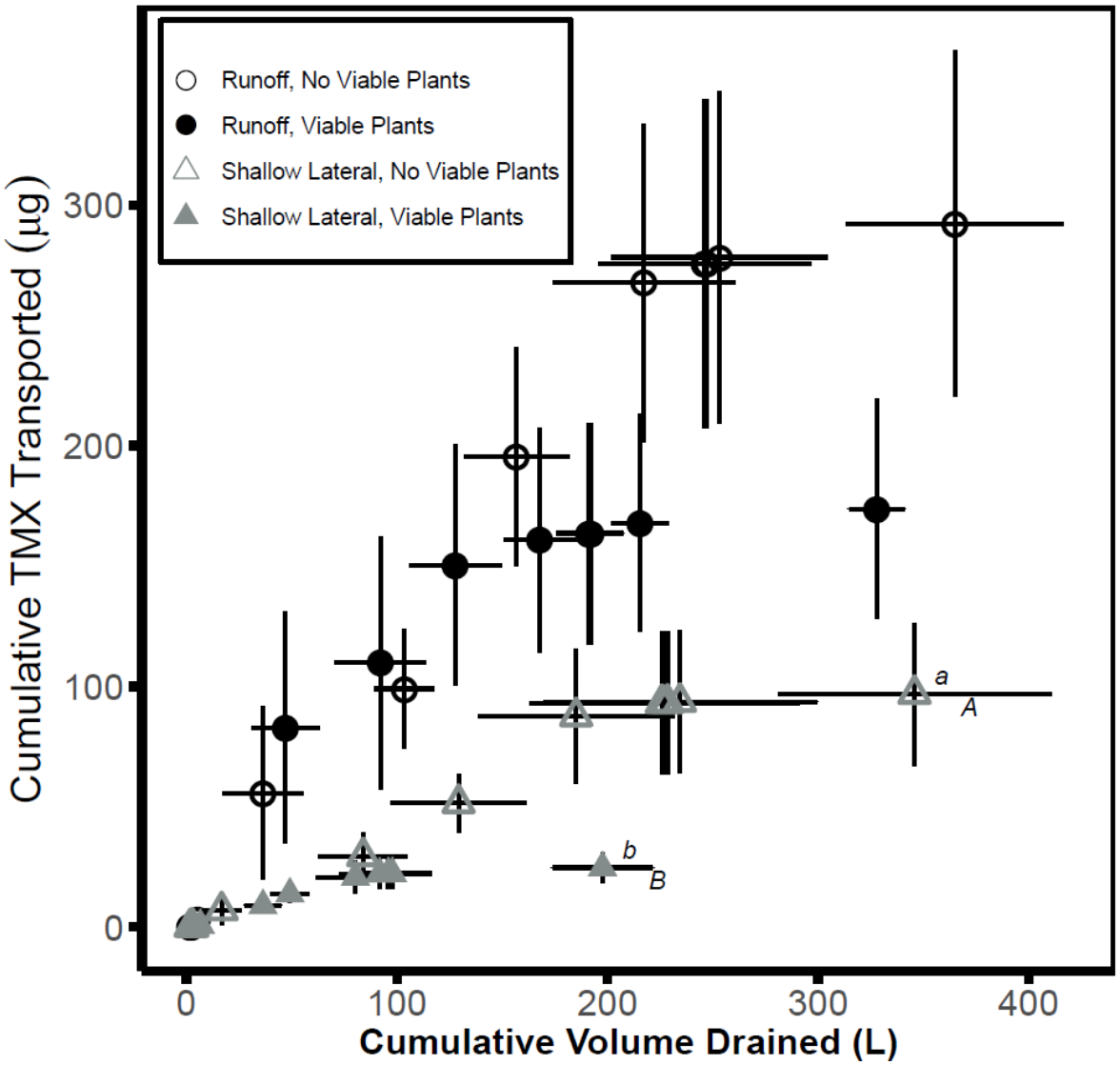


**Figure 3.2.** Cumulative mass of TMX transported in runoff and shallow lateral drainage vs cumulative volume drained. Note, deep drainage results are not considered here due to lack of flow records below the shallow lateral drainage outlet. *Lower case letters* denote significant differences between viable plant and no viable plant treatments in cumulative TMX while *capital letters* designate differences in cumulative drainage ( $p < 0.05$) and error bars represent SE (n = 3). All statistical tests compared the final cumulative observation points.

TMX mobility was also confirmed within the soil profile throughout the study period. For example, we detected vertical movement to the $B_t$ soil horizon by the V3 corn stage (i.e., Day 23; **Figures 3.3b** and **d**) and lateral migration between corn rows by the V5 stage (i.e., Day 36; **Figures 3.3c** and **d**). The presence of TMX in soil was therefore dependent on elapsed time

(two-way factorial ANOVA comparing concentrations at V3 and V5; $p < 0.05$), with a general trend of decreasing concentration through time for samples taken next to the plant (± 2 cm). In contrast, samples taken 25 cm from plants between rows showed TMX pulses at the V5 and VT corn stages.

The soil water content ($\theta$) and matric potential ($\Psi$) data revealed that living plant roots reduced soil water content via uptake (Figure S3), particularly at the 110 cm depth (**Figure 3.4b** and **c**). Here, the 110 cm water content sensors in the viable plant plots showed diurnal fluctuations (i.e. higher $\theta$ values at night; lower values during the day with peak $ET_o$) beginning at the end of July, an indication that plant roots at that depth were actively transpiring water during that period. Plant response ratios ($lnR_r$) in shallow lateral drainage were lowest during the same time period (**Figure 3.4a**) suggesting plant alteration of the flow field could have limited the dose of TMX leaving the plots.

TMX transport was dominated by surface and subsurface runoff processes throughout the growing season (**Figure 3.1** and **Figure 3.2; Table B1**), which likely resulted from rapid mixing of seed coatings via newly formed macropores (from root growth and corn emergence) and the erosion of TMX-bound colloids. Maximum TMX concentrations in surface runoff were detected early in the growing season when cumulative mass losses and $ET_o$ were low. The period of highest rainfall intensity (16 cm $h^{-1}$ in early July 2016; **Figure 3.1a** and **Table B2)** resulted in lower TMX concentrations in surface runoff compared to less intense rainfall events before and after (both with rainfall intensities $\leq$ 1 cm $h^{-1}$). Low rainfall intensity may have produced higher doses of TMX in surface runoff due to longer water residence time and greater mixing near the seed coating, whereas high intensity rain likely diluted the signal. Thus, we detected the highest

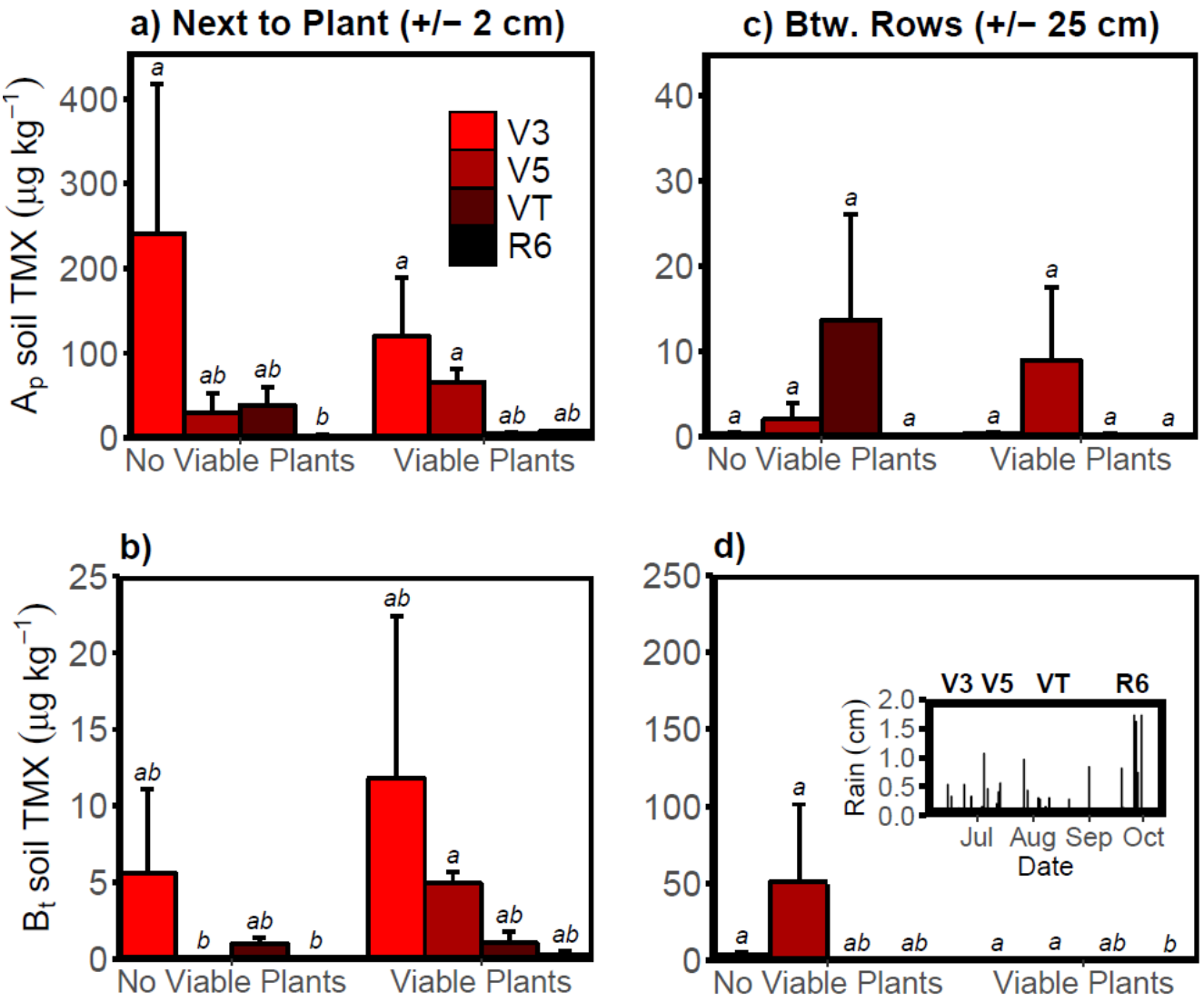


**Figure 3.3** TMX concentrations in soil collected at 0-5 cm (Ap soil horizon) and 25-30 cm (Bt soil horizon) at 2 cm (**a** and **b**) and 25 cm (between two rows) from corn plants or sown seeds (**c** and **d**). The inset of **d)** illustrates corn growth stage and rainfall during the growing season. *Different letters* denote significant differences between corn stage and with viable plant versus no viable plants treatments ($p < 0.05$) within each figure panel (i.e. sample location and depth) and errors bars represent SE ($n = 3$). **Note** that the scale in **c)** is 1/10 of that in **a)** and the scale in **d)** is 10 times that of **b)**.

concentrations of TMX in 0-5 cm soil (up to 241 µg kg$^{-1}$ at V3; **Figure 3.3a**) after low intensity rainfall preceding the V3 corn stage (**Figure 3.1a** and **b**). Similar early season losses to surface runoff may partially explain high concentrations of neonicotinoids detected in streams without comparable increases in discharge [*Hladik et al.*, 2014b; *Schnoebelen et al.*, 2003; *Thurman et al.*, 1992]. The potential risk to non-target organisms may be amplified under early season, low

intensity rainfall, as runoff samples contained enough TMX in 1 mL to physically impair honey bees (> 1.4 ng) [*Tosi et al.*, 2017] exposed to ponded water[*Samson-Robert et al.*, 2014]. Thus, fluxes into and out of this thin mixing layer [*McGrath et al.*, 2009; *Steenhuis et al.*, 1994] near the soil surface may have broad implications for rapid environmental contamination of neonicotinoids.

The low intensity rainfall preceding the V3 corn stage transported TMX through $B_t$ (**Figure 3.3b** and **3.1b)** soil into the deeper C horizon (**Figure 3.1c**), whereas larger, high intensity storms in early and late July 2016 produced lateral pulses of TMX throughout the profile (large spatial variation within **Figure 3.3c** and **d**). These latter data were characteristic of preferential flow events wherein high-intensity rainfall elevates pore water pressures and induces flow through larger macropores [*Jarvis*, 2007b]. This bypass flow process often results in higher concentrations being detected in soil and water than predicted by conventional transport equations (e.g., advection-dispersion) through a homogenous medium [*Allaire et al.*, 2009]. Non-equilibrium flow conditions may have accented the differing subsurface architecture of viable plant vs no viable plant plots. For example, high and often variable saturated hydraulic conductivity measurements (**Table 3.1**) depict a heterogeneous soil pore structure with the potential for rapid mobilization of the highly soluble neonicotinoids. Further, higher concentrations of TMX detected in Bt soil of viable plant treatments (vs no viable plant) at V5 (Tukey, $p = 0.02$; **Figure 3.3b**) suggest that corn plants facilitated vertical transport of the pesticide. High intensity rain events in early July 2016 could have caused preferential transport of TMX, as newly formed and existing root channels may have provided conduits for infiltrating water and greater connectivity to an existing macropore network [*Bundt et al.*, 2000; *Jørgensen et al.*, 2002]. This plant-mediated downward advection of neonicotinoids is consistent with

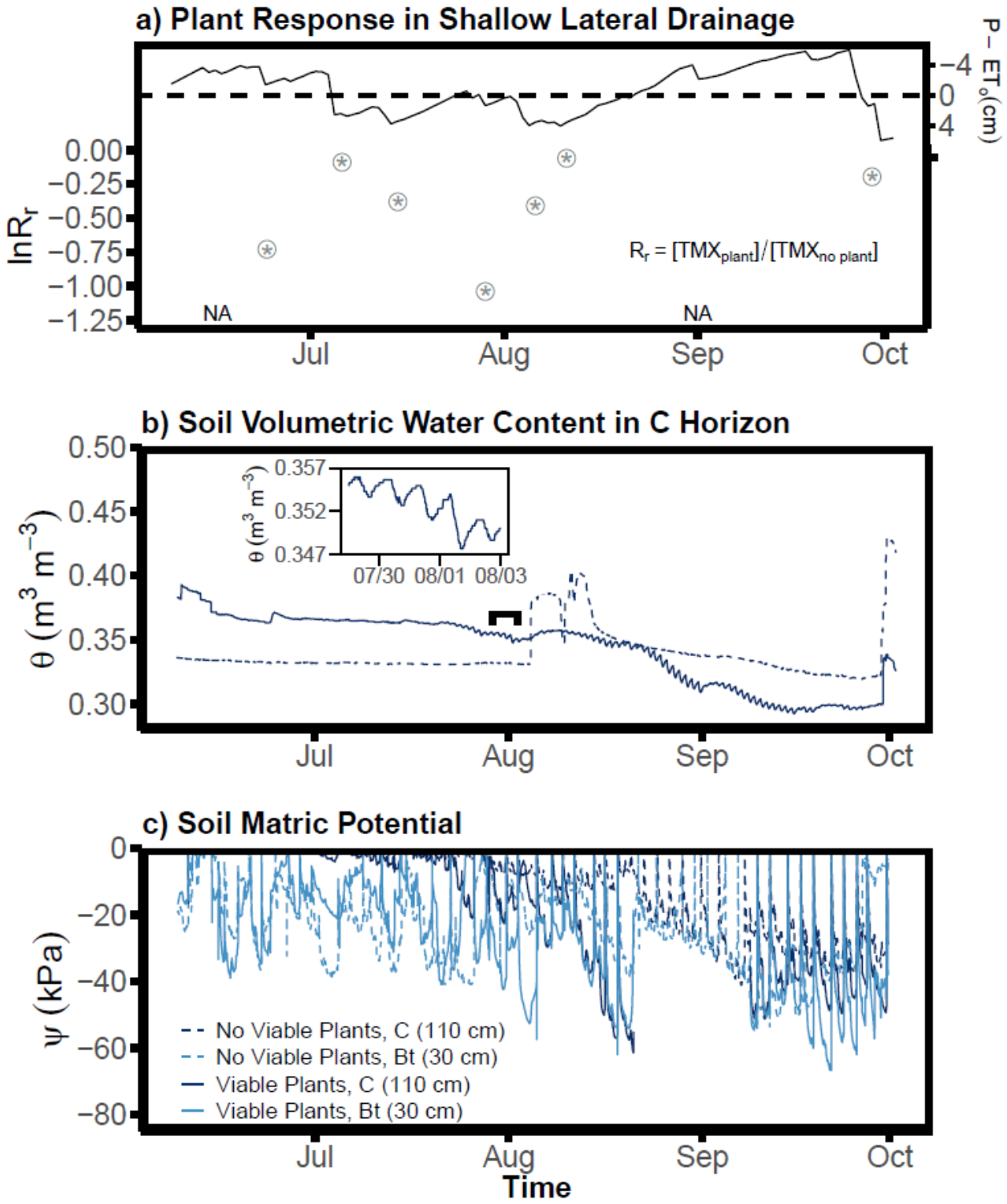


**Figure 3.4. a)** Temporal change of shallow $lnR_r$ and $P - ET_o$ (cumulative precipitation minus evapotranspiration). **b)** Volumetric soil water content ($\theta$; $n$ = 3 plots per treatment) and **c)** matric potential ($\Psi$; $n$ = 2 plots per treatment) in Bt and C horizon soil. The inset of **b**) Shows a 5-day period with plant-driven diurnal fluctuations in $\theta$. Sharp increases in $\Psi$ represent tensiometer refill events and missing time periods for plant treatments denote logger and probe

observations collected during a previous greenhouse study [*Radolinski et al.*, 2018a], which also detected maximum leachate concentrations and more vertical movement of TMX in soil containing viable plants around the V5 corn stage following heavy rainfall. However, after the V5 corn stage the subsurface network likely remained different between viable and no viable plant plots, yet we observed no significant differences between these treatments in soil TMX (**Figure 3.3**). Thus, drier soil conditions, less TMX mass available for transport (due to advective and degradation losses), and low intensity rainfall may have limited plant-driven mobility of the pesticide in the late growing season.

Though early July (V5 corn stage following intense rain) coincided with noticeable plant-mediated transport in the vertical soil profile (**Figure 3.3b**) and seasonal peak concentrations of TMX in shallow lateral flow (**Figure 3.1b**), this trend of higher plant-assisted pesticide mobility was not evident in drainage. Rather, plants appear to have restricted the mobility of TMX, seen as earlier peak concentrations for viable plant vs no viable plant plot drainage (**Figure 3.1b)** and significantly lower levels of the pesticide transported from plots containing viable corn plants in the late July event (one way ANOVA, $p < 0.05$; **Figure 3.1a** and **b**). As a result, the total mass of TMX in shallow lateral drainage became less sensitive to hydrological fluxes in plots containing viable plants, as indicated by asymptotic trend in **Figure 3.2**. The no-viable plant plots, in contrast, continued to leach TMX mass throughout the growing season. The cumulative mass of TMX transported from the shallow lateral compartment therefore differed by a factor of ~4 (no viable plants > with viable plants; one way ANOVA, $p < 0.05$; **Figure 3.2**), which may be partially attributed to reduced drainage volume in viable plant plots compared to those with no viable plants (one-way ANOVA, $p < 0.05$; **Figure 3.2**). Plants constrained the quantity of pesticide leaving the plots to a greater extent when cumulative $P - ET_o$ was at or below zero

(**Figure 3.4a**). Similarly, plants began to limit TMX loss through surface runoff (with viable plants vs no viable plants, one way ANOVA, $p < 0.05$; **Figure 3.1b**) as evaporative demands increased in late July and early August, 2016 (**Figure 3.1b, c** and **Figure 3.4a**).

The effect of growing plants on pesticide transport is further illustrated through the observed depletion of deeper water pools. For example, reduced shallow lateral transport in viable plant plots (**Figure 3.1b**; **Figure 3.2; Figure 3.4a**) corresponded to lower drainage volumes (**Figure 3.2**) and plant-mediated diurnal fluctuations in soil water content as deep as 110 cm (**Figure 3.4b**). These diurnal signals were also mirrored by a decrease in matric potential at depth, as plants exerted greater suction force on deeper water (110 cm soil, **Figure 3.4c**). Because the soil evaporation front in temperate North America rarely exceeds 30 cm in depth [*Sprenger et al.*, 2016], it can be deduced that diurnal signals in $\theta$ and steep decreases in $\Psi$ at the 110 cm depth are the result of plant-induced drying of the soil profile. While $\ln R_r$ values were lowest in late July, the lack of detectable TMX in subsurface lateral drainage for viable plant plots in early September (denoted as "NA" in **Figure 3.4a**) suggest that plants exerted the strongest influence on transport when diurnal $\theta$ signals were at their highest amplitude (**Figure 3.4a** and **b**). Similarly, the two events in early August produced higher $\ln R_r$ values as $P - ET_o$ became larger (**Figure 3.4a**), as low intensity rain contributed to recharge (**Figure 3.1a** and **Figure B4),** and as diurnal $\theta$ signals became more damped (**Figure 3.4b**). Plants prompted a physical equilibrium between $B_t$ and C horizons ($\Psi$ in Bt $\approx$ $\Psi$ in C; early-mid August, 2016; **Figure 3.4c**), while at the same time the matric potential decreased below -60 kPa, such that lysimeter water samples could no longer be obtained (**Figure 3.1c)**. Therefore, later in the growing season when evaporative demands were high, TMX likely diffused into the soil matrix (where pores held water at low $\Psi$). This process, which may have then physically isolated the

compound from rapid hydrological fluxes, appears to have been amplified by the presence of viable plants (e.g., slightly higher fraction of TMX in soil with viable plants at R6; **Table B1**).

Rate-limited diffusion into more "protected" soil pores has been proposed as a mechanism to explain apparent increases in solute-matrix affinity with time for neonicotinoids [*Oi*, 1999] and other highly soluble agrochemicals [*Jørgensen et al.*, 2002]. In an extreme example, incubating the herbicide imazethapyr in undisturbed soil for 16 days resulted in a tenfold increase in observed $K_d$ [*O'Dell et al.*, 1992]. Results of other sorption isotherms have also suggested that thiamethoxam displays a trend towards irreversible sorption in soil [*Li et al.*, 2018], The results shown here suggest that rain events in the late growing season will mobilize less TMX than similar storms in the early growing season, likely due to diminished TMX concentrations in the soil (**Figure 3.3**). For example, the high rainfall storms that occurred in late September (**Figure 3.1**) mobilized only trace amounts of TMX via surface runoff and shallow lateral drainage (**Figure 3.2**). Although irreversible sorption of TMX to soil is not excluded [*Li et al.*, 2018], degradation likely also played a role in the overall dissipation of TMX as this fertile soil (e.g. sufficient TOC, high porosity, and high CEC; **Table 3.1**) may have provided ideal conditions for microbial metabolism of the compound.[*Myresiotis et al.*, 2012]

## 3.6 Implications and Conclusions

Though levels of TMX transported from our experimental plots did not exceed any known lethal thresholds for non-target organisms, the apparent mobility of these compounds may still be concerning, as sub-part per billion exposure to neonicotinoids poses ecological risks to non-target terrestrial[*Tosi et al.*, 2017] and aquatic invertebrates [*Beketov and Liess*, 2008; *Sánchez-Bayo et al.*, 2016]. Moreover, this study can be taken as a conservative simulation of neonicotinoid transport potential due to: 1) the diminished dose of active ingredient (i.e. a

reduced density of 59,000 plants $ha^{-1}$), 2) disturbed soil properties (reduced structural flow due to tillage prior to plot construction), and 3) rate-limited flow conditions (low $K_s$ in Bt and C horizons; **Table 3.1**) in a highly reactive subsoil underlying the plow layer (e.g. high % clay and CEC in Bt and C horizons may retard movement due to partial positive charge on TMX; **Table 3.1**). Despite these potential limitations, TMX was transported via three drainage compartments and detected in the soil profile throughout the growing season. TMX concentrations were as high as 594 µg $kg^{-1}$ (**Figure 3.3a**) for individual soil samples taken at day 23 (V3), representing one of the highest concentrations of a neonicotinoid yet detected in soil under environmentally relevant conditions. Further, TMX concentrations detected in surface soil between corn rows exceeded those of the samples taken 25 cm below the corn seed by over an order of magnitude (**Figure 3.3b and c**), suggesting that TMX can be preferentially transported even under small hydraulic gradients (**Figure B2**). This pattern of rapid advective transport could be exacerbated as farmers continue to adopt no-till practices which can promote development of soil structure and preferential flow pathways [*Alletto et al.*, 2010]. As of 2011, no-till accounted for 40% of the US acreage dedicated to corn, soybean, cotton, and wheat,[*Wade et al.*, 2015] all of which currently employ neonicotinoid-coated seed treatments [*Douglas and Tooker*, 2015].

Our results suggested that TMX transport potential decreases with time, with alteration of the water flow field caused by plant-induced drying out of the matrix representing a potentially important factor for environmental contamination of neonicotinoids. Thus, even though growing plants appear to facilitate bypass flow, they also act to mitigate plot-scale transport of TMX by amplifying flow retardation. As a consequence, early season rain events (e.g. pre-VT stage), whether intense (peak shallow lateral concentrations in early July; **Figure 3.1**) or mild and frequent (peak runoff concentrations in late June; **Figure 3.1**), may dictate total mass transport of

these compounds. These early season pulses of TMX are consistent with rapid neonicotinoid transport to streams in the Midwest[*Hladik et al.*, 2014a; *Schnoebelen et al.*, 2003; *Thurman et al.*, 1992], and our work provides a mechanistic link from plot to catchment scale contamination of these compounds. Taken altogether, these data serve as definitive proof that seed coated neonicotinoids can be transported throughout the growing season both above and through the soil profile in potentially harmful doses.

# Chapter 4. Preferential flow alters solute mobility in the critical zone

Jesse Radolinski*, Hanh Le, Sheldon Hillaire, Kang Xia, Durelle Scott, and Ryan D. Stewart

To be submitted to *Water Resources Research*

## 4.1 Abstract

A multitude of organic contaminants are transmitted through the critical zone, yet the degree to which their chemical properties dictate transport in the presence of preferential flow remains unknown. We used a simple isotope mixing technique to understand how and to what extent preferential flow alters these chemical controls on solute transport through soil. Manure was spiked with eight common veterinary antibiotics with a range of mobility (estimated from their linear soil sorption coefficient $K_d$) and was applied to field runoff plots. Simulated rainfall was then spiked with $^2H$ as a conservative tracer and applied to the plots at a rate of 7 cm $h^{-1}$. Antibiotic concentrations and deuterium signals were recorded in soil pore water via suction lysimeters installed at 30 and 90 cm depths. The simulated rainfall produced nearly 3 orders of magnitude of variation in preferential flow (0.17% to 61% of applied water moving preferentially). Solute fluxes to lysimeters were similar at low ranges of preferential flow (i.e., <20%). However, when preferential flow exceeded ~20%, solute fluxes were higher for mobile contaminants than immobile contaminants, suggesting that bypass flow selects for more mobile compounds during exchange with the soil matrix. These non-intuitive findings contradict conventional understanding of solute transport, where the influence of compound properties is thought to be significantly reduced under increasing bypass flow. Rather, more preferential flow (~ >20%) appears amplifies these chemical controls. Altogether, we present novel data which can be used to build more accurate process-based transport models.

## 4.2 Graphical Abstract

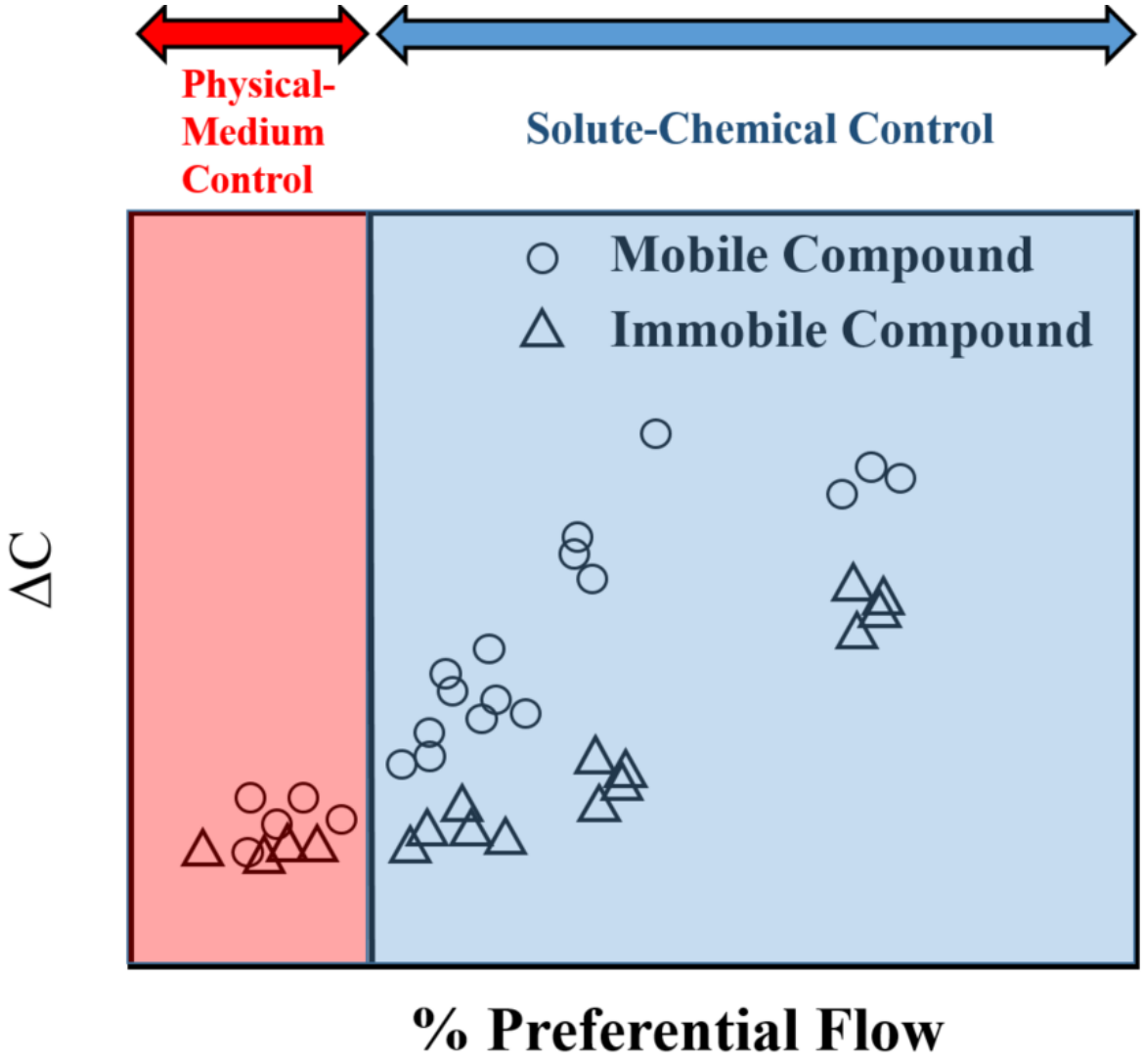


**Note:** Illustration of a system in which fluxes of two solutes with differing chemical mobility converge at low % preferential flow versus diverge at higher % preferential flow. Solute transport is thus controlled more by the structure of the medium at low preferential flow versus high preferential flow where chemical properties become influential. Here the solutes are assumed to be in kinetic equilibrium with the soil matrix prior to initiation of preferential flow.

## 4.3 Introduction

A growing and increasingly affluent human population has exposed the Earth's critical zone to new and potentially harmful compounds in ever-increasing loads [*McCance et al.*, 2018]. Many of these emerging contaminants are susceptible to rapid movement via non-equilibrium or

preferential flow [*Estévez et al.*, 2012; *Nham et al.*, 2015; *Vryzas*, 2018], which often leads to orders of magnitude greater solute leaching than predicted by equations specific to a homogenous soil matrix (e.g., the advection-dispersion equation) [*Allaire et al.*, 2009; *Radolinski et al.*, 2018a]. This rapid transport of contaminants can threaten water quality in nearby aquifers and streams, making it important to understand the physical and chemical controls on contaminant movement through unsaturated soils.

Preferential flow occurs as a disequilibrium between water flowing through the low-permeability bulk soil (matrix flow) and the highly conductive fraction of the total soil volume (e.g. macropores, root channels). Under such conditions, flow rates can sharply increase without analogous and uniform increases in soil pore water pressures [*Beven and Germann*, 2013; *Flühler et al.*, 1996; *Jarvis*, 2007b]. Preferential flow is ubiquitous in well-structured soils [*Graham and Lin*, 2011] and occurs over a broad range of water contents [*Flury et al.*, 1994; *Hardie et al.*, 2011; *Nimmo*, 2012]. In dry soils, bypass flow may occur as partially water-repellant layers destabilize the wetting front forming fingered flow [*Hardie et al.*, 2011], or as crack formation triggers macropore flow [*Greve et al.*, 2010; *Stewart et al.*, 2016]. As soils approach saturation, near positive pore water pressures can force water from the slow flowing matrix into highly conductive macropores [*Klaus et al.*, 2013; *Steenhuis et al.*, 1994], making total flow proportionally more preferential.

As ideal tracers, stable isotopes of water (e.g., $^{2}H$ and $^{18}O$) have been widely used to identify hydrological flow paths [*Gazis and Feng*, 2004] and determine water residence time [*Hrachowitz et al.*, 2013; *McGuire and McDonnell*, 2006]. These are used to detect preferential flow with traditional methods that tracking water transit through hydrological systems [*White et al.*, 1984]; however they are particularly useful for identifying water sources [*Good et al.*, 2015].

For this reason, stable isotopes can be used to distinguish water slowly flowing through the soil matrix from rapid from bypass flow [*Stumpp and Maloszewski*, 2010; *Stumpp et al.*, 2007; *Vogel et al.*, 2010]. Thus, these tracers can be employed as a simple tool for isolating and quantifying preferential flow.

In the presence of preferential flow, mobile contaminants (i.e., those with low soil partition coefficient, $K_d$, and low organic carbon normalized partition coefficient, $K_{oc}$) should move freely with little matrix interaction [*Kladivko et al.*, 1991; *Kurwadkar et al.*, 2014a; *Traub-Eberhard et al.*, 1994]. However, some dual-domain numerical simulations have suggested that immobile compounds (i.e. with high $K_d$, high $K_{oc}$) may be more susceptible to non-equilibrium flow [*Larsson and Jarvis*, 2000]. Other studies have reported that the total mass transport of readily leachable compounds may be reduced by up to 50% with preferential flow when compared to modeled advection-dispersion flow through a homogenous medium [*Larsson and Jarvis*, 1999] as infiltrating water bypasses contaminants stored in the soil matrix [*Ahuja et al.*, 1993; *Heathman et al.*, 1995]. Despite these varying observations, preferential flow is generally believed to weaken or eliminate chemical controls on solute transport [*Ghodrati and Jury*, 1992; *Larsson and Jarvis*, 2000]. Further, preferential flow in soils may represent as little as 1% [*Peterson and Wicks*, 2005] or more than 90% of total flow [*Leaney et al.*, 1993; *Zhang et al.*, 2018b], yet no study to date has defined the degree of preferential flow required to dampen this chemical influence.

Pharmaceuticals such as veterinary antibiotics are a group of contaminants that are widely used and possess a range of chemical properties, making them ideal for studying solute versus media controls. Every year, the U.S. purchases nearly 66 million kg of veterinary antibiotics to support the animal production industry, many of which are labeled as critically

important to the World Health Organization's strategy for controlling global antibiotic resistance [*Chen et al.*, 2018; *Collignon et al.*, 2016]. As much as 80% of initial antibiotic doses to livestock can be still be found in animal waste [*Chen et al.*, 2018; *Montforts et al.*, 1999]. This waste is often applied in agricultural systems as an amendment to replace synthetic fertilizer and improve soil structure [*Heuer et al.*, 2011], furthering the potential transport of antibiotics [*Le et al.*, 2018] and establishment of antibiotic resistant organisms [*D'Costa et al.*, 2011; *Wind et al.*, 2018]. Once antibiotics are exposed to the subsurface environment, a variety of reactive chemical structures interact with the soil matrix forming complexing solute distributions below-ground. These compounds can largely partition into soil organic matter [*Wegst-Uhrich et al.*, 2014], sorb strongly to soil mineral surfaces [*Chee-Sanford et al.*, 2009], or exist primarily in the aqueous phase with high susceptibility to macropore flow [*Boxall et al.*, 2002; *Kay et al.*, 2004; *Kay et al.*, 2005a; b]. The first two mechanisms are often considered to delay the transport of the compounds relative to water [*Van Genuchten and Cleary*, 1979] while the latter mechanism may cause compounds to move at similar or even faster velocities compared to the mean water velocity [*Beven and Germann*, 2013; *Dykaar and Kitandis*, 1996]. Veterinary antibiotics can thus be transported through a given soil faster or several orders of magnitude slower than water [*Boy-Roura et al.*, 2018].

The primary objectives of this study were to 1) quantify the transport of eight veterinary antibiotics under different preferential flow conditions and 2) specify a threshold of preferential flow required to eliminate chemical controls on the transport of these solutes. This threshold analysis is necessary to provide a fundamental understanding of how non-equilibrium flow alters contaminant mobility. These results can be used to build process-based transport models which can be used to manage water quality and thwart water resource degradation.

## 4.4 Materials and Methods

### 4.4.1 Soil Characterization and Field Study Site Preparation

The field experiment was conducted in the Spring of 2018 on a no-till agricultural field in Whitehorne, VA. The field had a 9 to 11% slope and was underlain by two loam-textured soil series: Braddock and Unison (Typic Hapludults) with moderate soil structure. At the beginning of the experiment, intact cores (5 x 5 cm; $n$ = 6 per horizon) and unconsolidated soil samples were taken from three soil horizons: Ap (5-10 cm), Bt1 (30-35 cm), and Bt2 (90-95 cm). Cores were used to determine soil bulk density [$M\ L^{-3}$], porosity [$L^3\ L^{-3}$], and saturated hydraulic conductivity ($K_s$) [$L\ T^{-1}$]. Core-derived $K_s$ was measured using the falling head method with a KSAT Benchtop Saturated Hydraulic Conductivity Instrument (UMS Inc., Munich, Germany). Unconsolidated soil samples were air dried, sieved to 2 mm, and analyzed for cation exchange capacity (CEC), pH, total organic carbon (TOC), and texture. CEC was measured via summation method [*Hajek et al.*, 1972], soil pH was measured in a 1:1 slurry (soil: $CaCl_2$), TOC was quantified by dry combustion using a Vario MAX CNS macro elemental analyzer (Elementar, Hanau, Germany), and textural analysis was conducted via the pipet method [*Day*, 1965]. Soil physiochemical and hydraulic properties are shown in **Table 4.1**.

A total of nine rainfall simulation plots were installed in the field consisting of 200 x 150 cm steel frames inserted 10 cm into the soil surface, with adjacent 40 cm x 200 cm buffer strips maintained outside of the frames for installation of soil pore-water samplers. Steel pans were fitted to the frames, sealed for runoff collection, and piped down gradient to a container for storage and quantification. Weed growth was then suppressed in all plots with glyphosate. Plots were differentiated into two treatments whereby manure was broadcasted on the soil surface (surface application; $n$ = 3 plots) or inserted into two 5 cm wide x 10 cm deep slits placed

perpendicular to the slope and spanning the width of the plot frame and buffer strip (subsurface injection; $n$ = 3 plots). The three remaining plots did not receive manure application and were treated as controls.

Prior to manure application, a series of suction lysimeters (200 kPa ceramic cups; Soil Moisture Equipment Corp., Santa Barbara, CA) were installed in the plot buffer strips to sample veterinary antibiotic transport in the subsurface. Soil pore water samples were withdrawn from two randomly positioned lysimeters in both the Bt1 (30 cm) and Bt2 horizons (90 cm) to detect vertical movement of VA's in surface application plots (2 probes per depth making 4 probes per plot, Figure S1). This same installation scheme was also adopted for control plots. In subsurface injection plots a series of nested (30 and 90 cm probes) lysimeters were installed both within and 25 cm down-gradient of the injection slit to detect vertical and lateral transport of antibiotics (2 probes per depth resulting in 8 probes per plot; **Figure C1**). A liquid slurry of dairy manure (5% solid content) was spiked with eight commonly used VAs, including two macrolides (erythromycin-ERY and tylosin-TYL), two sulfanomides (sulfamethazine-SMZ and sulfadimethoxine-SDM), three tetracyclines (oxytetracycline-OTC, chlortetracycline-CTC, and tetracycline-TC) and one lincosamide (pyrlimycin-PLY). The slurry was spiked to a target concentration of 500 µg $L^{-1}$ for all antibiotics and applied to plots at a rate of 56 Mg wet mass $ha^{-1}$ [*Le et al.*, 2018]. Manure was applied 7 days prior to rainfall simulations to limit losses of compounds via runoff [*Le et al.*, 2018], and natural rainfall was suppressed by covering the plots with plastic tarps during rain events.

Plots were a component of a wider effort to understand antibiotic resistant gene transmission in the environment as a result of manure application methods; however, the current study was specifically aimed at quantifying subsurface transport of VAs across a range of

preferential flow. Rather than comparing across treatments, we used manure application methods (contaminant locations) in combination with different soil horizons (depths), and slope positions (i.e., in slit vs down gradient) to express heterogeneity in solute and water transport. Thus, data were largely analyzed independent of manure application methods.

### 4.4.2 Field Rainfall Simulations and Water Sampling

Rainfall simulations were conducted after the 7-day equilibration period using deuterium-labeled well water to trace mobile infiltrating water and detect preferential flow contributions to pore water signature. The rainfall simulator (240 cm x 300 cm) followed the original design of *Humphry et al.* [2002], which has been adopted as standard protocol for the national research project for simulated rainfall-surface runoff studies [*SERA-17*, 2008] and provides constant droplet size and velocity between locations and studies. We conducted the rainfall simulations with the SERA-17 standard intensity of 7 cm $h^{-1}$ until the collection containers received 30 min of continuous runoff. Rainwater was labeled with a Dealglad venturi injector (90 x 55 x 55 mm; Shandong Jiujin Plastic Products Co., Shandong, China) fitted to the sprinkler inlet. This system dispensed an enriched deuterium solution into the well water at a ratio of ~ 4:100 (deuterium-spiked water: well water). Discrete pore water samples were taken from all lysimeters by applying 60 kPa of suction for 10 min, 1 h before the simulation, 0.5 h into the simulation, and 1 hour after the simulation (**Figure C2**).

### 4.4.3 Stable Isotope and Analysis Antibiotic Detection

All liquid samples (i.e., pore water from lysimeters and column leachate) were analyzed for $\delta^{18}O$ and $\delta^{2}H$ via cavity ring down spectroscopy (Model L1102-i, Picarro, Santa Clara, CA). All samples were expressed in per mil (‰) delta notation relative to Vienna Mean Standard Mean Ocean Water (VSMOW) via

$$\delta^{18}O \text{ or } \delta^{2}H = \left(\frac{R_{sample}}{R_{VSMOW}} - 1\right) \times 1000 \quad (1)$$

where $R_{sample}$ and $R_{VSMOW}$ are the respective ratios of heavy to light species in the sample and standard VSMOW water, respectively.

We used a modified post-processing method [*van Geldern et al.*, 2012] to apply drift and memory corrections to raw data, yielding a precision of 0.1‰ for $^{18}O$ and 0.2‰ for $^{2}H$. Liquid samples were analyzed for antibiotic concentration via HPLC MS/MS, as detailed in the Appendix C.

4.4.3 Preferential Flow Analysis

To analyze the deuterium tracer, we considered flow to be partitioned into two distinct and unmixed hydrological domains: faster advection-driven flow through preferential pathways (e.g., root channels and macropores) and slower flow through the soil matrix via classic advection dispersion mechanisms. Following the conceptual framework provided by *Stumpp et al.* [2007] the isotope mass balance can be described as

$$Q_t(t) = Q_{PF}(t) + Q_{MF}(t) \quad (2)$$

and

$$Q_t(t) \cdot C_t(t) = Q_{PF}(t) \cdot C_{PF}(t) + Q_{MF}(t) \cdot C_{MF}(t) \quad (3)$$

where the preferential flow, $Q_{MF}(t)$, and matrix flow, $Q_{PF}(t)$, sum up to total discharge $Q_t(t)$ [$L^3\ T^{-1}$] and $C_{MF}(t)$, $C_{PF}(t)$, and $C_t(t)$ [$M\ L^{-3}$] correspond to the isotope concentrations within each flow component. Assuming that preferential flow pathways translate to rainfall inputs during each sampling period, we consider the rainfall isotope signal to be equivalent to the preferential flow signal in the outlet

$$C_{PF}(t) = C_{rain}(t) \quad (4).$$

Thus, the fractional contribution of preferential flow to the outlet signal is

$$f_{PF}(t) = \frac{C_t(t) - C_{MF}(t)}{C_{PF}(t) - C_{MF}(t)} \quad (5)$$

and the preferential flow rate is

$$Q_{PF}(t) = f_{PF}(t) \cdot Q_t(t) \quad (6).$$

The $\delta^2H$ difference between individual pore water samples taken before the simulation was relatively small (standard deviation of 5 ‰ from all plots and depths) compared to the difference between these samples and labeled rainfall (average difference of 26 ‰; **Table 4.2**). Thus, we assumed that background lysimeter samples represented a uniform pre-event matrix signature $C_{MF}(t)$ which enabled calculation of $f_{PF}$ during and after field rainfall simulations for each lysimeter.

4.4.4. Assessment of Relative Antibiotic Mobility

To assess the relative mobility of our eight antibiotics, a simple solute partitioning test was performed on soil from the field site. One gram of dried and 2 mm sieved $A_p$ horizon soil was mixed with 500 mL of deionized water to reach target concentrations of each antibiotic at 2.5 µg $L^{-1}$ for SDM; 5 µg $L^{-1}$ for SMZ, PLY, and TC; 50 µg $L^{-1}$ for OTC, CTC, ERY, and TYL. The mixture was then left still to equilibrate for 1 h followed by vortexing, and shaking for 30 min. These concentrations ranges were chosen to be compatible with antibiotic detection in runoff samples taken previously from the same field [*Le et al.*, 2018]. After shaking for 30 min, the mixture was centrifuged at 5000 rpm for 5 min before a 1.5 mL aliquot of supernatant solution was mixed with 50 mg primary and secondary amine (PSA), vortexed, centrifuged, and

sequentially filtered with a 0.45 um PTFE syringe filterand the a 0.2 um PTFE syringe filter, before being injected into UPLC-MS/MS for analysis. The two macrolides (ERY and TYL) were not detected in supernatant (0.5 mL aliquots) even after three additional testing at concentration of 50, 250, and 500 μg $L^{-1}$, so the experimental $K_d$ could not be calculated for those two compounds. We thus assumed macrolides to be the most immobile compounds in our system. We used the USEPA's EPI (estimation program interface) Suite TM tool [*EPA*, 2010] to predict effective $K_{oc}$ values for ERY and TYL based on octanol water partitioning coefficients ($K_{ow}$) inputs, and assigned mobility rankings of 7 and 8 based on model outputs (**Table 4.3).** Additionally, we used EPI's BIOWIN model to estimate dissipation half-lives of our compounds in soil following the methods described in *Chen et al.* [2018]. Using these half-lives we projected that less than 10% of the originally applied VA mass would have degraded during our 7 day experiments, and thus assumed that decay played a minor role in relative transport of these compounds (**Table 4.3**). To accurately express the response of VAs to varying preferential flow estimates, the changes in concentration ($\Delta C$) from lysimeter samples taken 1 hour before simulations versus during, and 1 h after the event.

### 4.4.5. Statistical Analyses

We sought to compare solute fluxes ($\Delta C$) between the most immobile (ERY) and most mobile (SMZ) solutes at our highest ($f_{PF}$ = 0.35-0.61) and lowest ($f_{PF}$ < 0.2) ranges of preferential flow to clearly define where solute mobility governed transport to lysimeters. After separating the two ranges, rank transformed data were tested for normality via normal quantile plots and homogeneity of variance was detected using Fligner's test. Because the low range of preferential flow contained too much noise to pass normality and homogeneity assumptions, we performed a one way ANOVA on the highest range of preferential flow (ERY vs SMZ). To test

for difference and interaction of manure treatments (subsurface injection, surface application, and control plots with only levels of VAs) on $\Delta C$ across the range of preferential flow we used analysis of covariance (ANCOVA) to statistically compare the slope of lines fitted to log-transformed $\Delta C$ as function of preferential flow ($f_{PF} > 0$ and $\Delta C > 0$) by treatment. These log-transformed data were found to meet ANOVA assumptions using the approach outlined above. We used R version 3.2.2 to conduct all statistical analyses with $\alpha = 0.05$.

**Table 4.1.** Soil physiochemical and hydraulic properties. Note that cation exchange capacity (CEC), porosity, bulk density, saturate hydraulic conductivity $K_s$, pH and total organic carbon content (TOC) are expressed as mean ± standard deviation.

| Horizon | Depth (cm) | Texture | Sand (%) | Silt (%) | Clay (%) | CEC (cmol $kg^{-1}$) | Porosity (%) | Bulk density (g $cm^{-3}$) | $K_s$ (cm $d^{-1}$) | pH | TOC (%) |
|---|---|---|---|---|---|---|---|---|---|---|---|
| Ap | 0-23 | Loam | 44.5 | 41.6 | 25.8 | 16 ± 4.6 | 47± 0.009 | 1.36 ± 0.05 | 416 ± 486 | 6.0 ± 0.26 | 2 ± 0.45 |
| Bt1 | 23-33 | Sandy clay loam | 45.1 | 46.9 | 29.1 | 4.4 ± 1.7 | 37 ± 0.04 | 1.75 ± 0.13 | 43.8 ± 50.8 | 5.6 ± 0.27 | 0.25 ± 0.062 |
| Bt2 | 33-97 | Silty clay | 10.2 | 11.4 | 45.0 | 8.1 ± 0.30 | 54 ± 0.07 | 1.4 ± 0.04 | 44 ± 45.3 | 4.9 ± 0.07 | 0.40 ± 0.031 |

**Table 4.2.** Rainfall simulation information expressed as mean ± standard deviation.

| Rainfall Simulations | | |
|---|---|---|
| ***Time*** | Length of Simulation (h) | 1.2 ± 0.56 |
| | Time to Runoff (h) | 0.75 ± 0.53 |
| ***Rates*** | Rainfall Rate (cm $h^{-1}$) | 7 |
| | Infiltration Rate (cm $h^{-1}$) | 5.6 ± 0.76 |
| ***Depths*** | Rainfall (cm) | 8.7 ± 3.9 |
| | Infiltration (cm) | 6.9 ± 2.8 |
| | Runoff (cm) | 1.8 ± 1.3 |
| ***Tracer*** | Rainfall Label $\delta^2H$ (‰) | -12.7 ± 8.44 |
| | Background Pore Water $\delta^2H$ (‰) | -39 ± 5.0 |

**Table 4.3.** Veterinary antibiotics with experimentally determined "effective" sorption coefficient-$K_d$, Relative Mobility ranking, and EPI (estimation program interface) predicted dissipation kinetics. Macrolides (ERY and TYL) were most immobile based on our sorption analysis, but required the EPI tool to assess mobility rankings of 7 and 8 (see Methods).

| Veterinary Antibiotic (VA) | Effective $K_d$ | Relative Mobility | EPI Predicted Half Life (d) | EPI Predicted Decay Constant ($d^{-1}$) |
|---|---|---|---|---|
| Eryrthomycin (ERY) | *NA* | 8 | 360 | $2 \times 10^{-3}$ |
| Tylosin (TYL) | *NA* | 7 | 360 | $2 \times 10^{-3}$ |
| Tetracycline (TC) | 1140 | 6 | 120 | $6 \times 10^{-3}$ |
| Pirlimycin (PLY) | 997 | 5 | 75 | $9 \times 10^{-3}$ |
| Chlortetracycline (CTC) | 783 | 4 | 360 | $2 \times 10^{-3}$ |
| Oxytetracycline (OTC) | 368 | 3 | 120 | $6 \times 10^{-3}$ |
| Sulfadimethoxam (SDM) | 80.3 | 2 | 75 | $9 \times 10^{-3}$ |
| Sulfamethazine (SMZ) | 64.6 | 1 | 75 | $9 \times 10^{-3}$ |

## 4.5 Results and Discussion

Rainfall simulations lasted for an average of 1.2 h generating 8.7 cm of cumulative rainfall and 6.9 cm of infiltration, with the remainder lost as surface runoff (**Table 4.2**). Under the assumption that event water had infiltrated vertically via pure advection and soil moisture was at field capacity (~0.30 using soil texture contours in *Twarakavi et al.* [2009]) prior to rainfall, the average of 6.9 cm of infiltrated water would have filled and/or displaced ~23 cm of storage. This estimate suggests that a homogenous wetting front had not reached our 30 cm probes within the sampling period, and that the sampled water was derived from preferential flow or pre-event matrix storage. Thus, our assumption that any event water seen in lysimeter samples represented preferential flow (Equation 4) appears to have been valid for this experiment.

Of the 82 isotope-based estimates of $f_{PF}$, 19 (20%) resulted in zero or negative values. Based on our detection method, negative values indicate that our lysimeter samples taken during and after the simulation were equal to or more isotopically depleted than the estimated matrix signature (i.e., samples pulled ~1 h before simulated rainfall). Negative $f_{PF}$ values indicate a dominant contribution of pre-event water, so we considered these points to be entirely matrix derived ($f_{PF} = 0$). Including non-detect values caused a slight upward shift in the distribution of $f_{PF}$, as seen by the Isotope (Positive) versus Isotope (All) data (**Figure 4.1**). Though event water was applied at a constant rainfall intensity (7 cm $h^{-1}$) and infiltrated in similar rates between plots (**Table 4.2**), simulated rainfall produced nearly 3 orders of magnitude of variation in preferential flow ($f_{PF}$ from 0.0017 to 0.6; **Figure 4.1**)**.** These numerous point detections of bypass flow in space and time (during and after rainfall) accented the heterogeneous subsurface architecture in

this no-till agricultural field and enabled analysis of solute mobility across a wide range of preferential flow.

To understand how these preferential flow estimates affected the transport of our eight VAs, we quantified the change in concentration ($\Delta C$) as a function of estimated $f_{PF}$ across a spectrum of relative mobility. Similar to our preferential flow estimates, when veterinary antibiotic fluxes were negative or non-detectable, we considered $\Delta C$ to be zero (**Figure 4.2**). Despite one instance of ERY detection, control plot samples either showed no detectable antibiotcs or else strictly contained the highly mobile sulfanomide compounds (SMZ and SDM; **Figure C3**). Sulfanomide fluxes from control and manure-applied plots were similar in magnitude and range along a spectrum of preferential flow estimates. Additionally, we found no significant difference between the slope of lines fitted to $\Delta C$ data across the range of $f_{PF}$ for all treatments, and no significant treatment interactions on preferential flow estimates (subsurface injection, surface application, and control plots; ANCOVA, $p > 0.05$; **Figure 4.2**). Because the behavior of these compounds in control plots was nearly indistinguishable from experimental plots (similar linear trends with and without control; **Figure C3**) and all treatments produced similar trends in solute fluxes (**Figure 4.2**), we excluded treatments from subsequent analyses (**Figure 4.3)**. Our resulting range of $\Delta C$ extended from 0 to 3.85 µg $L^{-1}$, or from 0.006 to 3.85 µg $L^{-1}$ when only considering positive values (**Figure 4.3**). Lysimeter data displayed a general trend of increasing $\Delta C$ with preferential flow, though the relationship was noisy (**Figure 4.2**). For instance, high antibiotic concentrations were seen in samples without detectable preferential flow (e.g., ERY was measured with a $\Delta C$ value of 1.26 $L^{-1}$; **Figure 4.3**) whereas some samples with high $f_{PF}$ had no detectable VAs (e.g., ERY, TYL, and TC).

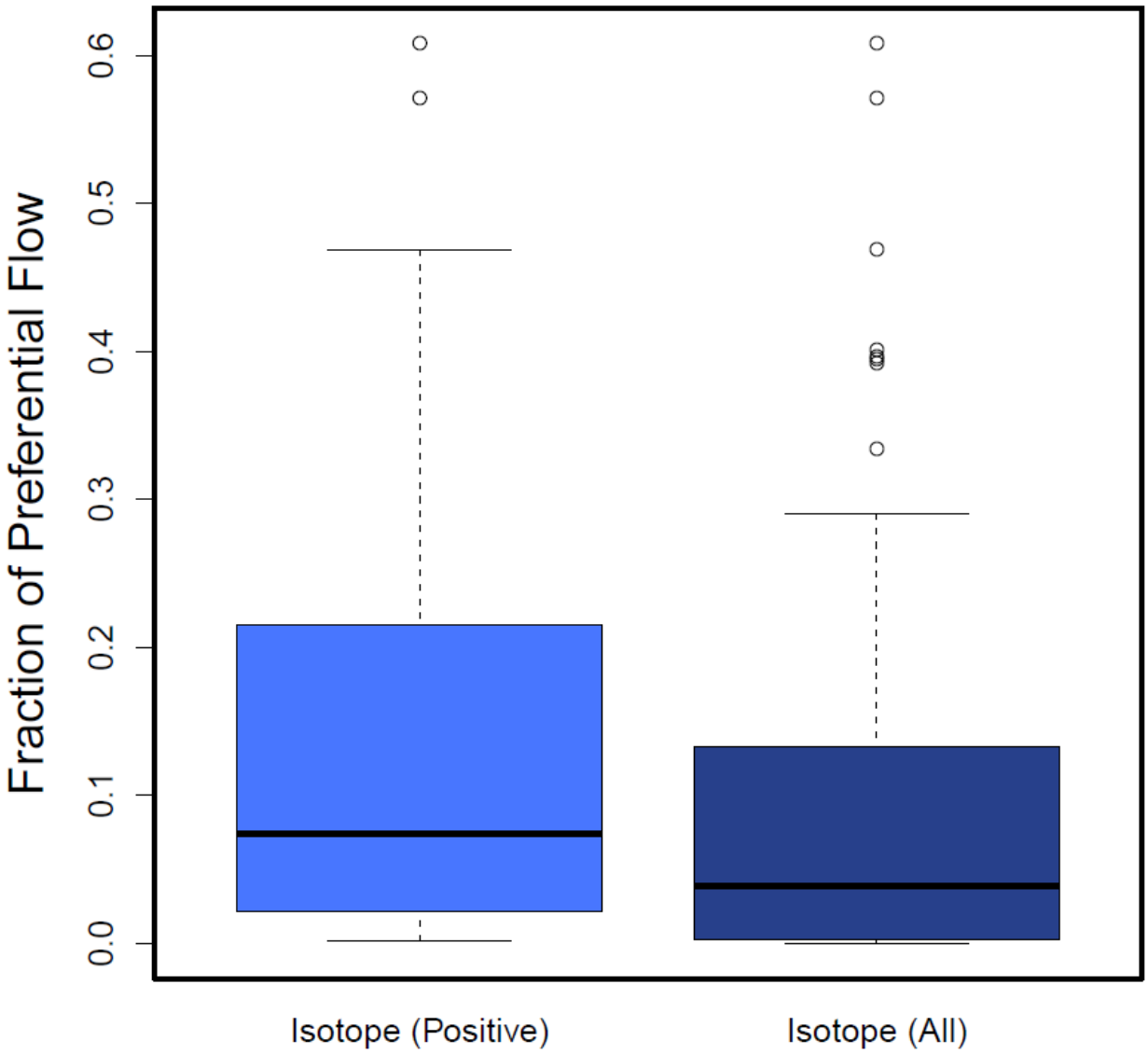


**Figure 4.1.** Experimental estimates of fraction of preferential flow ($f_{PF}$) using an isotope-mixing approach that included ("All") versus excluded ("Positive") samples in which $f_{PF} = 0$.

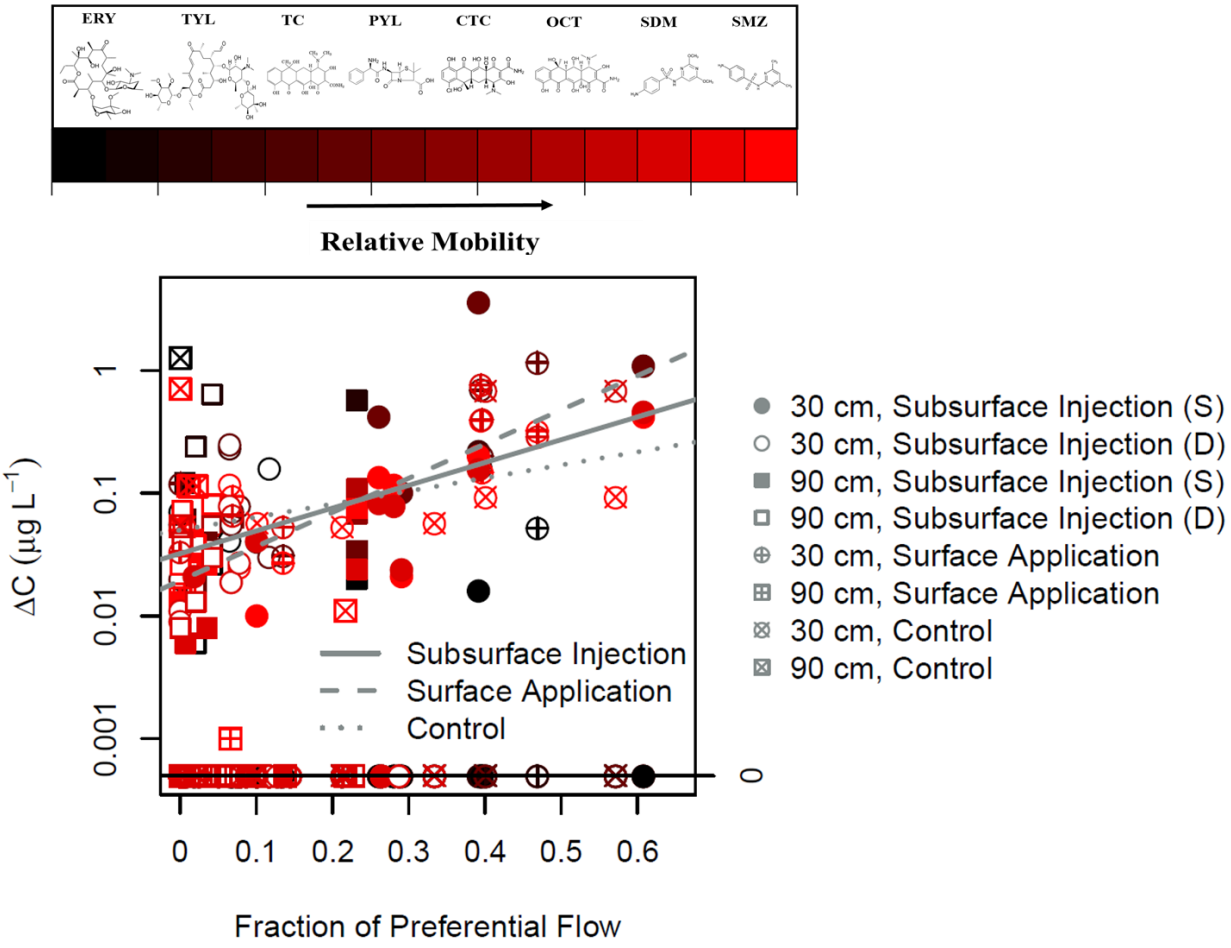


**Figure 4.2**. The change in VA concentration ($\Delta C$) versus the fraction of preferential flow ($f_{PF}$) estimated in lysimeter samples ($\Delta C = 0$ and $f_{PF} = 0$ included). Colors indicate relative mobility as estimated from effective $K_d$ values, wherein red is most mobile and black is least mobile. "S" and "D" refer to samples taken lysimeters installed in and down gradient of injection slits, respectively. Linear models were fit to Subsurface Injection, Surface Application and Control data points ($\Delta C = 0$ and $f_{PF} = 0$ excluded) and did not have significant difference between slopes (ANCOVA, $p > 0.05$). Slopes were 1.85 (subsurface injection), 2.78 (surface application), and 1.06 (control plots) and adjusted respective $r^2$ values were 0.27, 0.48 and 0.11.

The contaminants with the greatest contrast in relative mobility were similar in $\Delta C$ for the low range of preferential flow, but differed significantly in the highest range of preferential flow (SMZ vs ERY; one-way ANOVA, $p < 0.001$; **Figure 4.5b**). This finding suggests that chemical controls (solute-matrix interaction) on solute mobility were weakest when bypass flow was minimal. However, based on the distribution of positive $\Delta C$ and $f_{PF}$ values (**Figure 4.5a** and **Figure**

**4.4**), leachate had the greatest probability of having $\Delta C$ values < ~0.20 µg $L^{-1}$ and $f_{PF}$ values < ~0.2 even when excluding non-detect values. By contrast, bypass flow and leaching of antibiotics at high concentrations were relatively unlikely to occur.

Solute transport to our lysimeters also appears to have been most sensitive (e.g., $\Delta C/f_{PF}$ was highest) to preferential flow when $f_{PF}$ was < ~0.2 (**Figure 4.6**). The influence of preferential flow on the magnitude of $\Delta C$ was therefore dampened when chemical controls became more influential, suggesting a shift in flow partitioning. For example, in a situation where $\Delta C$ linearly increased across the range of $f_{PF}$ values (**Figure 4.6 inset**), the solute fluxes in drainage would respond similarly (i.e., nearly constant $\Delta C/f_{PF}$) across the spectrum of preferential flow. Instead we observed that minor additions of event water were sufficient to remove the influence of solute-matrix affinity. Altogether, these data illustrate that solute responses to bypass flow differ along a spectrum of preferential flow (**Figure 4.5** and **Figure 4.6**).

The detection of antibiotic fluxes in our lysimeters depicted a dynamic flow field that non-selectively sampled solutes under some conditions and selectively sampled solutes under other conditions. When preferential flow was minimal (i.e., $f_{PF}$ < ~0.2), antibiotics were transported in similar concentrations independent of their relative mobility (**Figure 4.5b**). At the highest observed range of bypass flow (i.e., $0.4 < f_{PF} \leq 0.61$), solute fluxes significantly differed between mobile and immobile compounds, indicating a fundamental shift in solute and flow partitioning.

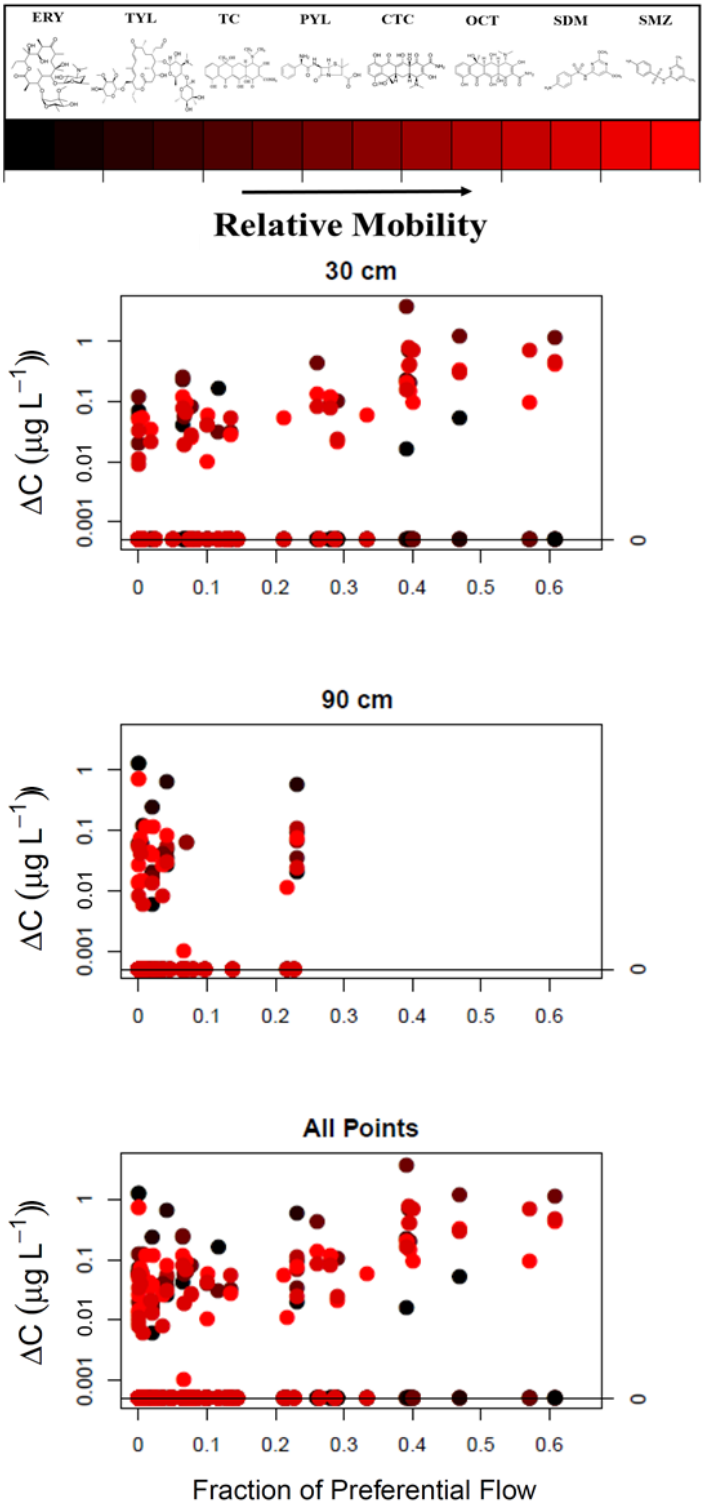


**Figure 4.3**. The change in veterinary antibiotic concentration (ΔC) versus the fraction of preferential flow estimated in lysimeter samples (ΔC = 0 and $f_{PF}$ = 0 included).

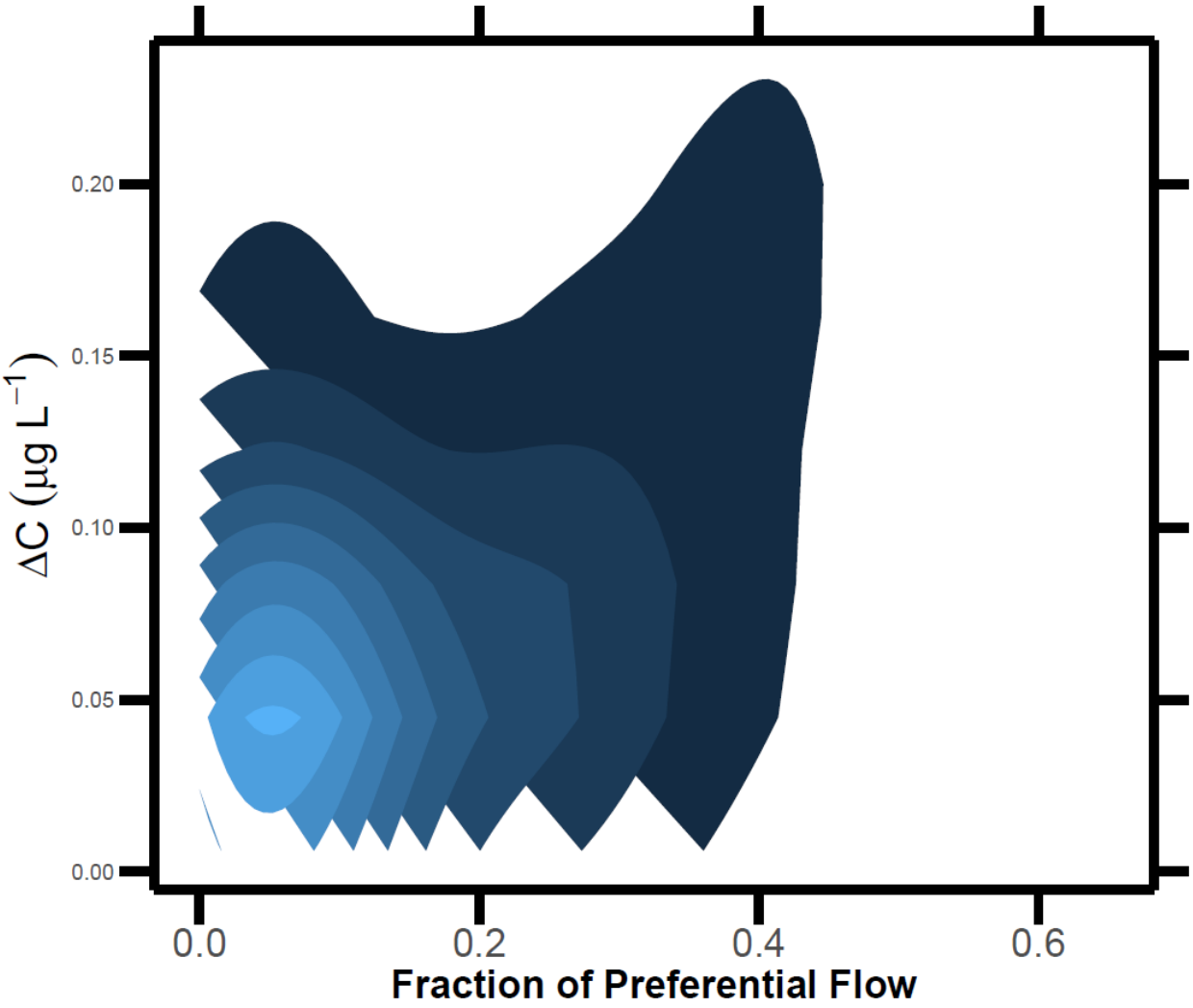


**Figure 4.4.** Bivariate kernel density plot depicting the distribution of results for positive Δ*C* and $f_{PF}$ values, where lightest areas are most probable and darkest areas are least probable.

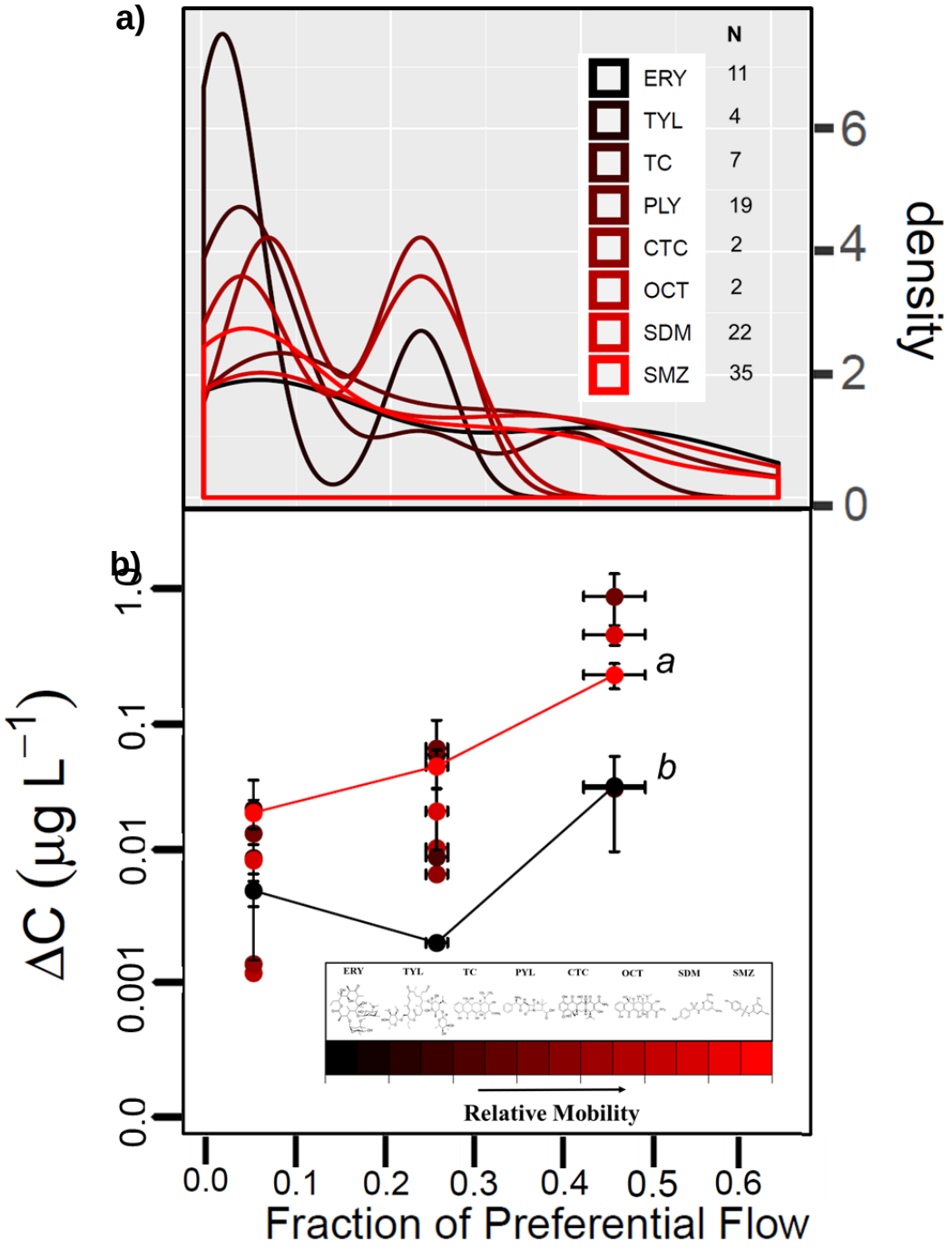


**Figure 4.5. a)** The smoothed density distribution of veterinary antibiotics in the detected range of estimated preferential flow (where $\Delta C > 0$ and $f_{PF} > 0$), indicating the total frequency of samples detected. Using the ranges of preferential flow with highest density, ($f_{PF}$ ~0 – 0.2, 0.2 – 0.35, and 0.35 – 0.61) $\Delta C$ was binned and compared for all compounds and all values of $\Delta C$ and $f_{PF}$ in **b)**. *Different letters* denote statistical differences ($p < 0.05$) in $\Delta C$ between our most mobile (SMZ) and immobile compounds (ERY) at the highest range of preferential flow. Error bars represent standard error of the mean (SE).

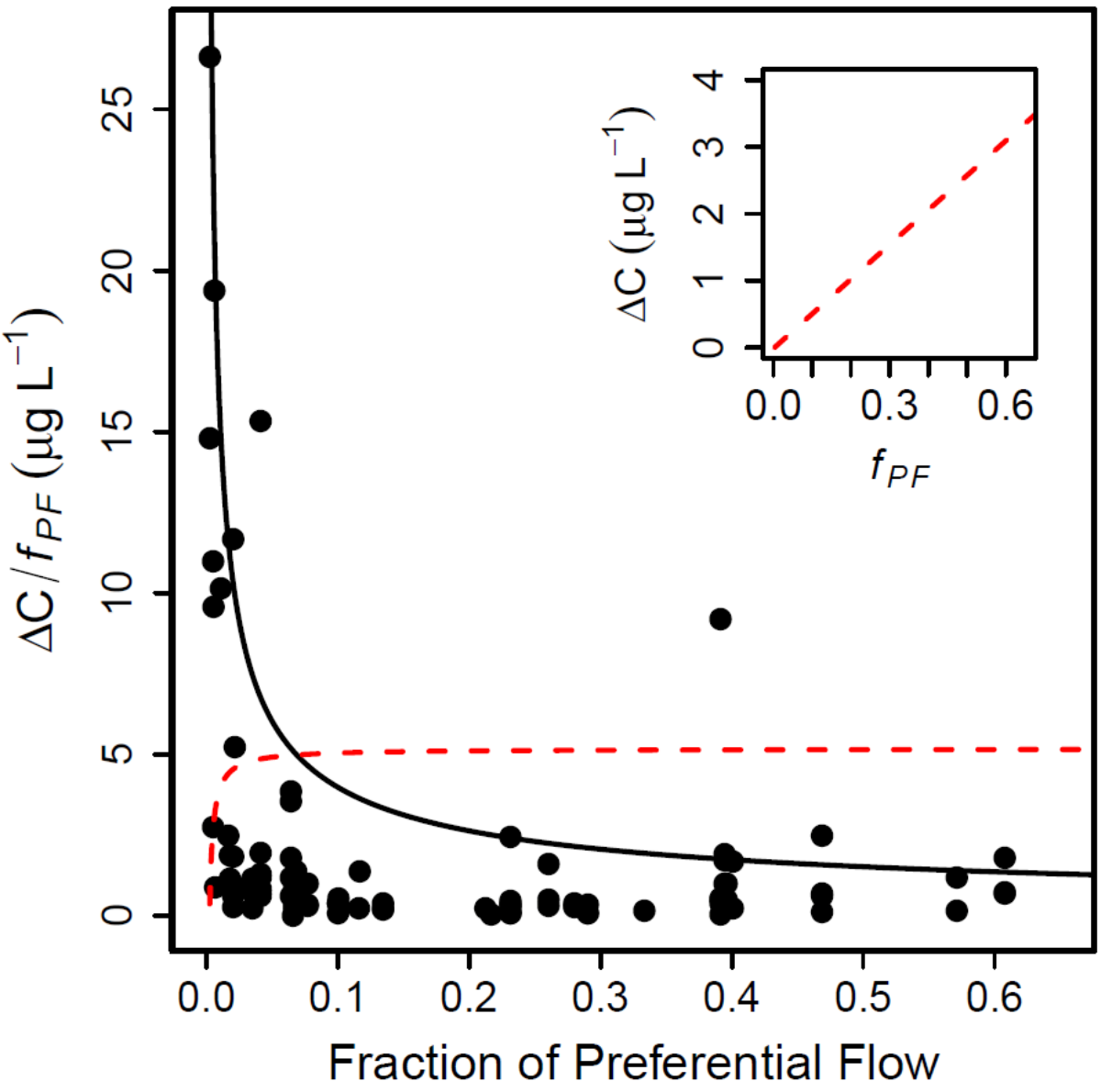


**Figure 4.6.** Solute sensitivity to preferential flow ($\Delta C/f_{PF}$) across the detected range of preferential flow. The solid black line shows a Markov Chain Monte Carlo fitted power law function (sensitivity = 1* $f_{PF}^{-0.6}$) and the red dashed line depicts a scenario where $\Delta C$ increases linearly across the range of $f_{PF}$. Note that $\Delta C$ extends from the lowest value, 0.006 µg $L^{-1}$ to the highest values 3.8 µg $L^{-1}$.

This selective vs non-selective transport behavior may be explained by both the amount of preferential flow and the ability of this bypass flow to access contaminants. For example, 7 d of equilibration and rainfall suppression would have been sufficient for compounds to diffuse into the soil matrix [*Jarvis*, 2007a; *Pignatello and Xing*, 1995; *Radolinski et al.*, 2019] and for sorption equilibrium to occur [*Le et al.*, 2018; *Thiele-Bruhn*, 2003]. Consequently, plots spiked with antibiotics produced nearly identical solute fluxes as the control plots (**Figure C3**), suggesting that these compounds may be stored in the soil matrix from previous applications. Therefore, when drainage water was less preferential (i.e., $f_{PF}$ < 20%), the likelihood of sampling all compounds was higher (**Figure 4.4**) as most of the drainage water originated in the matrix. Infiltrating water may have mixed with a greater volume of pre-event storage before triggering preferential flow events with trace levels of antibiotics, allowing for compounds strongly sorbed to the soil matrix (e.g., immobile antibiotics) and compounds weakly bound to macropore walls (e.g., mobile antibiotics) to be transported in similar proportions. Higher proportions of preferential flow would have excluded flow through matrix where the much of the compounds resided [*Heathman et al.*, 1995], causing the two hydrological domains (i.e., fast preferential flow versus slow matrix flow) to become more distinct [*Scaini et al.*, 2019; *Worthington*, 2019] and infiltrating water to select for contaminants with a higher affinity for the aqueous phase.

It should also be noted that our moderately mobile solute, PLY, produced the highest $\Delta C$ in drainage (high range of $f_{PF}$, **Figure 4.3** and **Figure 4.5b**); however, a previous antibiotic transport study conducted in the same field site reported PLY as being highly mobile with 50x more PLY transported compared to the sulfonamide sulfamerazine [*Le et al.*, 2018]. This result suggests either that 1) PLY sorption to the $A_p$ soil sample used for $K_d$ determination may not have been representative of the entire field or 2) our mobility ranking was accurate and the high

apparent mobility of PLY seen in similar field studies [*Kulesza et al.*, 2016; *Le et al.*, 2018] may be the result of more novel mechanisms (e.g., colloidal transport). Some numerical simulations have also suggested that moderately mobile solutes may be most sensitive preferential flow [*Larsson and Jarvis*, 2000]. Though the underlying mechanisms are not yet clear, we speculate that these compounds may be immobile enough to be sorbed throughout the soil medium, yet soluble enough to partition into local bypass flow. Thus, when $f_{PF}$ approached ~0.5 (i.e., roughly equal matrix and preferential influence) moderately mobile compounds could be selected in higher proportions relative to other antibiotics.

These non-intuitive findings contradict conventional understanding of solute transport, where the influence of compound properties is thought to be significantly reduced with bypass flow [*Barbash and Resek*, 1996; *Klein*, 1994; *Larsson and Jarvis*, 2000]. When preferential flow intensified, solute fluxes in drainage became more influenced by the physiochemical interactions with the medium (relative mobility) rather than just the medium itself (i.e., well-connected macropore network). Alternatively, if rainfall was applied much closer to the time of manure application one would expect the opposite trend: solute-matrix interactions might govern contaminant transport at low values of $f_{PF}$ but become less important as bypass flow samples mobile and immobile compounds equally. Using a similar experimental design *Le et al.* [2018] detected comparable losses to runoff for four antibiotics of varying mobility when rainfall happened just 2 hours after manure application, yet losses differed by an order of magnitude when manure was undisturbed for just 3 d. More directly, the timing appears to be an important factor in controlling contaminant behavior in the presence of preferential flow, due to sorption kinetics and physical partitioning of the compounds below-ground.

## 4.6 Implications and Conclusions

By simulating a range of preferential flow, we were able to evaluate conditions necessary to dampen versus amplify chemical controls on solute transport, thus providing novel insight into subsurface water and solute partitioning. Our results suggest that under field-relevant scenarios the influence of solute-chemical properties appear damped below ~20% preferential flow (**Figure 4b**), but amplified at higher contributions of event water. Mechanistically, this means that fast flow paths may preferentially select for more mobile solutes. Practically, this means that water quality may be threatened equally by a wide range of solutes with little bypass flow and though less probable (**Figure 4.4**), high preferential flow may still result in orders higher leaching in the vadose zone (**Figure 4.3**, and **Figure 4.4**).

Together, these results suggest that it may be necessary to re-evaluate common assumptions of solute transport under preferential flow conditions. Specifically, our findings indicate that: **1)** it is more probable that a chemical's matrix affinity has little bearing on contaminant transport under conditions of low preferential flow (e.g., < 20% of water moving preferentially + sorption into the soil matrix), and **2)** it appears to be more likely that traditional reactive transport models can better describe solute movement as the proportion of flow moving preferentially increases.

# Chapter 5. Conclusions

The objectives of this dissertation were to: 1) quantify the environmental transport of two emerging contaminant classes (neonicotinoids + veterinary antibiotics); and 2) and use these solutes to evaluate fundamental controls on contaminant mobility in the critical zone. We first determined the amount of neonicotinoids that could move from corn seed coatings into surrounding soil and leach from the soil environment, accounting for varying soil texture, soil structure, and the role of viable plants. We then further addressed the role of viable plant growth on neonicotinoid transport throughout the corn growing season. Though concentrations of neonicotinoids leaving our experimental systems (e.g., via leachate in Chapter 1) can be considered harmful to invertebrates, extrapolating risk to aquatic organisms requires integration from larger spatial scales (e.g., using previous landscape reconnaissance studies) and detailed incorporation of ecotoxicological data. For the final study, we used eight common veterinary antibiotics that ranged in mobility along with a simple isotope mixing method to determine how and to what degree preferential flow alters chemical controls on solute transport.

The results addressed these two main objectives by quantifying the amount of emerging contaminants that could move under environmentally relevant conditions and providing process-based insight that can be applied to a range of compounds in the critical zone. For example, we identified the first definitive link from environmental contamination of neonicotinoids to seed-coatings, and described novel behavior of veterinary antibiotics in the subsurface. The neonicotinoid studies showed that mobile contaminant transport is largely controlled by evaporative constraints (e.g., P-ET) and precipitation-driven preferential flow, which are both amplified by deep rooted plants such as the maize planted in these studies. Through our veterinary

antibiotic study we showed how the transport of compounds with a range of mobility can be altered by a spectrum of preferential flow estimates.

With these works we provided a several new insights to the disciplines of water resources and hydrology. When mobile contaminants are introduced to the soil environment their susceptibility to rapid leaching at high concentrations (i.e., "Transport Potential") is governed primarily by decay, center of mass position relative to some highly conductive outlet (e.g., $L_{soil}$ in **Figure 5.1**), and the evaporative constraints posed by the water budget (P-ET). Early in the growing season, the total mass loss to decay is minor; however, the transport potential also remains minimal unless total precipitation is sufficient to move the center of mass downward (Point 1, **Figure 5. 1**).

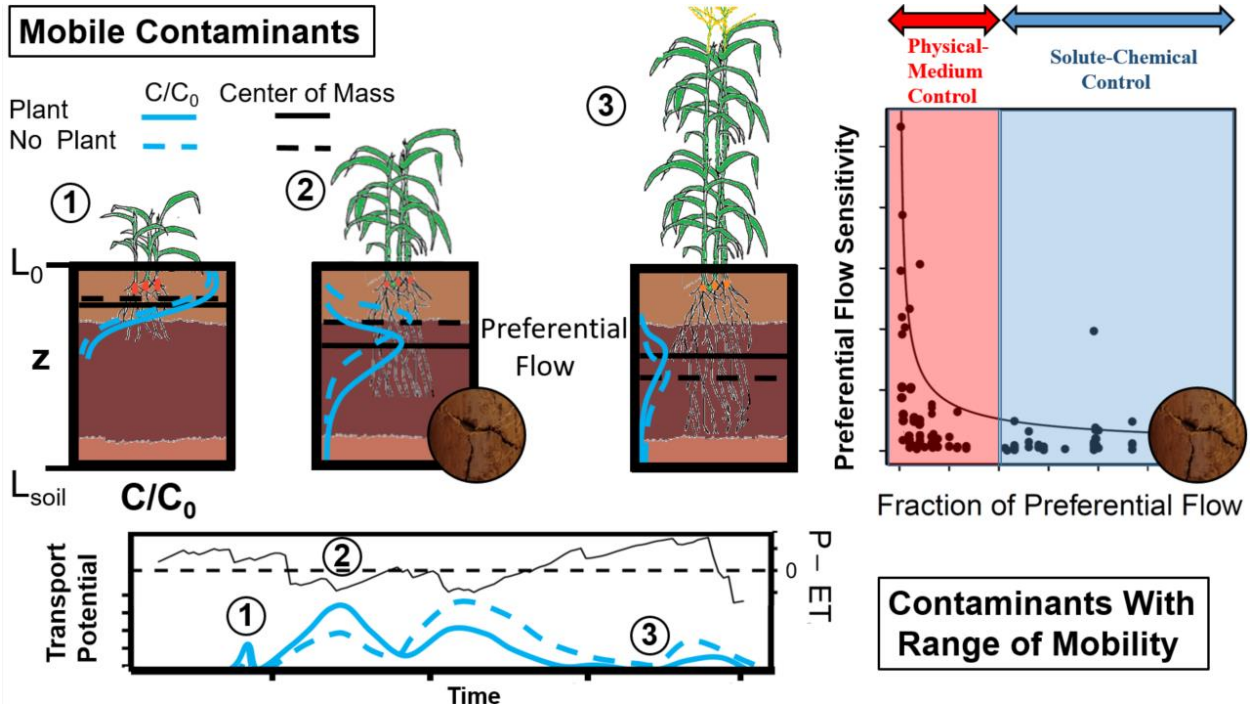


**Figure 5.1** Conceptual diagram showing how transport potential varies throughout a growing season for mobile contaminants with the influence of growing plants illustrated (**left**) and a depiction of solute sensitivity to a range of preferential flow (**right**).

The transport potential may peak when P-ET > 0, a substantial portion of original mass remains, and large rainstorms drive the center of mass downward with a higher likelihood bypass flow, which can be amplified by newly formed root channels (Point 2**, Figure 5.1**). Thus, later in the growing season, much of the contaminant may be lost to degradation, and any transport is constrained by evapotranspiration (P-ET < 0; Point 3, **Figure 5.1**). Additional rainfall may trigger the release of the contaminant from the profile, however, the transport potential is highly diminished and some contaminant mass may be partially immobilized in soil micropores. Small increases in preferential flow appear to affect contaminant transport most when the fraction of preferential flow is low (e.g., < 0.20). As preferential flow exceeds this low range the sensitivity to bypass flow dampens and compound properties better explain the relative fluxes to drainage (**Figure 5.1**).

Altogether, these concepts provide a framework for quantification of emerging contaminant transport, while also eliciting new scientific understanding of solute partitioning under heterogeneous subsurface flow. These studies were carefully conducted to make realistic measurements of contaminant transport in the critical zone and isolate mechanisms that govern solute mobility. We deliver these results to both the public and greater hydrology/water quality community for emerging contaminant risk assessment and mechanistic model development, in an effort to thwart global water resource degradation.

## References


Ahuja, L., D. DeCoursey, B. Barnes, and K. Rojas (1993), Characteristics of macropore transport studied with the ARS root zone water quality model, *Transactions of the ASAE*, *36*(2), 369-380.

Akbar, S., and S. Sultan (2016), Soil bacteria showing a potential of chlorpyrifos degradation and plant growth enhancement, *brazilian journal of microbiology*, *47*(3), 563-570.

Alix, A., C. Vergnet, and T. Mercier (2009), Risks to bees from dusts emitted at sowing of coated seeds: concerns, risk assessment and risk management, edited, pp. 131-132, Julius Kühn Institut, Bundesforschungsinstitut für Kulturpflanzen, Quedlinburg.

Allaire, S. E., S. Roulier, and A. J. Cessna (2009), Quantifying preferential flow in soils: A review of different techniques, *Journal of Hydrology*, *378*(1), 179-204.

Alletto, L., Y. Coquet, P. Benoit, D. Heddadj, and E. Barriuso (2010), Tillage management effects on pesticide fate in soils. A review, *Agronomy for sustainable development*, *30*(2), 367-400.

Anderson, J., C. Dubetz, and V. Palace (2015), Neonicotinoids in the Canadian aquatic environment: a literature review on current use products with a focus on fate, exposure, and biological effects, *Science of the Total Environment*, *505*, 409-422.

Anderson, T. A., C. J. Salice, R. A. Erickson, S. T. McMurry, S. B. Cox, and L. M. Smith (2013), Effects of landuse and precipitation on pesticides and water quality in playa lakes of the southern high plains, *Chemosphere*, *92*(1), 84-90.

Banerjee, K., S. H. Patil, S. Dasgupta, D. P. Oulkar, and P. G. Adsule (2008), Sorption of thiamethoxam in three Indian soils, *J Environ Sci Health B*, *43*(2), 151-156.

Barbash, J. E., and E. A. Resek (1996), *Pesticides in ground water: distribution, trends, and governing factors*, Ann Arbor Press.

Beketov, M. A., and M. Liess (2008), Potential of 11 pesticides to initiate downstream drift of stream macroinvertebrates, *Archives of environmental contamination and toxicology*, *55*(2), 247-253.

Beven, K., and P. Germann (2013), Macropores and water flow in soils revisited, *Water Resources Research*, *49*(6), 3071-3092.

Boxall, A. B., P. Blackwell, R. Cavallo, P. Kay, and J. J. T. l. Tolls (2002), The sorption and transport of a sulphonamide antibiotic in soil systems, *131*(1-2), 19-28.

Boy-Roura, M., J. Mas-Pla, M. Petrovic, M. Gros, D. Soler, D. Brusi, and A. Menció (2018), Towards the understanding of antibiotic occurrence and transport in groundwater: Findings from the Baix Fluvià alluvial aquifer (NE Catalonia, Spain), *Science of the total environment*, *612*, 1387-1406.

Brann, D. E. (1998), Optimum row width for corn -- revisited.

Brann, D. E., A. O. Abaye, P. R. Peterson, D. R. Chalmers, D. L. Whitt, G. F. Chappell, D. A. Herbert, S. McNeill, J. Baker, and S. J. Donohue (2009), Agronomy handbook.

Bundt, M., A. Albrecht, P. Froidevaux, P. Blaser, and H. Flühler (2000), Impact of preferential flow on radionuclide distribution in soil, *Environmental science & technology*, *34*(18), 3895-3899.

Chee-Sanford, J. C., R. I. Mackie, S. Koike, I. G. Krapac, Y.-F. Lin, A. C. Yannarell, S. Maxwell, and R. I. Aminov (2009), Fate and transport of antibiotic residues and antibiotic resistance genes following land application of manure waste, *Journal of environmental quality*, *38*(3), 1086-1108.

Chen, C., P. Ray, K. F. Knowlton, A. Pruden, and K. Xia (2018), Effect of composting and soil type on dissipation of veterinary antibiotics in land-applied manures, *Chemosphere*, *196*, 270-279.

Codling, G., Y. Al Naggar, J. P. Giesy, and A. J. Robertson (2016), Concentrations of neonicotinoid insecticides in honey, pollen and honey bees (Apis mellifera L.) in central Saskatchewan, Canada, *Chemosphere*, *144*, 2321-2328.

Collignon, P. C., J. M. Conly, A. Andremont, S. A. McEwen, A. Aidara-Kane, B. M. o. I. S. o. A. R. World Health Organization Advisory Group, Y. Agerso, A. Andremont, P. Collignon, and J. Conly (2016), World Health Organization ranking of antimicrobials according to their importance in human medicine: a critical step for developing risk management strategies to control antimicrobial resistance from food animal production, *Clinical Infectious Diseases*, *63*(8), 1087-1093.

Commission, E. (2002), Commission Decision of 12 August 2002 implementing Council Directive 96/23/EC concerning the performance of analytical methods and the interpretation of results, *Off. J. Eur. Commun.*, *221*, 8-36.

Conover, W. J. (2012), The rank transformation-an easy and intuitive way to connect many nonparametric methods to their parametric counterparts for seamless teaching introductory statistics courses, *Wiley Interdisciplinary Reviews: Computational Statistics*, *4*(5), 432-438.

Conover, W. J., and R. L. Iman (1981), Rank Transformations as a Bridge between Parametric and Nonparametric Statistics, *The American Statistician*, *35*(3), 124-129.

Cox, L., W. C. Koskinen, and P. Y. Yen (1997), Sorption− desorption of imidacloprid and its metabolites in soils, *Journal of agricultural and food chemistry*, *45*(4), 1468-1472.

Cox, L., A. Cecchi, R. Celis, M. C. Hermosín, W. C. Koskinen, and J. Cornejo (2001), Effect of Exogenous Carbon on Movement of Simazine and 2,4-D in Soils, *Soil Science Society of America Journal*, *65*, 1688-1695.

Cushman, J. A. (2017), Environmental Fate of Animal Manure-associated Antibiotics and Seed-coated Pesticide in Soils, Masters thesis, Virginia Tech.

D'Costa, V. M., C. E. King, L. Kalan, M. Morar, W. W. Sung, C. Schwarz, D. Froese, G. Zazula, F. Calmels, and R. Debruyne (2011), Antibiotic resistance is ancient, *Nature*, *477*(7365), 457.

Day, P. R. (1965), Particle fractionation and particle-size analysis, *Methods of soil analysis. Part 1. Physical and mineralogical properties, including statistics of measurement and sampling*, *9*(Agronomy), 545-567.

DCR, V. (2015), Virginia Nutrient Management Standards and Criteria. Richmond, VA, edited.

de Perre, C., T. M. Murphy, and M. J. Lydy (2015), Fate and effects of clothianidin in fields using conservation practices, *Environmental toxicology and chemistry*, *34*(2), 258-265.

Douglas, M. R., and J. F. Tooker (2015), Large-scale deployment of seed treatments has driven rapid increase in use of neonicotinoid insecticides and preemptive pest management in US field crops, *Environmental science & technology*, *49*(8), 5088-5097.

Douglas, M. R., J. R. Rohr, J. F. Tooker, and I. Kaplan (2015), EDITOR'S CHOICE: Neonicotinoid insecticide travels through a soil food chain, disrupting biological control of non-target pests and decreasing soya bean yield, *Journal of Applied Ecology*, *52*(1), 250-260.

Dykaar, B. B., and P. K. Kitandis (1996), Macrotransport of a biologically reacting solute through porous media, *Water Resources Research*, *32*, 307-320.

Elbert, A., M. Haas, B. Springer, W. Thielert, and R. Nauen (2008), Applied aspects of neonicotinoid uses in crop protection, *Pest management science*, *64*(11), 1099-1105.
EPA, U. (2010), Estimation Program Interface (EPI) Suite, edited, Ver.
Estévez, E., M. del Carmen Cabrera, A. Molina-Díaz, J. Robles-Molina, and M. del Pino Palacios-Díaz (2012), Screening of emerging contaminants and priority substances (2008/105/EC) in reclaimed water for irrigation and groundwater in a volcanic aquifer (Gran Canaria, Canary Islands, Spain), *Science of the Total environment*, *433*, 538-546.
Flühler, H., W. Durner, and M. Flury (1996), Lateral solute mixing processes—A key for understanding field-scale transport of water and solutes, *Geoderma*, *70*(2-4), 165-183.
Flury, M., H. Flühler, W. A. Jury, and J. Leuenberger (1994), Susceptibility of soils to preferential flow of water: A field study, *Water Resources Research*, *30*(7), 1945-1954.
FOCUS (2001), FOCUS Surface Water Scenarios in the EU Evaluation Process under 91/414/EEC: Report of the FOCUS Working Group on Surface Water Scenarios, edited, p. 245.
Gazis, C., and X. Feng (2004), A stable isotope study of soil water: evidence for mixing and preferential flow paths, *Geoderma*, *119*(1), 97-111.
Ghodrati, M., and W. A. Jury (1992), A field study of the effects of soil structure and irrigation method on preferential flow of pesticides in unsaturated soil, *Journal of contaminant Hydrology*, *11*(1-2), 101-125.
Girolami, V., M. Marzaro, L. Vivan, L. Mazzon, C. Giorio, D. Marton, and A. Tapparo (2013), Aerial powdering of bees inside mobile cages and the extent of neonicotinoid cloud surrounding corn drillers, *Journal of Applied Entomology*, *137*(1-2), 35-44.
Good, S. P., D. Noone, and G. Bowen (2015), Hydrologic connectivity constrains partitioning of global terrestrial water fluxes, *Science*, *349*(6244), 175-177.
Goulson, D., and D. Kleijn (2013), Review: An overview of the environmental risks posed by neonicotinoid insecticides, *Journal of Applied Ecology*, *50*(4), 977-987.
Graham, C. B., and H. S. Lin (2011), Controls and frequency of preferential flow occurrence: A 175-event analysis, *Vadose Zone Journal*, *10*(3), 816-831.
Greatti, M., R. Barbattini, A. Stravisi, A. G. Sabatini, and S. Rossi (2006), Presence of the ai imidacloprid on vegetation near corn fields sown with Gaucho® dressed seeds, *Bulletin of Insectology*, *59*(2), 99-103.
Greve, A., M. Andersen, and R. Acworth (2010), Investigations of soil cracking and preferential flow in a weighing lysimeter filled with cracking clay soil, *Journal of Hydrology*, *393*(1-2), 105-113.
Gupta, S., V. T. Gajbhiye, and R. K. Gupta (2008), Soil dissipation and leaching behavior of a neonicotinoid insecticide thiamethoxam, *Bulletin of environmental contamination and toxicology*, *80*(5), 431-437.
Hajek, B., F. Adams, and J. Cope (1972), Rapid Determination of Exchangeable Bases, Acidity, and Base Saturation for Soil Characterization 1, *Soil Science Society of America Journal*, *36*(3), 436-438.
Hallmann, C. A., R. P. Foppen, C. A. van Turnhout, H. de Kroon, and E. Jongejans (2014), Declines in insectivorous birds are associated with high neonicotinoid concentrations, *Nature*, *511*(7509), 341-343.
Hardie, M. A., W. E. Cotching, R. B. Doyle, G. Holz, S. Lisson, and K. Mattern (2011), Effect of antecedent soil moisture on preferential flow in a texture-contrast soil, *Journal of Hydrology*, *398*(3-4), 191-201.

Hartz, K. E. H., T. M. Edwards, and M. J. J. E. Lydy (2017), Fate and transport of furrow-applied granular tefluthrin and seed-coated clothianidin insecticides: Comparison of field-scale observations and model estimates, *26*(7), 876-888.

Hassanpour, B., B. K. Richards, L. D. Goehring, J.-Y. Parlange, and T. S. J. V. Z. J. Steenhuis (2019), Predicting the Fate of Preferentially Moving Herbicides, *18*(1).

Heathman, G., D. Timlin, L. Ahuja, and K. Johnsen (1995), Surface aggregates and macropore effects on chemical transport in soil under rainfall, *Soil Science Society of America Journal*, *59*(4), 990-997.

Heuer, H., H. Schmitt, and K. Smalla (2011), Antibiotic resistance gene spread due to manure application on agricultural fields, *Current opinion in microbiology*, *14*(3), 236-243.

Hladik, M. L., D. W. Kolpin, and K. M. Kuivila (2014a), Widespread occurrence of neonicotinoid insecticides in streams in a high corn and soybean producing region, USA, *Environmental Pollution 193*, 189-196.

Hladik, M. L., D. W. Kolpin, and K. M. Kuivila (2014b), Widespread occurrence of neonicotinoid insecticides in streams in a high corn and soybean producing region, USA, *Environmental pollution*, *193*, 189-196.

Hrachowitz, M., H. Savenije, T. Bogaard, D. Tetzlaff, C. J. H. Soulsby, and E. S. Sciences (2013), What can flux tracking teach us about water age distribution patterns and their temporal dynamics?

Hu, Q., and M. L. Brusseau (1996), Transport of rate-limited sorbing solutes in an aggregated porous medium: A multiprocess non-ideality approach, *Journal of contaminant hydrology*, *24*(1), 53-73.

Humphry, J., T. Daniel, D. Edwards, and A. Sharpley (2002), A portable rainfall simulator for plot–scale runoff studies, *Applied Engineering in Agriculture*, *18*(2), 199.

Ionescu, A. (1969), Suction force variation in double-hybrid maize as a function of soil moisture, *Biologia Plantarum*, *11*(5), 370-374.

Jarvis, N. (2007a), A review of non-equilibrium water flow and solute transport in soil macropores: Principles, controlling factors and consequences for water quality, *European Journal of Soil Science*, *58*(3), 523-546.

Jarvis, N. J. (2007b), A review of non-equilibrium water flow and solute transport in soil macropores: principles, controlling factors and consequences for water quality, *European Journal of Soil Science*, *58*(3), 523-546.

Jeschke, P., and R. Nauen (2007), Nicotinic acetylcholine receptor agonists, target and selectivity aspects, *Modern Crop Protection Compounds*, *3*, 1127-1165.

Jeschke, P., R. Nauen, M. Schindler, and A. Elbert (2011), Overview of the status and global strategy for neonicotinoids, *Journal of agricultural and food chemistry*, *59*(7), 2897-2908.

Jones, A., P. Harrington, and G. Turnbull (2014), Neonicotinoid concentrations in arable soils after seed treatment applications in preceding years, *Pest management science*, *70*(12), 1780-1784.

Jørgensen, P. R., M. Hoffmann, J. P. Kistrup, C. Bryde, R. Bossi, and K. G. Villholth (2002), Preferential flow and pesticide transport in a clay-rich till: Field, laboratory, and modeling analysis, *Water Resources Research*, *38*(11), 28-21-28-15.

Katagi, T. (2013), Soil Column Leaching of Pesticides, in *Reviews of Environmental Contamination and Toxicology Volume 221*, edited, pp. 1-105, Springer.

Kay, P., P. A. Blackwell, and A. Boxall (2004), Fate of veterinary antibiotics in a macroporous tile drained clay soil, *Environmental Toxicology and Chemistry*, *23*(5), 1136-1144.
Kay, P., P. A. Blackwell, and A. B. Boxall (2005a), A lysimeter experiment to investigate the leaching of veterinary antibiotics through a clay soil and comparison with field data, *Environmental Pollution*, *134*(2), 333-341.
Kay, P., P. A. Blackwell, and A. B. Boxall (2005b), Column studies to investigate the fate of veterinary antibiotics in clay soils following slurry application to agricultural land, *Chemosphere*, *60*(4), 497-507.
Kladivko, E., G. Van Scoyoc, E. Monke, K. Oates, and W. Pask (1991), Pesticide and nutrient movement into subsurface tile drains on a silt loam soil in Indiana, *Journal of environmental quality*, *20*(1), 264-270.
Klarich, K. L., N. C. Pflug, E. M. DeWald, M. L. Hladik, D. W. Kolpin, D. M. Cwiertny, and G. H. LeFevre (2017), Occurrence of neonicotinoid insecticides in finished drinking water and fate during drinking water treatment, *Environmental Science & Technology Letters*, *4*, 168-173.
Klaus, J., E. Zehe, M. Elsner, C. Külls, and J. McDonnell (2013), Macropore flow of old water revisited: experimental insights from a tile-drained hillslope, *Hydrology and Earth System Sciences*, *17*(1), 103-118.
Klein, M. (1994), Evaluation and comparison of pesticide leaching models for registration purposes. Results of simulations performed with the pesticide leaching model, *Journal of Environmental Science & Health Part A*, *29*(6), 1197-1209.
Koleva, N. G., and U. A. Schneider (2010), The impact of climate change on aquatic risk from agricultural pesticides in the US, *International Journal of Environmental Studies*, *67*(5), 677-704.
Kulesza, S. B., R. O. Maguire, K. Xia, J. Cushman, K. Knowlton, and P. Ray (2016), Manure injection affects the fate of pirlimycin in surface runoff and soil, *Journal of environmental quality*, *45*(2), 511-518.
Kunkel, K. E., T. R. Karl, H. Brooks, J. Kossin, J. H. Lawrimore, D. Arndt, L. Bosart, D. Changnon, S. L. Cutter, and N. Doesken (2013), Monitoring and understanding trends in extreme storms: State of knowledge, *Bulletin of the American Meteorological Society*, *94*(4), 499-514.
Kurwadkar, S., R. Wheat, D. G. McGahan, and F. Mitchell (2014a), Evaluation of leaching potential of three systemic neonicotinoid insecticides in vineyard soil, *Journal of contaminant hydrology*, *170*, 86-94.
Kurwadkar, S., R. Wheat, D. G. McGahan, and F. Mitchell (2014b), Evaluation of leaching potential of three systemic neonicotinoid insecticides in vineyard soil, *Journal of contaminant hydrology*, *170*, 86-94.
Lamers, M., M. Anyusheva, N. La, V. V. Nguyen, and T. Streck (2011), Pesticide pollution in surface-and groundwater by paddy rice cultivation: a case study from northern Vietnam, *Clean–Soil, Air, Water*, *39*(4), 356-361.
Larsson, M., and N. Jarvis (1999), Evaluation of a dual-porosity model to predict field-scale solute transport in a macroporous soil, *Journal of Hydrology*, *215*(1-4), 153-171.
Larsson, M. H., and N. J. Jarvis (2000), Quantifying interactions between compound properties and macropore flow effects on pesticide leaching, *Pest Management Science*, *56*(2), 133-141.
Lauer, J. (2009), Corn plant density for maximum grain and silage production, edited.

Le, H. T., R. O. Maguire, and K. J. J. o. E. Q. Xia (2018), Method of dairy manure application and time before rainfall affect antibiotics in surface runoff.

Leaney, F., K. Smettem, and D. Chittleborough (1993), Estimating the contribution of preferential flow to subsurface runoff from a hillslope using deuterium and chloride, *Journal of Hydrology*, *147*(1-4), 83-103.

Leiva, J. A., P. Nkedi-Kizza, K. T. Morgan, and J. A. Qureshi (2015), Imidacloprid sorption kinetics, equilibria, and degradation in sandy soils of Florida, *Journal of agricultural and food chemistry*, *63*(20), 4915-4921.

Li, Y., P. Su, Y. Li, K. Wen, G. Bi, and M. Cox (2018), Adsorption-desorption and degradation of insecticides clothianidin and thiamethoxam in agricultural soils, *Chemosphere*, *207*, 708-714.

Limay-Rios, V., L. G. Forero, Y. Xue, J. Smith, T. Baute, and A. Schaafsma (2016), Neonicotinoid insecticide residues in soil dust and associated parent soil in fields with a history of seed treatment use on crops in southwestern Ontario, *Environmental Toxicology and Chemistry*, *35*(2), 303-310.

Main, A. R., N. L. Michel, J. V. Headley, K. M. Peru, and C. A. Morrissey (2015), Ecological and Landscape Drivers of Neonicotinoid Insecticide Detections and Concentrations in Canada's Prairie Wetlands, *Environmental science & technology*, *49*(14), 8367-8376.

Main, A. R., N. L. Michel, M. C. Cavallaro, J. V. Headley, K. M. Peru, and C. A. Morrissey (2016), Snowmelt transport of neonicotinoid insecticides to Canadian Prairie wetlands, *Agriculture, Ecosystems & Environment*, *215*, 76-84.

Mallants, D., M. T. Van Genuchten, J. Šimůnek, D. Jacques, and S. Seetharam (2011), Leaching of contaminants to groundwater, in *Dealing with Contaminated Sites*, edited, pp. 787-850, Springer.

McCance, W., O. Jones, M. Edwards, A. Surapaneni, S. Chadalavada, and M. Currell (2018), Contaminants of emerging concern as novel groundwater tracers for delineating wastewater impacts in urban and peri-urban areas, *Water research*.

McGrath, G. S., C. Hinz, and M. Sivapalan (2009), A preferential flow leaching index, *Water resources research*, *45*(11).

McGuire, K. J., and J. J. McDonnell (2006), A review and evaluation of catchment transit time modeling, *Journal of Hydrology*, *330*(3-4), 543-563.

McWilliams, D. A., D. R. Berglund, and G. Endres (2010), Corn growth and management quick guide.

Miranda, G. R., C. G. Raetano, E. Silva, M. A. Daam, and M. J. Cerejeira (2011), Environmental fate of neonicotinoids and classification of their potential risks to hypogean, epygean, and surface water ecosystems in Brazil, *Human and Ecological Risk Assessment: An International Journal*, *17*(4), 981-995.

Molz, F. (2015), Advection, dispersion, and confusion, *Ground Water*, *53*(3), 348-353.

Montforts, M. H., D. F. Kalf, P. L. van Vlaardingen, and J. B. Linders (1999), The exposure assessment for veterinary medicinal products, *Science of the total environment*, *225*(1-2), 119-133.

Myresiotis, C. K., Z. Vryzas, and E. Papadopoulou-Mourkidou (2012), Biodegradation of soil-applied pesticides by selected strains of plant growth-promoting rhizobacteria (PGPR) and their effects on bacterial growth, *Biodegradation*, *23*(2), 297-310.

Nham, H. T. T., J. Greskowiak, K. Nödler, M. A. Rahman, T. Spachos, B. Rusteberg, G. Massmann, M. Sauter, and T. Licha (2015), Modeling the transport behavior of 16

emerging organic contaminants during soil aquifer treatment, *Science of the Total Environment*, *514*, 450-458.
Nimmo, J. R. (2012), Preferential flow occurs in unsaturated conditions, *Hydrological Processes*, *26*(5), 786-789.
Nuyttens, D., W. Devarrewaere, P. Verboven, and D. Foqué (2013), Pesticide-laden dust emission and drift from treated seeds during seed drilling: a review, *Pest management science*, *69*(5), 564-575.
O'Dell, J. D., J. D. Wolt, and P. M. Jardine (1992), Transport of imazethapyr in undisturbed soil columns, *Soil Science Society of America Journal*, *56*(6), 1711-1715.
Oi, M. (1999), Time-dependent sorption of imidacloprid in two different soils, *Journal of agricultural and food chemistry*, *47*(1), 327-332.
Øygarden, L., J. Kværner, and P. Jenssen (1997), Soil erosion via preferential flow to drainage systems in clay soils, *Geoderma*, *76*(1-2), 65-86.
Peterson, E. W., and C. M. Wicks (2005), Fluid and solute transport from a conduit to the matrix in a carbonate aquifer system, *Mathematical geology*, *37*(8), 851-867.
Pignatello, J. J., and B. Xing (1995), Mechanisms of slow sorption of organic chemicals to natural particles, *Environmental science & technology*, *30*(1), 1-11.
Radolinski, J., J. Wu, K. Xia, and R. Stewart (2018a), Transport of a neonicotinoid pesticide, thiamethoxam, from artificial seed coatings, *Science of the Total Environment*, *618*, 561-568.
Radolinski, J., J. Wu, K. Xia, W. C. Hession, and S. Stewart (2018b), Transport of a Neonicotinoid Pesticide under Field Conditions, *Chemosphere (pre-print)*.
Radolinski, J., J. Wu, K. Xia, W. C. Hession, and R. D. Stewart (2019), Plants mediate precipitation-driven transport of a neonicotinoid pesticide, *Chemosphere*, *222*, 445-452.
Raes, D., and G. Munoz (2009), The ETo Calculator, *Reference Manual Version*, *3*.
Richard, T. L., and T. S. Steenhuis (1988), Tile drain sampling of preferential flow on a field scale, *Journal of Contaminant Hydrology*, *3*(2-4), 307-325.
Roger, E., A. Mahdi, and H. Mark (2013), Corn seeding depth: back to the basics, Iowa State University Extension Iowa State University.
Samson-Robert, O., G. Labrie, M. Chagnon, and V. Fournier (2014), Neonicotinoid-contaminated puddles of water represent a risk of intoxication for honey bees, *PloS one*, *9*(12), e108443.
Sanchez-Bayo, F. (2014a), Environmental science. The trouble with neonicotinoids, *Science*, *346*(6211), 806-807.
Sanchez-Bayo, F. (2014b), Environmental science. The trouble with neonicotinoids, *Science*, *346*(6211), 806-807.
Sanchez-Bayo, F., and K. Goka (2014), Pesticide residues and bees--a risk assessment, *PloS one*, *9*(4), e94482.
Sánchez-Bayo, F., K. Goka, and D. Hayasaka (2016), Contamination of the aquatic environment with neonicotinoids and its implication for ecosystems, *Frontiers in Environmental Science*, *4*, 71.
Sandrock, C., L. G. Tanadini, J. S. Pettis, J. C. Biesmeijer, S. G. Potts, and P. Neumann (2014), Sublethal neonicotinoid insecticide exposure reduces solitary bee reproductive success, *Agricultural and Forest Entomology*, *16*(2), 119-128.

Scaini, A., N. Amvrosiadi, C. Hissler, L. Pfister, and K. Beven (2019), Following tracer through the unsaturated zone using a Multiple Interacting Pathways model: implications from laboratory experiments, *Hydrological Processes*, *33*.

Schaafsma, A., V. Limay-Rios, T. Baute, J. Smith, and Y. Xue (2015), Neonicotinoid insecticide residues in surface water and soil associated with commercial maize (corn) fields in southwestern Ontario, *PloS one*, *10*(2), e0118139.

Schnoebelen, D. J., S. J. Kalkhoff, K. D. Becher, and E. Thurman (2003), Water-quality assessment of the eastern Iowa basins: Selected pesticides and pesticide degradates in streams, 1996–98, *US Geological Survey Water-Resources Investigations Report*, *3*(4075), 62.

SERA-17 (2008), National research project for simulated rainfall: Surface runoff studies, edited.

Smalling, K. L., M. L. Hladik, C. J. Sanders, K. M. J. J. o. E. S. Kuivila, and P. B. Health (2018), Leaching and sorption of neonicotinoid insecticides and fungicides from seed coatings, *53*(3), 176-183.

Sprenger, M., H. Leistert, K. Gimbel, and M. Weiler (2016), Illuminating hydrological processes at the soil-vegetation-atmosphere interface with water stable isotopes, *Reviews of Geophysics*, *54*(3), 674-704.

Starner, K., and K. S. Goh (2012a), Detections of the neonicotinoid insecticide imidacloprid in surface waters of three agricultural regions of California, USA, 2010-2011, *Bulletin of environmental contamination and toxicology*, *88*(3), 316-321.

Starner, K., and K. S. Goh (2012b), Detections of the neonicotinoid insecticide imidacloprid in surface waters of three agricultural regions of California, USA, 2010-2011, *Bull Environ Contam Toxicol*, *88*(3), 316-321.

Steenhuis, T. S., J. Boll, G. Shalit, J. S. Selker, and I. A. Merwin (1994), A simple equation for predicting preferential flow solute concentrations, *Journal of Environmental Quality*, *23*(5), 1058-1064.

Stewart, R. D., D. E. Rupp, M. R. A. Najm, and J. S. Selker (2016), A unified model for soil shrinkage, subsidence, and cracking, *Vadose Zone Journal*, *15*(3).

Stone, W. W., R. J. Gilliom, and K. R. Ryberg (2014), Pesticides in U.S. streams and rivers: occurrence and trends during 1992-2011, *Environmental Science & Technology 48*(19), 11025-11030.

Straw, A. (2009), Vegetable Planting Guide and Recommended Planting Dates.

Stumpp, C., and P. Maloszewski (2010), Quantification of preferential flow and flow heterogeneities in an unsaturated soil planted with different crops using the environmental isotope δ 18 O, *Journal of Hydrology*, *394*(3), 407-415.

Stumpp, C., P. Maloszewski, W. Stichler, and S. Maciejewski (2007), Quantification of the heterogeneity of the unsaturated zone based on environmental deuterium observed in lysimeter experiments, *Hydrological Sciences Journal*, *52*(4), 748-762.

Tapparo, A., D. Marton, C. Giorio, A. Zanella, L. Solda, M. Marzaro, L. Vivan, and V. Girolami (2012), Assessment of the environmental exposure of honeybees to particulate matter containing neonicotinoid insecticides coming from corn coated seeds, *Environmental science & technology*, *46*(5), 2592-2599.

Thiele-Bruhn, S. (2003), Pharmaceutical antibiotic compounds in soils–a review, *Journal of plant nutrition and soil science*, *166*(2), 145-167.

Thurman, E. M., D. A. Goolsby, M. T. Meyer, M. S. Mills, M. L. Pomes, and D. W. Kolpin (1992), A reconnaissance study of herbicides and their metabolites in surface water of the

midwestern United States using immunoassay and gas chromatography/mass spectrometry, *Environmental science & technology*, *26*(12), 2440-2447.
Tosi, S., G. Burgio, and J. C. Nieh (2017), A common neonicotinoid pesticide, thiamethoxam, impairs honey bee flight ability, *Scientific reports*, *7*(1), 1201.
Traub-Eberhard, U., W. Kördel, and W. Klein (1994), Pesticide movement into subsurface drains on a loamy silt soil, *Chemosphere*, *28*(2), 273-284.
Twarakavi, N. K., M. Sakai, and J. J. W. R. R. Šimůnek (2009), An objective analysis of the dynamic nature of field capacity, *45*(10).
Uğurlu, P., E. Ünlü, and E. I. Satar (2015), The toxicological effects of thiamethoxam on Gammarus kischineffensis (Schellenberg 1937)(Crustacea: Amphipoda), *Environmental toxicology and pharmacology*, *39*(2), 720-726.
USDA (2017), Acreage, edited by A. S. B. National Agricultural Statistics Service (NASS), United States Department of and A. (USDA).
USEPA (2008), Fate, Transport and Transformation Test Guidelines: OPPTS 835.0001 Principles and Strategies Related to Biodegradation Testing of Organic Chemicals under the Toxic Substances Control Act (TSCA), edited.
UVA (2015), University of Virginia Climatology Office, edited, Charlottesville, VA.
van Geldern, R., J. A. J. L. Barth, and O. Methods (2012), Optimization of instrument setup and post-run corrections for oxygen and hydrogen stable isotope measurements of water by isotope ratio infrared spectroscopy (IRIS), *10*(12), 1024-1036.
Van Genuchten, M. T., and R. Cleary (1979), Movement of solutes in soil: Computer-simulated and laboratory results, in *Developments in soil science*, edited, pp. 349-386, Elsevier.
Vogel, T., M. Sanda, J. Dusek, M. Dohnal, and J. Votrubova (2010), Using oxygen-18 to study the role of preferential flow in the formation of hillslope runoff, *Vadose Zone Journal*, *9*(2), 252-259.
Vryzas, Z. (2018), Pesticide fate in soil-sediment-water environment in relation to contamination preventing actions, *Current Opinion in Environmental Science & Health*, *4*, 5-9.
Wade, T., R. L. Claassen, and S. Wallander (2015), *Conservation-Practice Adoption Rates Vary Widely by Crop and Region*, United States Department of Agriculture, Economic Research Service.
Wegst-Uhrich, S. R., D. A. Navarro, L. Zimmerman, and D. S. Aga (2014), Assessing antibiotic sorption in soil: a literature review and new case studies on sulfonamides and macrolides, *Chemistry Central Journal*, *8*(1), 5.
Wettstein, F. E., R. Kasteel, M. F. Garcia Delgado, I. Hanke, S. Huntscha, M. E. Balmer, T. Poiger, and T. D. Bucheli (2016), Leaching of the neonicotinoids thiamethoxam and imidacloprid from sugar beet seed dressings to subsurface tile drains, *Journal of agricultural and food chemistry*, *64*(33), 6407-6415.
White, R., G. Thomas, and M. Smith (1984), Modelling water flow through undisturbed soil cores using a transfer function model derived from 3HOH and Cl transport, *Journal of soil science*, *35*(2), 159-168.
Whitehorn, P. R., S. O'Connor, F. L. Wackers, and D. Goulson (2012), Neonicotinoid pesticide reduces bumble bee colony growth and queen production, *Science*, *336*(6079), 351-352.
Wind, L., L.-A. Krometis, W. C. Hession, C. Chen, P. Du, K. Jacobs, K. Xia, and A. Pruden (2018), Fate of pirlimycin and antibiotic-resistant fecal coliforms in field plots amended with dairy manure or compost during vegetable cultivation, *Journal of environmental quality*, *47*(3), 436-444.

Worthington, S. R. (2019), How preferential flow delivers pre-event groundwater rapidly to streams, *Hydrological Processes*.
Zalom, F. G., N. Toscano, and F. J. Byrne (2005), Managing resistance is critical to future use of pyrethroids and neonicotinoids, *California Agriculture*, *59*(1), 11-15.
Zhang, P., C. Ren, H. Sun, and L. Min (2018a), Sorption, desorption and degradation of neonicotinoids in four agricultural soils and their effects on soil microorganisms, *Science of The Total Environment*, *615*, 59-69.
Zhang, Y., Z. Zhang, Z. Ma, J. Chen, J. Akbar, S. Zhang, C. Che, M. Zhang, and A. Cerdà (2018b), A review of preferential water flow in soil science, *Canadian Journal of Soil Science*, *98*(4), 604-618.

# Appendix A (Appendix for Chapter 2)

## A1 Background TMX in Soil

At each field location loose soil samples ($n$ = 6 per soil) were taken from the $A_p$ (0-20 cm) and $B_t$ (20-60 cm) horizons and combined into one aggregate sample per soil type and horizon. These soils were then analyzed for background concentrations of TMX prior to the column leaching experiment (**Table A1a** and **Table A1b**). Though TMX concentrations were three orders of magnitude higher than the detection limit in the sand $B_t$ layer, it was assumed, based on the relatively rapid transport observed in the main study, that the majority of mass in this lower layer leached out of the column after the pre-experiment saturation event. Additionally, by the V1 corn stage (8 days of growth), the highest concentrations of TMX found in sand $B_t$ soil (0.599 µg $kg^{-1}$; 30-45 cm) were nearly an order of magnitude less than those detected in the field (5.92 µg $kg^{-1}$), suggesting that the majority of background TMX was removed by the start of the leaching experiment.

**Table A1a**. Background levels of TMX in soil

| | | Background TMX | |
|---|---|---|---|
| **Soil** | **Depth (cm)** | **TMX (µg $kg^{-1}$)** | **TMX (µg)** |
| **Loam $A_p$** | 0-20 | 0.30 | 2.58 |
| **Loam $B_t$** | 20-60 | 0.37 | 7.63 |
| **Sand $A_p$** | 0-20 | 0.52 | 4.97 |
| **Sand $B_t$** | 20-60 | 5.92 | 124 |

**Table A1b.** Background TMX in 60 cm Soil Columns Compared to Total Mass from Seeds

| Soil | Background TMX / TMX from Seeds |
|---|---|
| **Loam** | 0.0057 |
| **Sand** | 0.072 |

## A2 Column Design Details

Following packing, all soil columns were fitted with a flat PVC end cap containing a 1.3 cm thread to 0.64 cm barbed hose fitting. 1 cm of mixed sand (fine and coarse grained) was placed between the cap and the bottom soil surface to maintain hydraulic connection between the soil and outlet drain. 1 g of glass wool was added inside the hose fitting and a 250 µm steel mesh screen was sealed above the fitting to prevent fine soil particles from leaching.

To minimize the erosion of surface soil and formation of preferential flow pathways, 2 g of glass wool was placed on top of the soil column, and 8 g of sodium bentonite was applied to the soil-PVC interface. All columns were housed in a greenhouse with a constant temperature of 24 °C.

## A3 Details to Soil Characterization

Soil pH was measured in a 1:1 (soil weight: $CaCl_2$) suspension. CEC was determined colorimeterically via ammonium acetate at pH 7 with a Lachat Quickchem 8500 autoanalyzer. TOC was quantified by dry combustion using a Vario MAX CNS macro elemental analyzer (Elementar, Hanau, Germany). Soil texture was obtained via the pipet method [*Day*, 1965].

## A4 Experimental Design

**Figure A1** shows treatment structure for the TMX Leachate and Distribution study.

## A5 Analytical Approach

Prior to analysis, plant tissue samples were frozen with liquid $N_2$, ground, freeze-dried and stored at -20 °C. Soil samples were homogenized, freeze-dried and stored at -20 °C. For extraction of TMX, 10 mL of acetonitrile was added to either 1 g of dried soil or 0.2 g of tissue in a 35 mL glass centrifuge tube and vortexed for 10 seconds. The centrifuge tube was then filled with 0.5 g of sodium chloride and 2 g of anhydrous magnesium sulfate, vortexed for 2

minutes, and centrifuged at 10,000 rpm for 10 minutes at 15°C. The supernatant was transferred into a 35 mL centrifuge vial with 0.5 g of anhydrous magnesium sulfate and 0.10 g of Primary Secondary Amine (PSA). Another 5 mL of acetonitrile was added to extract targets, as described above, and the two resulting supernatants were combined, vortexed for 1 min, and centrifuged at 4,000 rpm for 5 minutes at 15 °C. A 5.0 mL aliquot was extracted from the supernatant, transferred into a glass vial, and dried in a Rapidvap. The dehydrated sample was then reconstituted by adding 1 mL of 5 mM $NH_4Ac$-$H_2O$ and $NH_4Ac$-MeOH, filtered with a 0.2 µm polyvinylidene fluoride filter (Fisher, USA), and added to an amber glass vial for analysis via UPLC-MS/MS. For column leachate preparation, samples were filtered twice through a polyvinylidene fluoride syringe filter (0.45 µm and 0.2 µm, respectively), and transferred into an amber glass for analysis via UPLC-MS/MS.

Seeds recovered for TMX extraction were added to a 35 mL glass centrifuge with 10 mL of acetonitrile, sonicated for 20 mins, and centrifuged at 4,000 rpm for 10 minutes at 15 °C. A 50 µL aliquot of supernatant was dried via Rapidvap and diluted in 1 mL of 5 mM NH4Ac-H2O and 5 mM NH4Ac-MeOH. The reconstituted sample was then filtered with a 0.2 µm polyvinylidene fluoride filter (Fisher, USA), and added to an amber glass vial for analysis via UPLC-MS/MS.

TMX was detected using an Agilent 1290 UPLC coupled with Agilent 6490 Triple Quad tandem mass spectrometry. Separation occurred on a Zorbax Extend-C18 Column (4.6 × 50mm, 5 µm; Agilent, USA) at 30°C, using a mobile phase of (A) 5 mM $NH_4Ac$-$H_2O$ and (B) $NH_4Ac$-MeOH at a flow rate of 0.5 mL $min^{-1}$. Samples were subject to gradient elution at t = 0, 5, 6, 6.5, and 9.5 mins and A:B v/v ratios of 90:10, 5:95, 5:95, 90:10 and 90:10. The operation was performed using the positive ion mode with a desolvation gas flow rate of 14.0 L $min^{-1}$, gas

temperature of 250 °C, capillary voltage of 3000 V, and nebulizer gas pressure of 45.0 psi. The multiple reaction monitoring mode was used, with a resulting detection limit of 0.005 ng $g^{-1}$.

## A6 Statistical Analysis of Ancillary Data

Total soil organic carbon (TOC) and cation exchange capacity (CEC) were analyzed via one way ANOVAs ($n$ = 6 per soil type). For estimated cumulative ET,

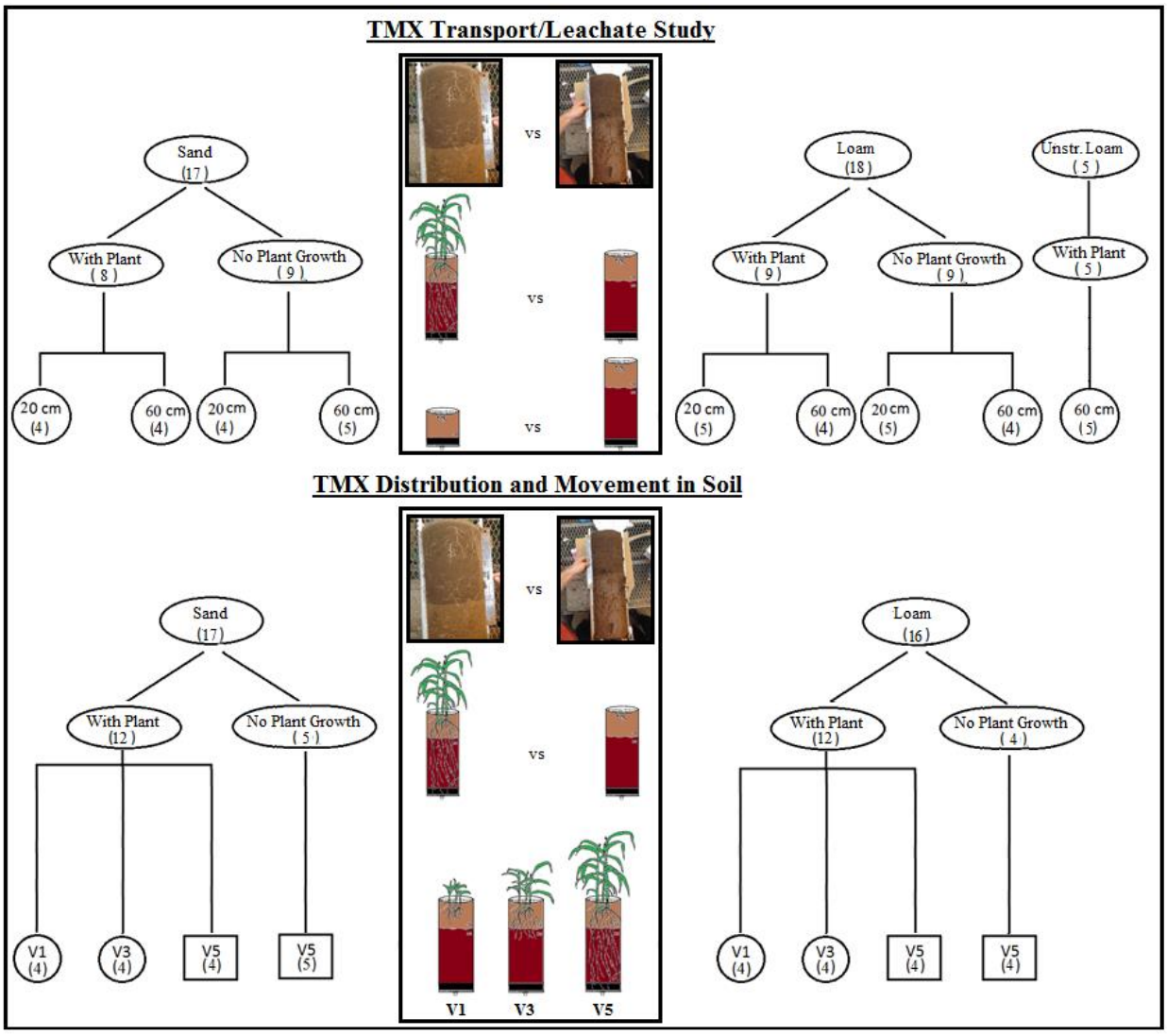


**Figure A1.** Treatment structure for the two studies (TMX Transport and Distribution) with number of column replicates in parentheses. Square outlines indicate columns also used in transport study.

two way ANOVAs were conducted on log-transformed data whereby texture and plant influence (plant and no plant) were treated as factors. Two way ANOVAs were conducted on TMX mass (**Figure A3**) and log transformed concentrations in plant-associated soil, again, treating plant influence and texture as factors. For TMX concentration in plant associated soil a combined V5, No Plant treatment (comprised of seed soil) was created to understand the effect of corn plant growth on TMX distribution. Normality was determined via visual inspection of histogram and normal quantile plot results. Homogeneity of variances was confirmed via Fligner's test. Tukey's multiple comparisons test was run on all resulting ANOVA results. All statistical tests were conducted in R version 3.2.2 with an alpha level of 0.05.

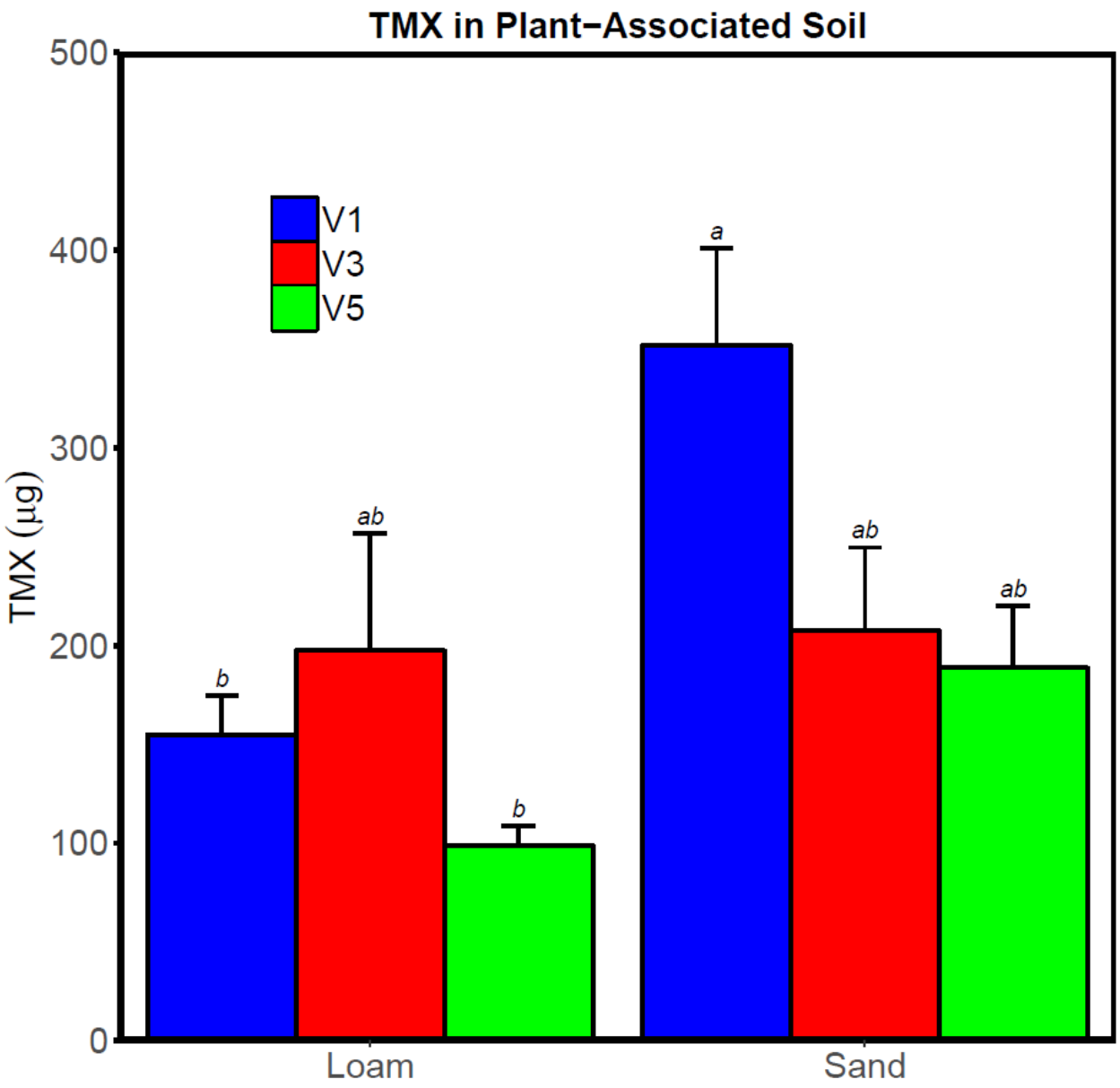


**Figure A2.** TMX mass recovered in plant-associated soil (combined from root and rhizosphere soil). V5 No Plant treatment represents seed soil (see description in Methods section). Error bars represent SE and different letters represent significant differences ($p \leq 0.05$)

## A7 Estimation of Evapotranspiration

Cumulative column Evapotranspiration (ET) was approximated by:

$$ET = I - L \quad [3]$$

where *ET* [L] represents evapotranspiration, *I* [L] is infiltration and *L* [L] is drainage in the form of column leachate. Column infiltration *I* was assumed to equal the amount of artificial precipitation applied, *P*. Equation [3] was applied on a cumulative basis over the entire experiment, with the assumption that the change in storage between the beginning and end of the experiment was zero (because the columns were at a water content close to field capacity in both cases). To convert cumulative ET into mean daily ET rates [L $T^{-1}$], the total amount estimated by Equation [3] was divided by the total number of elapsed days (i.e., 33 days). This approach assumed that the ET rate was constant throughout the experiment.

## A8 Details on Destructive Sampling of Soil

Trend discrepancies between TMX concentration and mass of soil in the 0-30 cm column section reflected differences in total root soil mass between corn stages, or decreases in total mass of bulk soil as the plant roots proliferated. For example, **Figure A2** reports slightly higher concentrations of TMX in V5 soil (sand, 0-30 cm) compared to V3 soil; however, in **Figure A4** relative differences between TMX mass in both stages are lower. In other words, by the V5 corn stage (as plant roots have grown in size and number) the mass of soil considered to be "root soil" had increased whereas the amount of bulk soil mass had decreased. Similarly, the trend of decreasing TMX concentrations in plant-associated soil through time (V1 to V5) as seen in **Figure A3** is not matched in terms of TMX mass for this section (**Figure A3**), where in the latter pesticide mass was found to increase from V1 to V3. Here, the significant decrease in TMX concentration between the two corn stages is counteracted by greater root soil mass at V3.

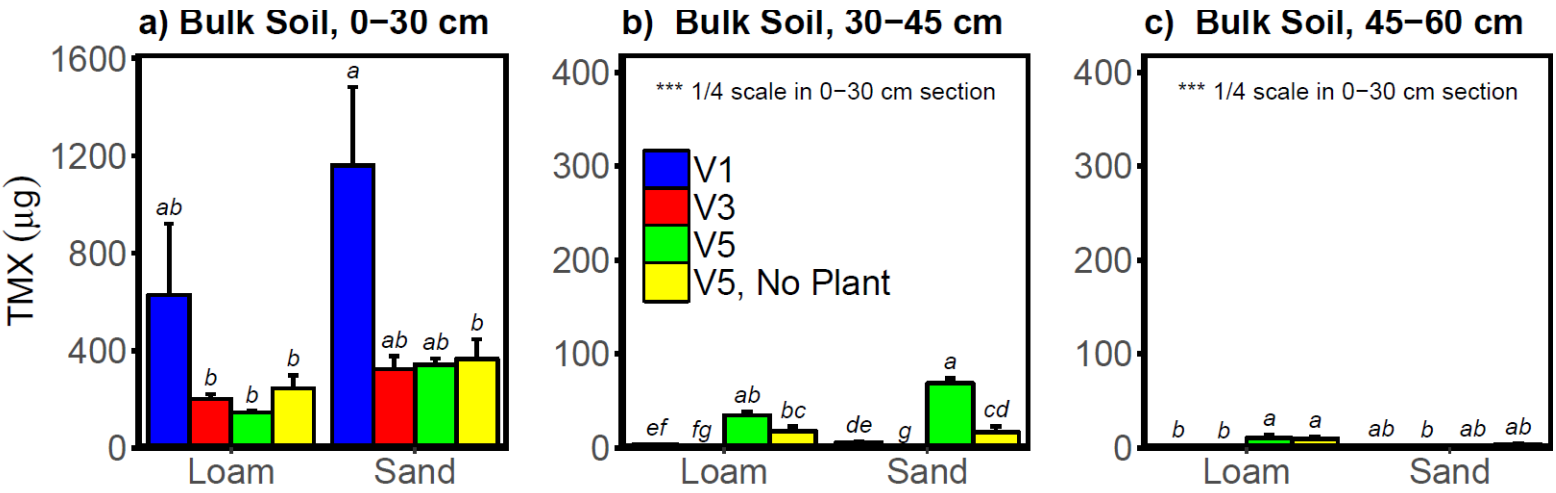


**Figure A3.** TMX mass recovered in bulk soil fractions 0-30 cm **a)**, 30-45 cm **b)**, and 45-60 cm **c)** over three corn stages (V1, V3, and V5). Error bars represent SE and different letters represent significant differences ($p \leq 0.05$). Y axes in 30-45 cm and 45-60 cm fractions are 25% that of the 0-30 cm section.

**Figure A4.** "sand" (**left** ) vs "loam" (**right**) soil columns (60 cm) cut longitudinally. Notice the layer of dry soil on the surface of the sand column, indicating higher ET (compared to loam columns) throughout the experiment.

# Appendix B (Appendix for Chapter 3)

## B1 Analytical Approach

The following methodology was adopted from *Radolinski et al.* [2018a] to measure thiamethoxam (TMX) concentrations in plant tissue, seeds, soil, and water samples: Prior to analysis, plant tissue samples were frozen with liquid $N_2$, ground, freeze-dried and stored at -20 °C. Soil samples were homogenized, freeze-dried and stored at -20 °C.

For extraction of TMX from a plant or soil sample, 10 mL of acetonitrile was added to either 1 g of freeze dried soil or 0.2 g of freeze dried plant tissue in a 35 mL glass centrifuge tube and vortexed for 10 seconds. The centrifuge tube was then filled with 0.5 g of sodium chloride and 2 g of anhydrous magnesium sulfate, vortexed for 2 minutes, and centrifuged at 10,000 rpm for 10 minutes at 15°C. The supernatant was transferred into a 35 mL centrifuge vial with 0.5 g of anhydrous magnesium sulfate and 0.10 g of Primary Secondary Amine (PSA). Another 5 mL of acetonitrile was added to extract targets, as described above, and the two resulting supernatants were combined, vortexed for 1 min, and centrifuged at 4,000 rpm for 5 minutes at 15 °C. A 5.0 mL aliquot was extracted from the supernatant, transferred into a glass vial, and dried in a Rapidvap. The dehydrated sample was then reconstituted by adding 1 mL of 5 mM $NH_4Ac$-$H_2O$ and $NH_4Ac$-MeOH (V/V, 1/9), filtered with a 0.2 µm polyvinylidene fluoride filter (Fisher, USA), and added to an amber glass vial for analysis via UPLC-MS/MS.

For drainage water, samples were filtered twice through a polyvinylidene fluoride syringe filter (0.45 µm and 0.2 µm, respectively), and transferred into an amber glass for direct analysis via UPLC-MS/MS.

One seed before planting and three seed castings recovered from each plot were added to a 35 mL glass centrifuge with 10 mL of acetonitrile, sonicated for 20 mins, and centrifuged at

4,000 rpm for 10 minutes at 15 °C. A 20 µL aliquot of supernatant was dried via Rapidvap and diluted in 1 mL of 5 mM $NH_4Ac$-$H_2O$ and 5 mM $NH_4Ac$-MeOH (V/V, 1/9). The reconstituted sample was then further diluted 100 times for the pre-planting seed and V1 seed castings, 20 times for the V3 seed castings, and 10 times for the V5 seed castings before filtered with a 0.2 µm polyvinylidene fluoride filter (Fisher, USA) and analysis for TMX via UPLC-MS/MS.

TMX was analyzed in the extracts or water sample using an Agilent 1290 UPLC coupled with Agilent 6490 Triple Quad tandem mass spectrometry. Separation occurred on a Zorbax Extend-C18 Column (4.6 × 50mm, 5 µm; Agilent, USA) at 30°C, using a mobile phase of (A) $H_2O$ (5 mM $NH_4Ac$) and (B) MeOH (5 mM $NH_4Ac$) at a flow rate of 0.5 mL $min^{-1}$. Samples were subject to gradient elution at t = 0, 5, 6, 6.5, and 9.5 mins and A:B v/v ratios of 90:10, 5:95, 5:95, 90:10 and 90:10. The operation was performed using the positive ion mode with a desolvation gas flow rate of 14.0 L $min^{-1}$, gas temperature of 250 °C, capillary voltage of 3000 V, and nebulizer gas pressure of 45.0 psi. The multiple reaction monitoring mode was used with resulting method detection limits of 0.005 µg $kg^{-1}$ for plant and soil matrices, and 0.005 µg $L^{-1}$ for water. The LOD and LOQ of the target (i.e., TMX) were 0.005 and 0.01 µg $kg^{-1}$ (or µg $L^{-1}$) in the matrices (i.e., plant, soil and water). The recoveries of TMX were 100.5 ± 5.1%, 82.9 ± 5.5% and 104.2 ± 5.3% in plant, soil and water, respectively.

## B2 Drainage Collection Design

The field plot design and drainage collection system are illustrated in **Figure B1**.

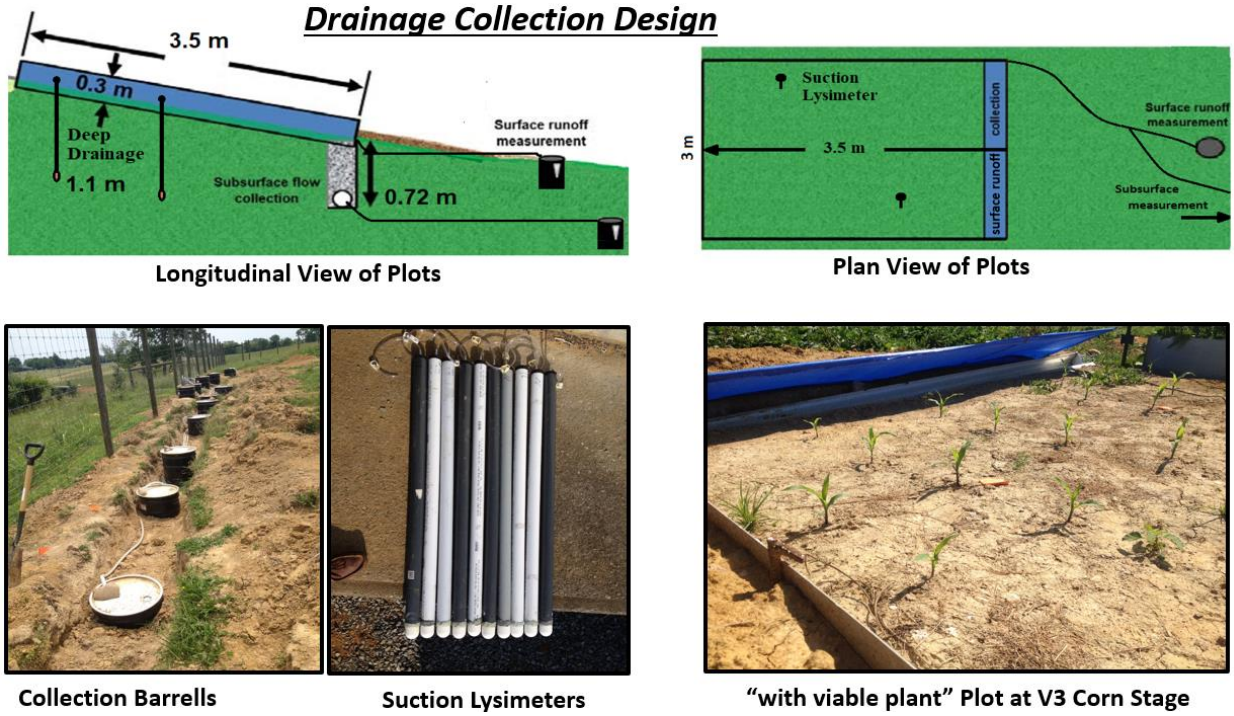


**Figure B1.** Field plot and drainage collection design.

## B3 Soil Sampling Details

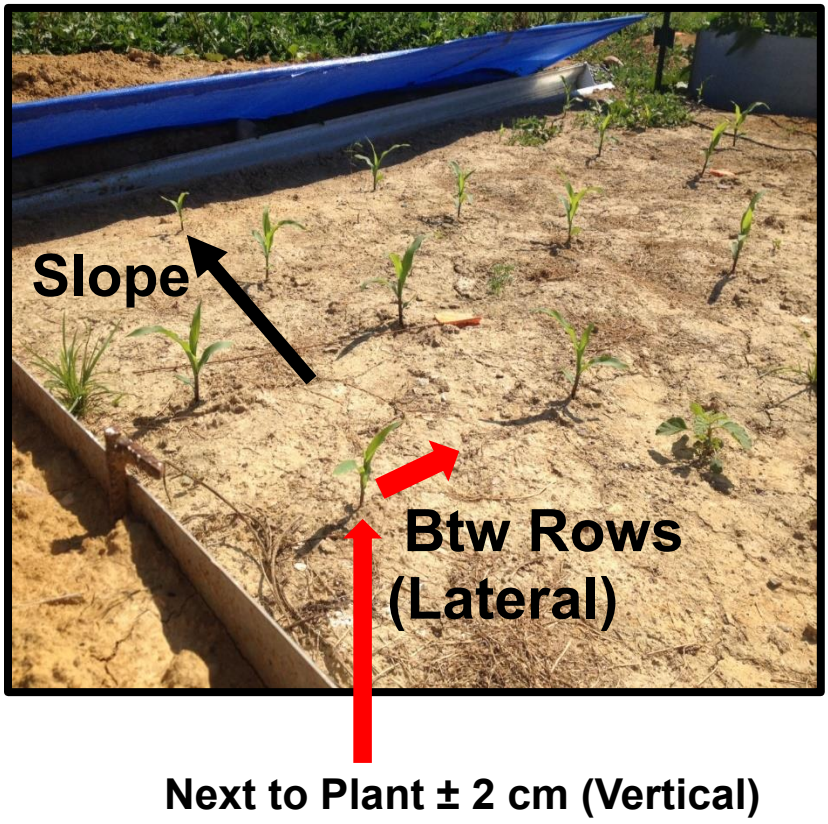


**Figure B2**. Soil sampling scheme, highlighting the significance of TMX detection between rows (i.e. 25 cm perpendicular to the plot slope).

## B4 Soil Water Content

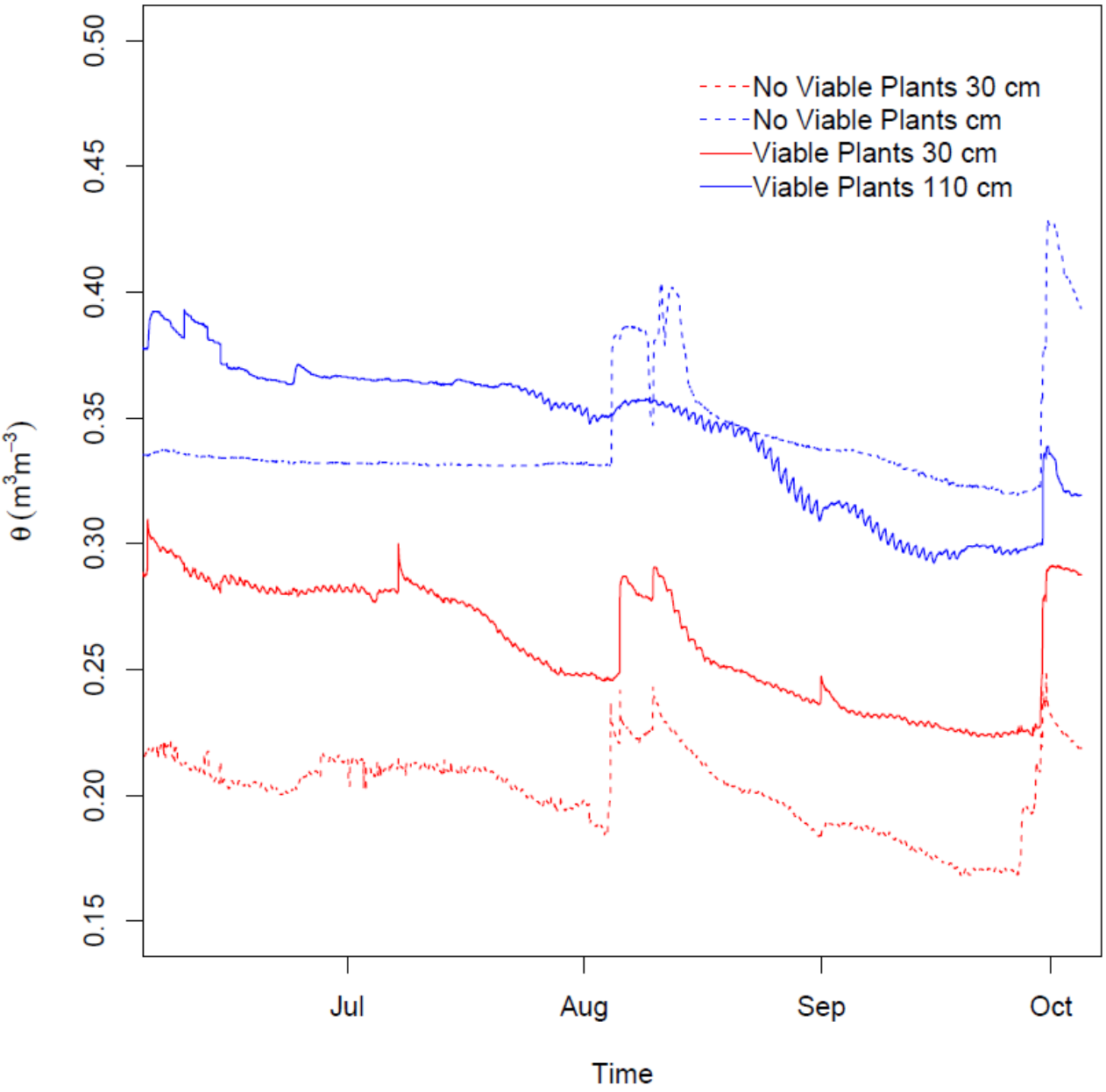


**Figure B3.** Soil water content ($\theta$) in upper $B_t$ (30 cm) and C horizons (110 cm) from $n$ = 3 plots per plant treatment (viable vs no viable plants).

## B5 Total TMX in Drainage and Soil Compartments

**Table B1.** Estimated cumulative mass of TMX transported (%) via runoff and shallow lateral drainage over the growing season and mass of TMX remaining in soil at different corn growth stages as a fraction of the initial input from the coating of 60 seeds per plot (1.21 ± 0.04 mg of TMX per seed).

| | % of Initial TMX Input (Per Plot) | |
|---|---|---|
| | **No Viable Plants** | **Viable Plants** |
| ***Drainage Compartment (Cumulative)*** | | |
| Runoff | 0.41 ± 0.17 | 0.24 ± 0.11 |
| Shallow Lateral | 0.13 ± 0.071 | 0.034 ± 0.016 |
| ***Soil Compartment*** | | |
| V3 | 43 ± 55 | 23 ± 24 |
| V5 | 16 ± 25 | 14 ± 7.6 |
| VT | 9 ± 10 | 1.1 ± 0.9 |
| R6 | 0.51 ± 0.44 | 1.4 ± 0.43 |

## B6 Details Regarding Rainfall Events

Rainfall event characteristics are reported in **Table B2**. Rainfall intensity measurements are reported as the ratio of rainfall accumulation to accumulation time for contiguous rain gauge recordings with 15 minute resolution. “Max Intensity” describes the maximum rainfall intensity measurement recorded during the preceding period of precipitation.

**Table B2.** Rainfall event period and drainage sampling details. Note that drainage sampling typically followed multiple days of rainfall accumulation.

| Event Period | Sampling Date | Event Number | Days after Planting | Accumulation (cm) | Max Intensity (cm $hr^{-1}$) |
|---|---|---|---|---|---|
| 6/15/2016 - 6/16/2016 | 6/16/2016 | 1 | 10 | 0.96 | 1.2 |
| 6/21/2016 - 6/24/2016 | 6/24/2016 | 2 | 18 | 3.4 | 0.91 |
| 7/2/2016 -7/6/2016 | 7/6/2016 | 3 | 30 | 7.3 | 16 |
| 7/12/2016 - 7/14/2016 | 7/15/2016 | 4 | 39 | 3 | 1 |
| 7/26/2016 - 7/29/2016 | 7/29/2016 | 5 | 53 | 3.4 | 1.4 |
| 8/3/2016 - 8/6/2016 | 8/6/2016 | 6 | 61 | 4.2 | 0.83 |
| 8/7/2016 - 8/10/2016 | 8/11/2016 | 7 | 66 | 1.7 | 0.6 |
| 9/1/2016 | 9/1/2016 | 8 | 87 | 2 | 1.8 |
| 9/26/2016- 9/28/2016 | 9/29/2016 | 9 | 115 | 7.8 | 2 |

## B7 Detailed Statistical Analysis

Rank transforming data to normality permitted the use of more flexible parametric tests (one-way ANOVA, factorial ANOVA); which altogether is the functional equivalent of running traditional non-parametric comparisons [*Conover*, 2012; *Conover and Iman*, 1981].

# Appendix C (Appendix for Chapter 4)

## C1 Analytical Approach

Each collected leachate sample was first cleaned up by mixing 1.8 mL leachate with 60 mg primary and secondary amine (PSA), vortexing for 2 min, and centrifuging at 5000 rpm for 5 min. The supernatant was then filtered first through a 0.45 µm PTFE syringe filter and then through a 0.2 µm PTFE syringe filter immediately before being analyzed using an online solid phase extraction (SPE) system coupled with a Ultra-Performance Liquid Chromatography/tandem mass spectrometry (UPLC/MS/MS) (Agilent 1290 Infinity LC system with Flexible Cube and Agilent 6490 Triple Quadrupole system, Agilent, Santa Clara, CA). Six hundred µL of a filtered leachate was loaded onto the online SPE installed with Agilent PLRP-S cartridges (15-20 µm, 4.6 × 12.5mm, Agilent). A Flow of 1 mL $min^{-1}$ was run though the cartridges at 0.1 min with 100% water, 4.6 min with 100% acetonitrile, and 13 min with 100% water. Separation of target analytes was conducted on a Zorbax SB-C18 analytical column (3.0 × 100 mm, 3.5-µm particle size, Agilent) at 40$^{o}$C with a mobile phase flow rate of 0.4 mL $min^{-1}$. A Zorbax SB-C18 guard column (2.1 × 50 mm, 1.8-µm particle size, Agilent) was installed before the analytical column to remove matrix interference. The mobile phase included (A) 0.1% formic acid in water and (B) 90% acetonitrile with the following A:B gradient of 80:20, 80:20, 80:20, 39:61, 0:100, 0:100, and 80:20, measured at respective times of 0, 0.1, 4.6, 11.1, 12.6, 14.1, and 14.6 min.

The tandem mass spectrometry system was set up using an electrospray ionization positive mode at nitrogen gas temperature of 250$^{o}$C, nitrogen gas flow of 14 L $min^{-1}$, nebulizer gas pressure of 310 kPa, and capillary voltage of 3500 V. The mass to charge ratios (m/z) for the parent ion and qualifier and quantifier daughter ions are listed in **Table C1**. Due to significant

matrix interference, concentrations of all target analytes in the leachate samples were quantified against matrix-matched standards [*Commission*, 2002]. The method detection limits and recoveries of the target analytes are listed in **Table C2**.

**Table C1.** Method detection limit and recovery of target compounds in their matrix

| Antibiotic | Method detection limit (ng $L^{-1}$) | Recovery (%) ($n$ =10) |
|---|---|---|
| Tylosin (TYL) | 249 | 102 ± 14 |
| Pirlimycin (PYL) | 12.5 | 100 ± 8 |
| Tetracycline (TC) | 6.39 | 108 ± 14 |
| Erythromycin (ERY) | 6.25 | 90 ± 12 |
| Oxytetracycline (OTC) | 124 | 111 ± 7 |
| Sulfadimethoxine (SDM) | 25.7 | 102 ± 9 |
| Sulfamethazine (SMZ) | 6.35 | 96 ± 13 |
| Chlorotetracycline (CTC) | 63.2 | 91 ± 7 |

**Table C2.** Mass to charge (m/z) of the parent ion and daughter ions for target analytes

| Antibiotic | Parent Ion (m/z) | Qualifier Daughter Ion (m/z) | Quantifier Daughter Ion (m/z) |
|---|---|---|---|
| Tylosin (TYL) | 916.0 | 772.0 | 174.0 |
| Pirlimycin (PYL) | 411.0 | 363.0 | 112.0 |
| Tetracycline (TC) | 445.2 | 154.0 | 410.0 |
| Erythromycin (ERY) | 734.6 | 576.5 | 158.2 |
| Oxytetracycline (OTC) | 461.6 | 443.0 | 426.0 |
| Sulfadimethoxine (SDM) | 311.2 | 92.1 | 156.1 |
| Sulfamethazine (SMZ) | 279.0 | 156.0 | 186.0 |
| Chlorotetracycline (CTC) | 479.1 | 153.9 | 443.9 |

## C2 Field Plot Design and Lysimeter Placement

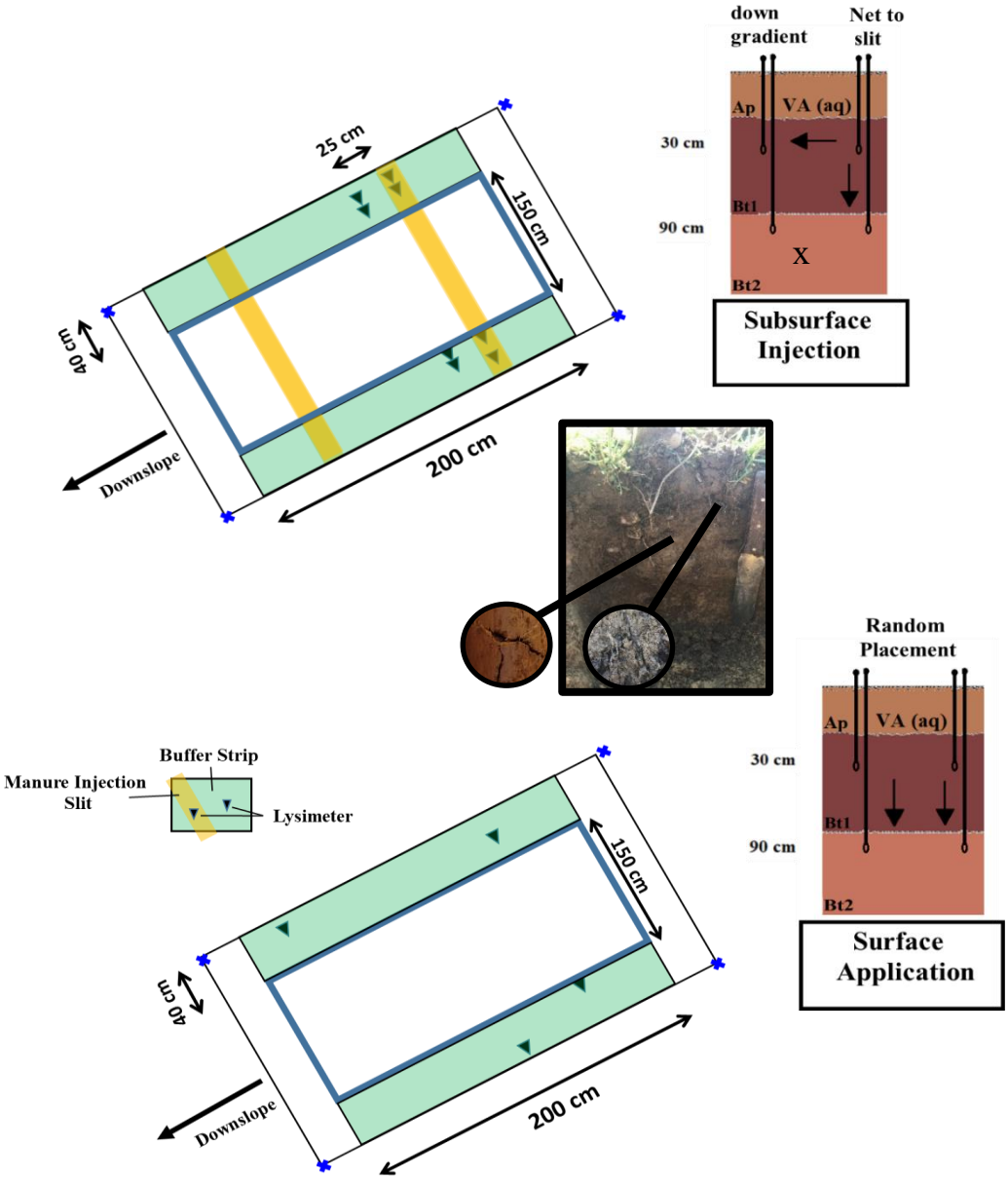


**Figure C1.** Schematic showing the basic design for Subsurface Injection (**top**) and Surface Application (**bottom**) runoff plots along with their respective lysimeter installation schemes. The center photograph shows soil structure development in the A and B horizons. **Note**: Control Plots were designed and sampled in an identical manner to the Surface Application plots.

## C3 Lysimeter Sampling Details

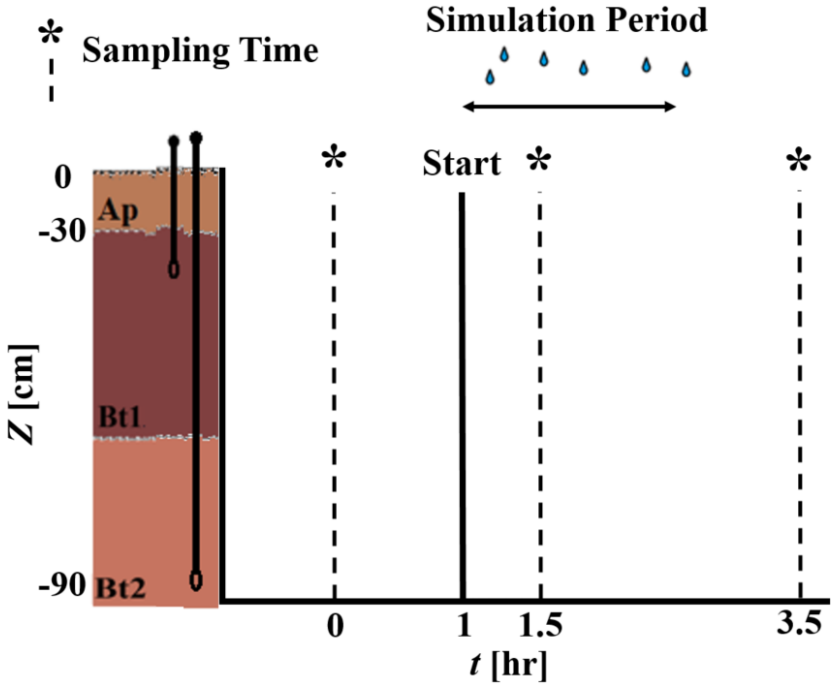


**Figure C2.** Lysimeter sampling regiment for field rainfall simulations in space (30 and 90 cm depths) and time (1 hour before, 0.5 hours into, and 1 hour after rainfall simulations).

## C4 Behavior of Veterinary Antibiotics in Control Plots

In the presence of preferential flow, solute transport was similar between control and experimental plots for the most mobile VAs (Sulfonamides: SDM and SMZ; **Figure C3**). After only 7 days of equilibration with the soil matrix, newly introduced VAs behaved similarly to compounds introduced in previous growing seasons. This shows that mobile compounds are still susceptible to preferential flow despite long term persistence in the soil matrix (e.g., > 6 months).

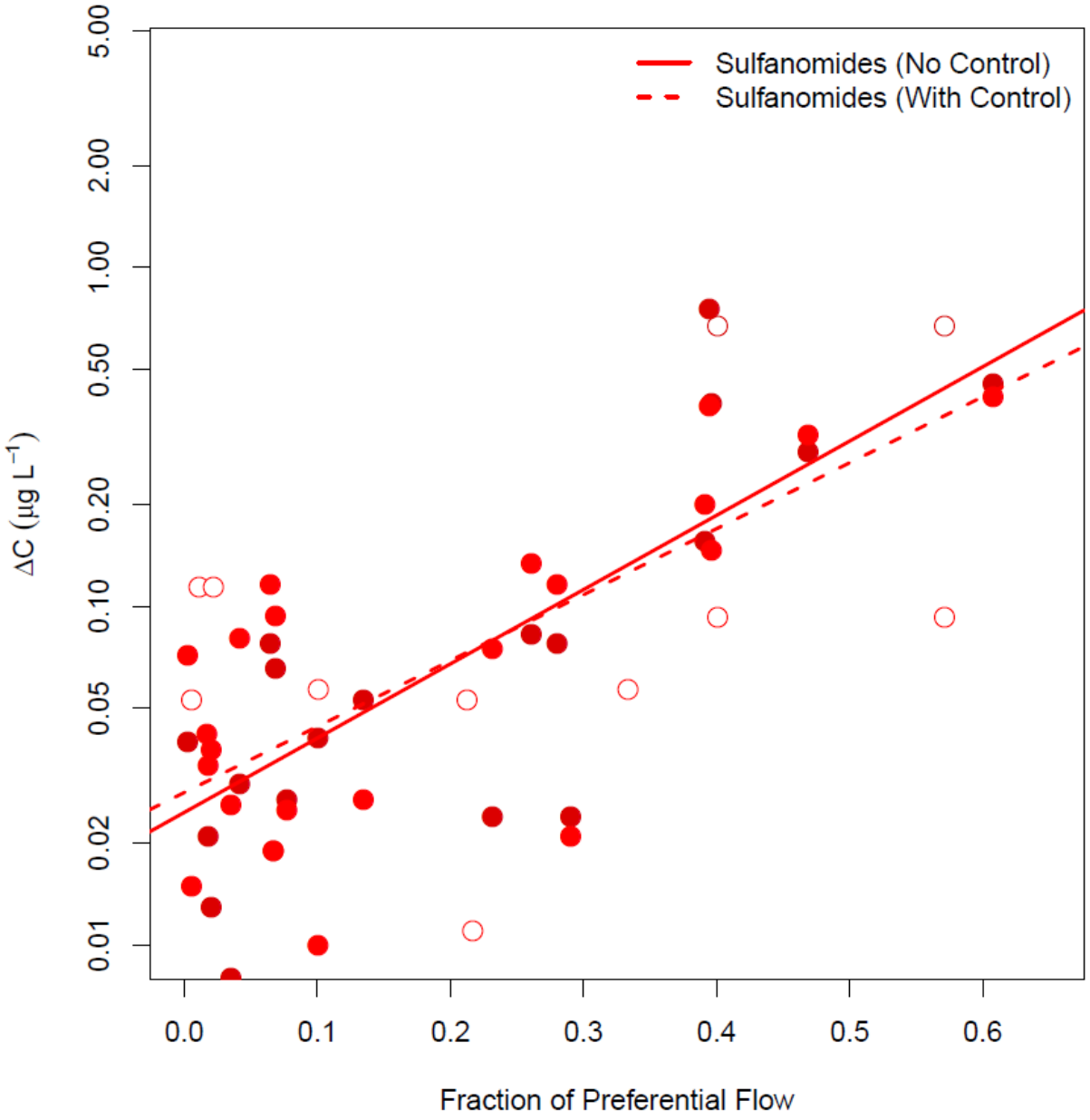


**Figure C3.** The change in concentration of sulfanomides (SMZ and SDM) versus the estimated fraction of preferential flow from lysimeter samples. Open circles represent samples taken from control plots, whereas filled circles represent those taken from plots where antibiotic-spiked manure was applied. Only samples with non-zero ΔC were included.